主　論　文

A study of reflection height of tweek atmospherics in the D- and lower E-region ionosphere

（D 領域・下部 E 領域電離圏における

トウィーク空電反射高度の研究）

by
Hiroyo Ohya

大矢　浩代

Nagoya University

2012

Acknowledgements

I am grateful to the members of my thesis advisory committee at the Solar–Terrestrial Environment Laboratory (STEL), Nagoya University: the chairman, Professor Takashi Kikuchi, and Professors Kazuo Shiokawa, Munetoshi Tokumaru, Masafumi Hirahara, and Yuichi Otsuka. The research presented in this thesis was conducted in collaboration with Professors Kazuo Shiokawa, Masanori Nishino, and Yoshizumi Miyoshi of the STEL. Professor Masanori Nishino is greatly acknowledged for his advice and encouragement.

I am also grateful to the late K. Hidaka and late M. Takasuka of Kagoshima Observatory, STEL, for their continuous operation of the VLF observations, and to M. Satoh, Y. Katoh, Y. Hamaguchi, and Y. Yamamoto of STEL for their technical support of the VLF/ELF measurements. This research was supported by Project 2 and the cooperative research program of STEL.

The 210 MM magnetic field data were provided by Professor Kiyohumi Yumoto of the Space Environment Research Center, Kyushu University. The plots of these data were reprinted from the 210 MM database site at STEL.

I also wish to acknowledge the contributions of many professors and staff members of the Graduate School of Engineering and Graduate School of Science, Chiba University, for their help and encouragement.

I thank Professor Yukihiro Takahashi of Hokkaido University, and Dr. Fuminori

Tsuchiya of Tohoku University, and Dr. Kozo Yamashita of Salesian Polytechnic for providing me with the opportunity to participate in the AVON project.

The AVON project has been supported by the joint research program of STEL. My research was supported by a grant from the Career-support Program for Women Scientists at Chiba University.

Finally, I extend my sincere thanks to my husband, Satoru Makita, for his support and help with childcare, housekeeping, and nursing my parents. Thanks from the bottom of my heart. Special thanks, too, to my children, Hitomi and Ryo, for their help in the installation of the AVON system in Taiwan. My heartfelt thanks and gratitude also go to my late parents, Seishiro and Kiyo Ohya, for their encouragement and emotional support during my studies.

Contents

Notation

General Notation

H: geomagnetic field strength

R: Fresnel reflection coefficient

T: electron temperature

c: speed of light

e: electron charge (=1.60218 × 10^{-19} C)

f: frequency

f_H: electron gyro frequency

f_N: plasma frequency

k: Boltzmann constant

m_e: electron mass (=9.10938 × 10^{-31} kg)

m_i: ion mass

n_e: electron density (cm^{-3})

q: photoionization rate

t: time

v: electron velocity

v_g: group velocity

v_p: phase velocity

α_{eff}: recombination rates

ε_0: electric permittivity in a vacuum (=8.854188 × 10^{-12} F/m)

θ: wave normal angle

λ: wavelength

μ_0: permeability in a vacuum (= 4π × 10^{-7} H/m)

ν_{en}: collision frequency between electrons and neutrals

ω: angular frequency

ω_H: electron gyro frequency

ω_N: angular plasma frequency

Specific Notation

A: total column absorption of the radio waves

A_o: amplitude of ordinary mode

A_x: amplitude of extraordinary mode

K: imaginary part of the refraction index in the Appleton–Hartree formula

L: dipole L shell

N: peak electron density in the E-region

ionosphere (cm^{-3})

P: power flux density of the scattered waves

P_0*:* power flux density of the transmitted radio waves

R_o*:* reflection coefficients of ordinary mode

R_s: smoothed relative sunspot number

R_x*:* reflection coefficients of extraordinary mode

S: effective surface area of rocket probe

T_g*:* time delay from lightning to the observation point

V: scattering volume

V_p*:* voltage between rocket probe and plasma

V_x*:* *x*-direction components of rocket speed (orbital plane of the rocket: *x*–*z* plane, and *z* is vertical upward direction)

V_y*:* *y*-direction components of rocket speed

a: Earth's radius

d: horizontal propagation distance of tweek atmospherics

f_c*:* cut-off frequency of tweek atmospherics

h: reflection height of tweek atmospherics

h': virtual height of the ionosphere

i: electric current in rocket probe

n: order of mode

q: ionization production rate ($cm^{-3}s^{-1}$)

β*:* angle between the horizontally projected direction of propagation vector and the positive *x*-direction

δ*:* angle between horizontal component of the propagation vector and magnetic meridian plane

κ_o*:* absorption coefficients of ordinary mode

κ_x*:* absorption coefficients of extraordinary mode

λ_n*:* ratio of negative ions ($=n^-/n_e$)

μ*:* refractive index in the Appleton–Hartree formula

ρ*:* angle between the propagation vector and the positive *z*-direction

ρ_0*:* initial value of the incident angle of the radio waves from transmitter

σ_0: radar scattering cross section

φ: angle between external magnetic field vector and z-axis

χ: absorption of the radio waves $(=K\omega/c)$

Abstract

The D- and lower E-region ionosphere at altitudes below ~100 km has been studied using rockets, very low frequency (VLF) radio waves, and ionosondes over the past six decades. However, the nighttime lower ionosphere at low latitudes has remained a relatively blank region of study due to the limited locations of measurement by rockets and VLF radio waves. Conventional ionosondes cannot measure the lower ionosphere below ~100 km because of the high collision frequency between plasma and the neutral atmosphere.

This thesis presents three results obtained from analysis of tweek atmospherics. Specifically, this thesis describes 1) the development of an automatic procedure to estimate the reflection height and propagation distance of tweek atmospherics, 2) the long-term variation in the tweek reflection height, and 3) the variation in tweek reflection height during a magnetic storm. Tweek atmospherics are an effective tool for deriving long-term height variations in the D- and lower E-region ionosphere. Passive measurement of tweeks is much easier and cheaper than measurement by rockets and active radio sounding techniques and can be used to observe the ionosphere even over the sea. We developed an automatic procedure to estimate the reflection height and propagation distance of tweeks to investigate long-term variations in the tweek reflection height. Use of the maximum entropy method (MEM) instead of the fast Fourier transform (FFT) significantly improved the accuracy of estimated reflection height and particularly propagation distance. These results show that the automatic procedure can clearly detect the rapid frequency changes of tweeks.

The main aspect of this thesis is that we show, for the first time, long-term (1976–2010) variations in the reflection heights of tweek atmospherics based on VLF

observations at Kagoshima, Japan. The tweek reflection heights were investigated on the geomagnetically quietest days of each month over three solar cycles using an automated procedure of spectral fitting to estimate the cut-off frequency. The results are compared with various effects of solar-cycle variation on the nighttime lower ionosphere at low latitudes. The average and standard deviation of the reflection heights were 95.9 km and 3.1 km, respectively. Typical time variations of the reflection heights were identified as 13.3, 3.2, 1.3, 1.0, 0.6, and 0.5 years. These variations in the tweek reflection heights did not show simple anti-correlation with solar activity. The correlation coefficient between the tweek reflection height and the sunspot number was 0.03 throughout the three solar cycles. Hilbert–Huang transform analysis revealed variations of 0.5–1.5 years and ~10 years to be intrinsic mode functions (IMFs). The decomposed IMF with the ~10-year variation was positively correlated with sunspot number and negatively correlated with galactic cosmic rays (GCRs). These variations in the tweek reflection heights could be caused by coupling of several ionization effects in the D and lower E regions: geocorona, GCRs, particle precipitation, and variations in neutral density in the lower thermosphere. GCRs may have played a role in the long-term variations until 2006. In these processes, the geocorona and particle precipitation could show negative correlations, whereas the GCRs and neutral density could show positive correlations with solar activities.

Another new and interesting result is the response of the nighttime D-region ionosphere to the great magnetic storm of 2–12 October 2000. We found that the tweek reflection height significantly decreased by approximately 10 km at 15:50–16:50 UT on 2 October and at 12:50 UT on 3 October. We compared these characteristic negative excursions of the tweek reflection heights with amplitude variations of 40-kHz radio-wave signals, electron density profiles obtained by two medium-frequency radars, and the *h'F* values measured by an ionosonde, ground magnetic field data, and GCRs.

Possible mechanisms for the drop in tweek reflection heights may be coupling with the F-region downward motion caused by westward electric fields associated with substorm activities during the great storm and large-scale traveling ionospheric disturbances (LSTIDs) propagating from high to low latitudes.

This thesis also describes new network observations of tweek atmospherics over southeastern Asia. These continuous measurements of tweek atmospherics provide useful information for monitoring short- and long-term variations in the D and lower E-region ionosphere at low latitudes.

Chapter 1.
General Introduction

In nature, very-low-frequency (VLF, 3–30 kHz) waves originate from lightning and are categorized into atmospherics and emissions. The two major characteristic atmospherics in VLF waves are whistlers and tweeks, and the main VLF emissions are hiss emissions, discrete emissions, periodic emissions, chorus emissions, quasi-periodic emissions, and triggered emissions (Obayashi, 1970). The VLF emissions are caused by resonance between particles and waves in the magnetosphere. Whistlers propagate in the atmosphere, ionosphere, and magnetosphere, whereas tweeks propagate in the atmosphere through the Earth–ionosphere waveguide with reflection between the bottom edge of the ionosphere and the Earth's surface.

Tweeks are a useful tool for investigating the D- and lower E-region ionosphere. The altitude ranges of these regions are 60–90 km for the D region and 90–150 km for the E region (Brekke, 1997). Conventional ionosondes (1–30 MHz) cannot measure the D region below 100 km. Radio waves at frequencies of more than 1 MHz can pass through this altitude region because they are higher than the critical frequency for the D region electron density. However, radio waves below several MHz are significantly absorbed due to the high collision frequency in the D region. Thus, it is usually difficult to observe the D and lower E regions using conventional ionosondes.

However, tweeks are reflected only in the D or lower E regions. The reflection height is a sensitive indicator of the vertical density profile of the D and lower E regions. Thus, tweeks are useful for investigating the bottom part of the ionosphere.

This chapter presents a brief overview of tweek atmospherics in Section 1.1. In

Section 1.2, nighttime ionization sources in the D- and lower E-region ionosphere are described. Section 1.3 describes the method of observing electron density in the D- and lower E-region ionosphere. Variations in electron density in the D- and lower E-region ionosphere are then described in Section 1.4, followed by a presentation of the purpose of this thesis in Section 1.5.

1.1. Tweek Atmospherics

Tweek atmospherics at frequencies of 1.5–10.0 kHz originate from lightning discharge and propagate over several thousand kilometers in the Earth–ionosphere waveguide reflecting between the bottom edge of the ionosphere and the Earth's surface. These atmospherics were given the name "tweeks" because there are audible and sound like a bird's "tweet." Figure 1.1 shows a schematic diagram of the waveguide propagation of tweeks. The letters *h* and *d* indicate the reflection height (the waveguide height) and the propagation distance, respectively. Figure 1.2 shows a typical dynamic spectrum of a tweek observed at Kagoshima, Japan (31.48ºN, 130.72ºE), at 14:51:18 UT on 11 March 2011. The frequency of the tweeks fell from 10 kHz to about 2 kHz during 118 ms, which can be seen on the dynamic spectrum as characteristic frequency–time dispersion. In any season, tweeks can be observed only at night because attenuation due to solar ionization is much greater in daytime.

Tweeks consist of several order modes, including zero-, first-, and second-order and higher modes. Figure 1.2 shows the zero- to third-order modes. The zero- and first-order modes are less than 1.7 kHz and around 1.7 kHz, respectively. The second- and third-order modes are seen at 3.3 and 5.3 kHz, respectively.

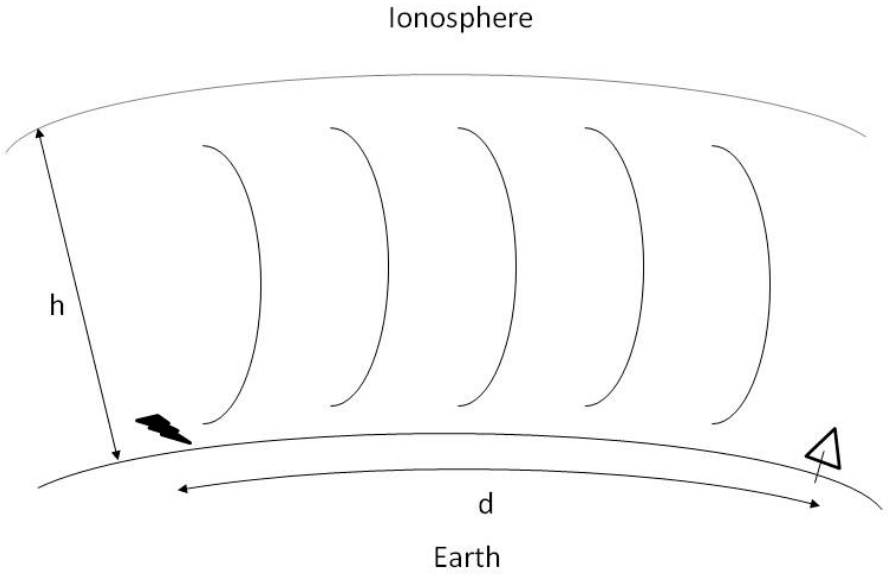

Figure 1.1. Schematic diagram of the waveguide propagation of tweeks.

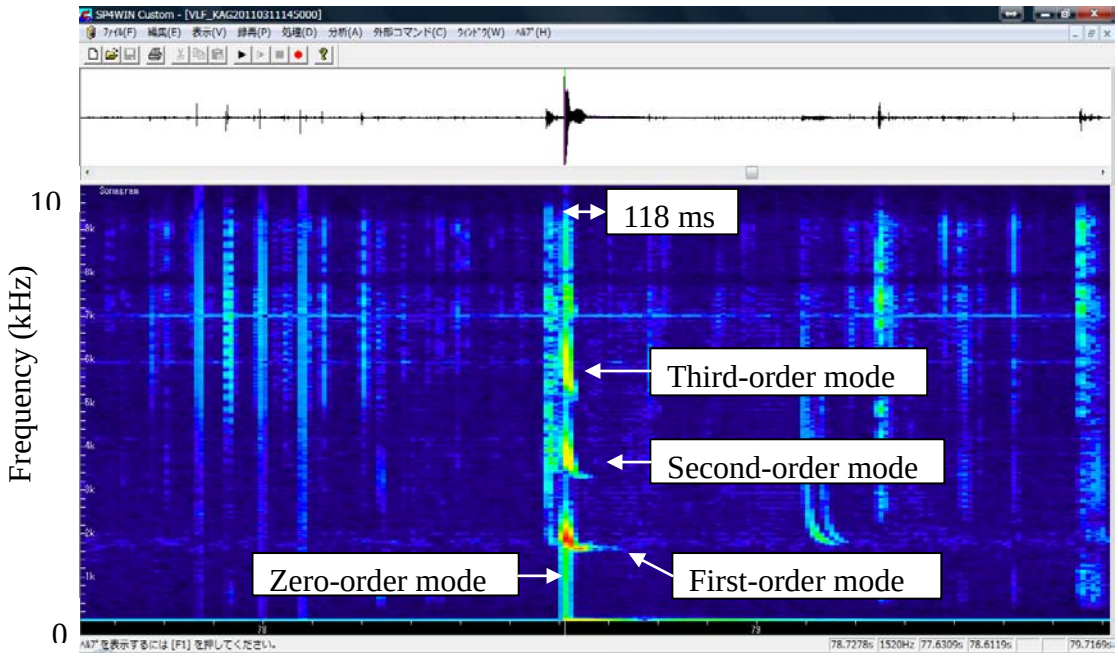

Figure 1.2. Typical dynamic spectrum of a tweek observed at Kagoshima, Japan, at 14:51:18 UT on 11 March 2011.

The mode represents the number of field patterns in the plane perpendicular to the propagation direction in the Earth–ionosphere waveguide. Figure 1.3 (a) and (b) show the electric-field patterns of the first- and second-order modes, respectively, assuming that the Earth is an electrically perfect conductor (Fresnel reflection coefficient $R = +1$) and the ionosphere is a magnetically perfect conductor ($R = -1$). The figures show the transverse magnetic (TM) mode. The mode pattern can be obtained based on the Maxwell equations when the ionosphere is located at the surface, where the vertical electric field is zero and just under the upper perfect conductor. The zero-order mode of tweeks is the TM_0 mode (Wait, 1970; Hayakawa et al., 1994). Regarding the first-order mode, both TM and transverse electric (TE) modes have been considered based on an inhomogeneous and anisotropic ionosphere model (Hayakawa et al., 1994). Yamashita (1978) calculated the attenuation coefficient and excitation factor of a waveguide near the cut-off frequency and demonstrated that the quasi-TE mode plays a dominant role in the formation of tweeks.

Some earlier studies of tweeks were not interested in the tweeks in themselves but as signals prior to whistlers (Baba et al., 1992). In the era before satellites, whistlers were considered more important than tweeks because whistlers contain information on the magnetosphere. Tweeks were examined to investigate whistler propagation, particularly the direction of whistlers (Baba et al., 1992). In this earlier period, the idea of using tweeks to study the lower ionosphere and lightning distribution had been raised. However, tweeks occur in large numbers (several tens in a minute) and were difficult to analyze with the lack of computer resources at the time. Thus, tweeks have generally attracted little attention, although there are several notable studies.

Research on tweeks can be divided into four main themes: studies of the lower ionosphere, lightning distribution, whistler propagation, and the propagation mechanism of tweeks. To my knowledge, Burton and Boardman (1933a) published the earliest

paper on tweek atmospherics in the lower ionosphere. They analyzed tweeks using data obtained by submarine cable interference observations in the USA and Cuba in 1928–1931. In their paper, tweeks were well explained by simple reflection theory. The reflection height and propagation distance were estimated. They showed nocturnal variations in the cut-off frequency and the tweek occurrence rate. Additionally, they described seasonal variations in the first and last arrival times of tweeks around sunset and sunrise. They reported that the cut-off frequencies were 2.30 kHz (corresponding to the reflection height of 65.17 km) at sunset, 1.65 kHz (90.85 km) at midnight, and 1.86 kHz (80.59 km) at sunrise.

Tweeks can also be observed from about 30 minutes before sunset and until about 20 minutes after sunrise in summer. The frequency–time dispersion of tweeks was numerically studied by Outsu (1960). He showed that if the imperfectly conducting layer is calculated as a perfectly conducting layer, the errors in the reflection height and propagation distance are larger by 5% and 9% than the true values, respectively. Rafalsky et al. (1995) introduced a technique to estimate the reflection height and propagation distance of tweeks. The accuracy of the estimation was on the order of 1% for the ionospheric height and 7% for the distance. Kishore et al. (2005) showed that the cut-off frequency of tweeks obtained in the South Pacific region ranged from 1.62 to 1.79 kHz and that the reflection height varied between 80 and 95 km. Kumar et al. (2008) concluded that the tweek reflection heights observed in the South Pacific region (18.2ºS, 178.3ºE) during low solar activity varied in the range of 83–92 km; these heights were higher by about 1–1.5 km than those estimated during a period of high solar activity.

Tweek studies of lightning distribution have investigated the source of lightning and discussed the estimation of propagation distance. Kashiwagi et al. (1970) reported a peak propagation distance of around 2000 km based on observations at Sakushima,

Japan (34.7ºN, 137.0ºE), using a direction-finder atmospheric location network. Hayakawa et al. (1994) and Nagano et al. (2007) also reported directional findings based on tweeks.

Studies of tweeks as signals prior to whistlers have estimated the locations of the source lightning as well as whistler ducts using field-analysis methods (Ohta et al., 1991; Hayakawa et al., 1992; Baba et al., 1992).

Research on the propagation mechanism of tweeks has examined various parameters such as the phase velocity, group velocity, attenuation factor, polarization mixing ratio, and excitation factor based on waveguide mode theory (Outsu, 1960; Wait, 1970; Yamashita, 1978; Ryabov, 1992; Shevets and Hayakawa, 1998). Lynn and Crouchley (1967) reported that about four times as many tweeks arose from the east than from the west in observations at Brisbane, Australia. Prasad (1981) showed the effects of a mixed path of ground and sea on the formation of tweeks. Baba et al. (1991) found that the incident angle of the cut-off frequency for the first-order mode was zero, i.e., the cut-off frequency could be regarded as the vertical reflection. Kishore et al. (2005) showed that sea paths have less attenuation than do ground paths.

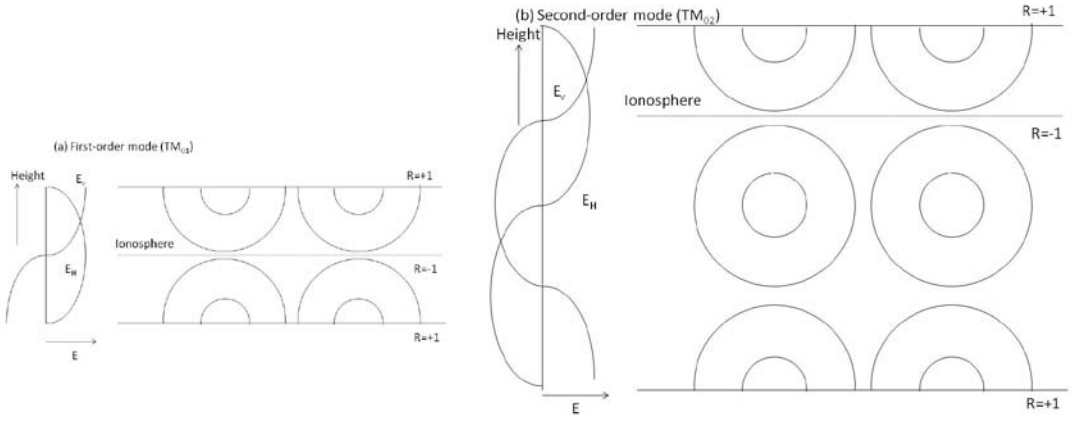

Figure 1.3. Electric field pattern of (a) the first-order mode and (b) second-order mode of tweeks in the Earth–ionosphere waveguide. The circles indicate equipotential contours.

1.2. Nighttime Ionization Sources in the D and Lower E Region Ionosphere

The heights of the D region, E region, and F region of the ionosphere are roughly 60–90 km, 90–130 km, and 130–1000 km, respectively. The regions are divided according to electron density. Figure 1.4 shows the electron density profiles of the ionosphere (Schunk and Nagy, 2000). Nighttime electron densities in the D, E, and F regions are roughly ~10^3 cm^{-3}, 10^3–10^4 cm^{-3}, and ~10^5 cm^{-3}, respectively.

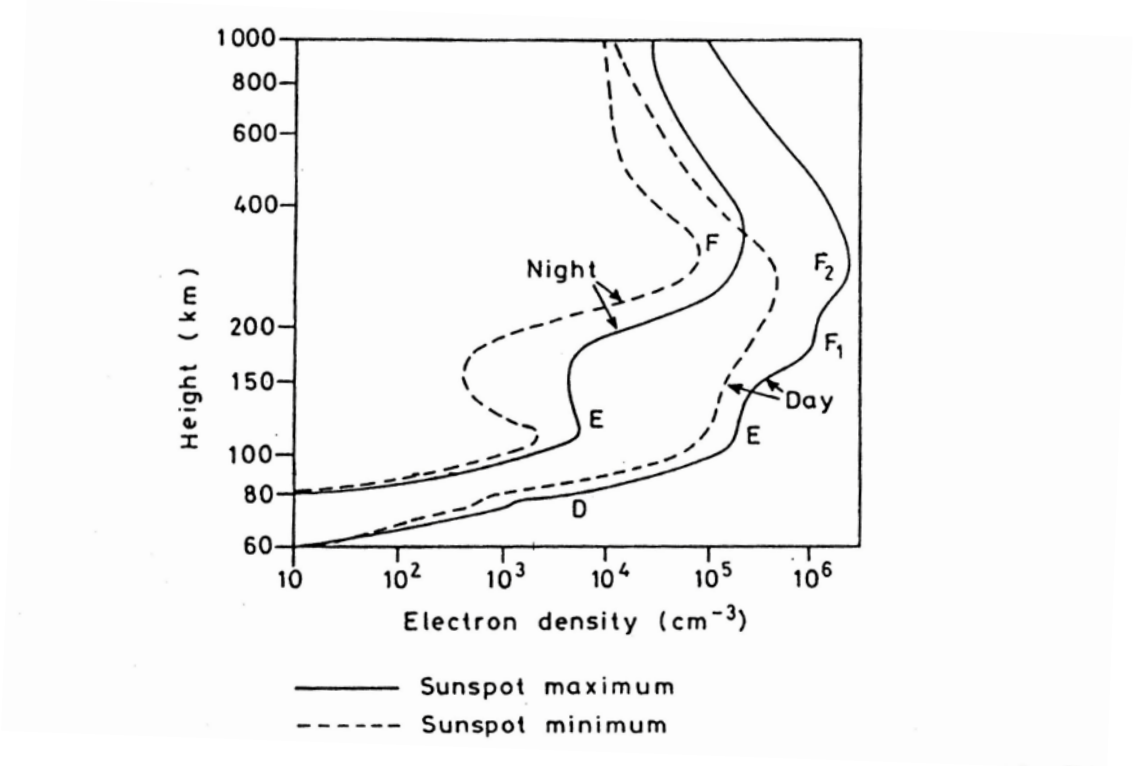

Figure 1.4. Electron density profiles in the ionosphere (Hargreaves, 1992).

In 1901, Marconi identified the ionosphere using a radio-signal experiment. In 1902, Kennelly and Heaviside suggested that free electrical charges in the upper atmosphere

could reflect radio waves (Ratcliffe, 1967). The first rough measurements of the height of the reflecting layer were made by Forest and Fuller in San Francisco, California, USA, in 1912–1914 (Schunk and Nagy, 2000). Using transmitter–receiver radio signals, the reflecting-layer height was estimated to be about 500 km (Villard, 1976). However, the Forest–Fuller results did not become well known. More widely known measurements of the reflecting-layer height were made in 1924 by Breit and Tuve (1925) and by Appleton and Barnett (1925). In 1926, the name “ionosphere” was proposed by Watson-Watt in a letter to the United Kingdom Radio Research Board, but it did not appear in the literature until three years later (Watson-Watt, 1929). The names of the D, E, and F regions originated from Appleton, who assigned the letter “E” to the first reflected electric field he recognized. Later, when he identified a second layer at higher altitudes, he assigned it the letter “F” to maintain alphabetical order. Subsequently, he conjectured that there may be another layer at lower altitudes, which he named “D” (Silberstein, 1959).

The D- and lower E-region ionosphere is known to be maintained by several ionization sources, even during nighttime when solar radiation is not present (e.g., Nagata and Tohmatsu, 1973). After sunset, electron density in the ionosphere abruptly decreases. However, this decrease stops at a certain level, and weak ionization is maintained throughout the night. Figure 1.5 shows the nighttime ionization production rate for each ionization source (Nagata and Tohmatsu, 1973; Tohmatsu, 1990). There are five main nighttime ionization sources in the D-region and lower E-region ionosphere below 100-km height:

(1) Magnetospheric particles (ionization rate: 10^{-1} – 1 $cm^{-3}\cdot s^{-1}$)

(2) Geocoronal hydrogen Lyman (HLy)-α(1216 $\mathring{A}$) and HLy-β(1027 $\mathring{A}$) (10^{-3} – 1 $cm^{-3}\cdot s^{-1}$)

(3) Primary cosmic rays (10^{-3} – 10^{-1} $cm^{-3}\cdot s^{-1}$)

(4) Scorpius X-1 (10^{-3} –10^{-2} cm^{-3} · s^{-1})

(5) Galactic X-rays (10^{-3} cm^{-3} · s^{-1}).

For source (1) above, the ionization production rate due to the magnetospheric particles is considered to largely depend on the geomagnetic latitude and magnetic activities. The main ionization source in nighttime is the geocoronal emission (2), which constitutes about 1% of daylight production. The HLy-α (1216 Å) and -β (1027 Å) of the geocorona photoionize NO and O_2, respectively (Tohmatsu, 1990). For source (3), in general, the two primary types of cosmic rays are galactic cosmic rays (GCRs) and solar cosmic rays (SCRs). GCRs are the dominant source in nighttime because SCRs cannot reach the night side of the Earth. GCRs are known to have anti-correlation with solar activities (Heaps, 1978). The difference in the ionization production rate due to GCRs between solar maximum and solar minimum is not as significant as seen in Figure 1.5. Nagata and Tohmatsu (1973) reported that when X-ray bursts occurred in (4) and (5), considerable increase in D-region electron density was observed by low-frequency (LF) waves.

According to Nagata and Tohmatsu (1973), the nighttime photoionization rate q by geocoronal emission for NO^+ is ~2.0×10^{-1} $cm^{-3}s^{-1}$ at 95 km, with a peak of ~1 $cm^{-3}s^{-1}$ at 105 km. For O_2^+, q is ~10^{-1} $cm^{-3}s^{-1}$ at 95 km, with a peak of ~10 $cm^{-3}s^{-1}$ at 105 km. The recombination rates α_{eff} for $NO^+ + e^-$ and $O_2^+ + e^-$ at 176 K [the nighttime neutral temperature at 95 km by the Mass Spectrometer Incoherent Scatter 90 (MSIS90) model] are ~5.1×10^{-7} cm^3s^{-1} and ~2.8×10^{-7} cm^3s^{-1}, respectively (Sheehan and St. Maurice, 2004). Thus, the electron density from this photoionization of NO^+ and O_2^+ at 95 km is given as (Brekke, 1997; Thomson et al., 2007)

$$n_e = \sqrt{\frac{q}{(1+\lambda_n)\alpha_{eff}}}, \qquad (1\text{-}1)$$

where $\lambda_n (=n^-/n_e)$ is the ratio of negative ions. The value of λ_n can be assumed to be ~3.0

$\times 10^{-1}$ at 95 km at night (Brekke, 1997). Equation (1-1) is on the condition of $dn_e/dt = 0$, which means that the photoionization rate is equal to the loss rate (Brekke, 1997). Based on Equation (1-1), the nighttime electron densities at 95 km for NO^+ and O_2^+ are calculated to be 5.5×10^2 cm^{-3} and 5.2×10^2 cm^{-3}, respectively. Using the International Reference Ionosphere 2007 (IRI-2007) model, the nighttime electron density at 95 km is 1.6×10^3 cm^{-3}. Accordingly, about 67% of total electron density at 95 km at night is produced by HLy-α and -β of the geocorona.

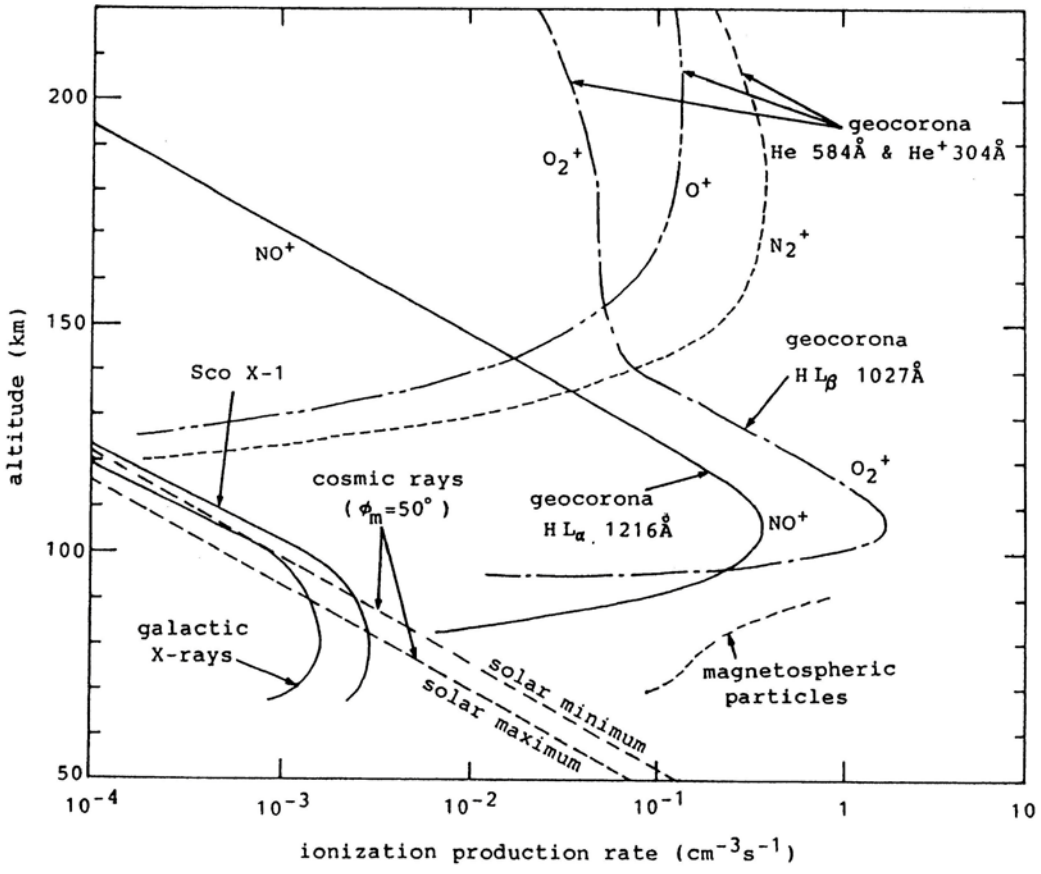

Figure 1.5. Nighttime ionization sources (Tohmatsu, 1990).

1.3. Techniques for Measuring Electron Density in the D- and Lower E-region Ionosphere

This section describes measurement techniques for electron density in the D- and lower E-region ionosphere. The following methods are available: LF (below 1 MHz) ionosonde, medium-frequency (MF) radar, incoherent-scatter radar (ISR), riometer, wave interaction or cross-modulation method, VLF and LF sounding techniques, and rocket measurements.

1.3.1 Low-frequency Ionosonde

Currently, Japanese ionosondes use the frequency range from ~1 to 30 MHz, as mandated by radio-regulation law. In the 1950s, however, lower frequency (50–2000 kHz) was used by an ionosonde near Boulder, Colorado, USA (Blair et al., 1953; Wakai, 1971). In principle, an ionosonde works as follows. Radio waves are transmitted vertically from a loop antenna. The wave is impulsive, with a duration of about 10 μs and a repetition frequency of several tens of hertz. The receiving unit observes the wave echo reflected from the ionosphere. The set of transmitting and receiving devices is called the “ionosonde.”

Given that the transmitted pulse propagates at the group velocity, v_g ($= c\sqrt{1- f_N^2 / f^2}$), in the ionosphere, the virtual height *h’* is defined as

$$h' \equiv \frac{1}{2}ct = \int_0^h \frac{cdz}{v_g} = \int_0^h \frac{1}{\sqrt{1-\frac{f_N^2}{f^2}}}dz \quad , \qquad (1\text{-}2)$$

where *c* is the speed of light, *t* is the time lag between transmission and reception of the

wave, h is the true height of the reflection point, f_N is the plasma frequency (in Hz), and f is the wave frequency. As the frequency of the transmitted wave changes, the reflection point h and virtual height h' change. f_N is a function of the electron density n_e (in m^{-3}) as follows:

$$f_N = \sqrt{\frac{e^2 n_e}{4\pi^2 m_e \varepsilon_0}} = 8.98 \times 10^{-3} \sqrt{n_e} \quad \text{(1-3)}$$

where e = 1.60218 × 10^{-19} C for electron charge, m_e = 9.10938 × 10^{-31} kg for electron mass, and ε_0 = 8.854188 × 10^{-12} F/m for electric permittivity in a vacuum. h' is calculated from t and depends on the electron density distribution below h.

Using observations by the LF ionosonde (50–2000 kHz) at Boulder, Wakai (1971) showed that the nighttime f_oE in the sunspot minimum period was lower by about 0.3 MHz than that in the sunspot maximum period. The estimated f_oE corresponded to electron densities at heights between 105 and 120 km. Wakai further derived the following empirical expression of the peak electron density, N electrons/cm^3 at midnight, versus the smoothed relative sunspot number R_s for E-region virtual heights $h'E$ of less than 100 km:

$$N = 1.62 \times 10^3 \left(1 + 0.0098 R_s\right). \quad \text{(1-4).}$$

However, these results were obtained for solar cycle 19 and thus do not include recent solar cycles. Because of new legal restrictions on radio transmission, it will be difficult to use such low frequencies with ionosondes in the future.

1.3.2. Medium-frequency Radar

Radio waves at MF of about 2 MHz are known to be partially reflected by a steep vertical gradient of electron density in the D region. In MF radar measurements, the electron density in the D region is estimated from the amplitude ratio of the

extraordinary (A_x) to the ordinary (A_o) modes based on the differential absorption method (DAE) (Murayama et al., 2000). The ratio, A_x/A_o, is represented as follows:

$$\frac{A_x}{A_o} = \frac{R_x}{R_o} \exp\left[-2 \int_0^h (\kappa_x - \kappa_o) dz \right], \qquad (1\text{-}5)$$

where R_o and R_x are the reflection coefficients of the ordinary and extraordinary waves, and κ_o and κ_x are absorption coefficients of the ordinary and extraordinary waves, respectively (Gardner and Pawsey, 1953; Belrose and Burke, 1964). The electron density n_e is given from the height variation of the amplitude ratio A_x/A_o as

$$n_e = \frac{\ln\left(\frac{R_x}{R_o}\right)_2 - \ln\left(\frac{R_x}{R_o}\right)_1 - \left[\ln\left(\frac{A_x}{A_o}\right)_2 - \ln\left(\frac{A_x}{A_o}\right)_1 \right]}{\frac{2(\kappa_x - \kappa_o)(h_2 - h_1)}{n_e}}, \qquad (1\text{-}6)$$

where 1 and 2 denote parameters at two heights separated by, for example, about 2 km. The absorption at the two heights is assumed to be equal (Belrose and Burke, 1964; Murayama et al., 2000). In the denominator, $(\kappa_x - \kappa_o)/n_e$ is a function of the collision frequency ν between electrons and neutrals, as follows (Gardner and Pawsey, 1953; Sen and Wyller, 1960):

$$\frac{\kappa_x - \kappa_o}{n_e} = \frac{5}{4} \frac{e^2}{m_e \varepsilon_0 c \nu} \left[C_{\frac{5}{2}}\left(\frac{\omega - \omega_L}{\nu} \right) - C_{\frac{5}{2}}\left(\frac{\omega + \omega_L}{\nu} \right) \right]$$

$$C_p(x) \equiv \frac{1}{p!} \int_0^\infty \frac{\varepsilon^p \exp(-\varepsilon) d\varepsilon}{\varepsilon^2 + x^2} \qquad (1\text{-}7)$$

$$\varepsilon = \frac{m_e v^2}{2kT},$$

where ω is the angular frequency of the radio wave, $\omega_L = 2\pi f_H \cos\theta$, f_H is the electron gyro frequency, θ is the wave normal angle, v is the electron velocity, k is the Boltzmann constant, and T is the electron temperature. R_x/R_o is also a function of the collision frequency as follows:

$$\left|\frac{R_x}{R_o}\right| = \sqrt{\frac{\left\{\frac{\omega-\omega_L}{\nu}C_{\frac{3}{2}}\left(\frac{\omega-\omega_L}{\nu}\right)\right\}^2 + \left\{\frac{5}{2}C_{\frac{5}{2}}\left(\frac{\omega-\omega_L}{\nu}\right)\right\}^2}{\left\{\frac{\omega+\omega_L}{\nu}C_{\frac{3}{2}}\left(\frac{\omega+\omega_L}{\nu}\right)\right\}^2 + \left\{\frac{5}{2}C_{\frac{5}{2}}\left(\frac{\omega+\omega_L}{\nu}\right)\right\}^2}} \quad \text{(1-8)}.$$

The values of $(\kappa_x - \kappa_o)/n_e$ and $|R_x/R_o|$ should depend on the collision frequency. However, in the DAE method, it is assumed that the dependence does not affect the estimation of the electron density.

Using the MF radar, midnight electron density was estimated to be 100–1000 cm^{-3} at altitudes of 93–99 km (Holdsworth et al., 2002). However, estimations of electron density by the DAE method usually have large error because $(\kappa_x - \kappa_o)/n_e$ actually depends on the electron density (Kawamura et al., 2007). Improvement of this estimation is currently under discussion.

1.3.3. Incoherent-scatter Radar

If powerful radio waves from a ground radar antenna are transmitted to the ionosphere, waves backscattered by free electrons can be observed on the ground. The scattering of radio waves by free electrons is known as Thomson scattering. The electron density is estimated from the total power returned from the scattering region. Such incoherent-scatter observations have been made using very- to ultra-high-frequency waves (50–1000 MHz) for measurement of the electron density at altitudes of 60–700 km.

The electron density n_e can be estimated from the power flux density of the scattered waves P as follows:

$$n_e = \frac{4\pi h^2 P}{P_0 \sigma_0 V}, \quad \text{(1-9)}$$

where P_0 is the power flux density of the transmitted radio waves, σ_0 is the radar scattering cross section, and V is the scattering volume.

At present, numerous ISR facilities are operational including the Arecibo (Puerto Rico), EISCAT (Tromso and Svalbard, Norway), Irkutsk (Russia), Jicamarca (Peru), Kharkov (Ukraine), Millstone Hill (Massachusetts, USA), MU (Shigaraki, Japan), and Sondrestrom (Greenland) facilities. These ISRs are useful for ionospheric research. However, they need large transmitting/receiving facilities, and care must be taken to avoid interference with radio communications and broadcasts.

1.3.4. Riometer

A riometer (Relative Ionospheric Opacity METER) measures cosmic noise absorption. Radio waves from cosmic noise sources can be observed on the ground. The intensity of the noise is modulated by ionospheric absorption as well as by the celestial distribution of the sources. By monitoring this noise intensity, we can observe variation in the electron density in the D region. The ratio of the noise intensity on the ground to that above the ionosphere corresponds to the total absorption. In the ionosphere, total column absorption A (dB) of the radio waves with the angular frequency ω is represented as follows:

$$A = 20\log_{10}\left[\exp\left\{\int \chi \cdot dl\right\}\right] = 4.6\times10^{-5}\int \frac{n_e \nu_{en}}{\omega^2 + \nu_{en}^2} dl \quad , \qquad (1\text{-}10)$$

where $\chi(=K\omega/c)$ is the absorption of the radio waves (K is the imaginary part of the refraction index in the Appleton–Hartree formula), $\int dl$ is the integration along the path length, and ν_{en} is the collision frequency.

Riometers are usually operated in the frequency band of 20–60 MHz and are useful for observing D-region ionization due to auroral particles and solar protons in the polar

region. However, it is difficult to observe D-region density variation at low latitudes using a riometer because the variation amplitude at low latitudes is very small.

1.3.5. Wave Interaction or Cross-modulation Method

A radio wave causes the electron temperature in the D region to increase. If another radio wave propagates in the same region, that wave is modulated by the first wave. That is, variation in its attenuation rate will synchronize with the amplitude of the first radio wave. In this method, two artificial radio waves are used, and the electron density can be derived from the fact that the modulation is proportional to the attenuation rate, which corresponds to the electron density. This method is useful for the altitude range of 65–85 km (Tohmatsu, 1990).

1.3.6. Very-low-frequency and Low-frequency Sounding Techniques

Several studies have employed artificial VLF and LF radio wave propagation from transmitters at both steep and oblique incidences to the ionosphere together with the full-wave analysis method to derive electron-density profiles in the lower ionosphere (Deeks, 1966; Bain and May, 1967; Shellman, 1970; Bain and Harrison, 1972; Krasnushkin and Knyazeva, 1970; Sechrist, 1974). This method essentially uses an inversion technique to derive the electron-density profiles from measurements of reflection and conversion coefficients at several frequencies (Jones and Wand, 1970; Backus and Gilbert, 1970).

1.3.7. Rocket Measurements

Sounding rockets can directly measure the electron density in the D- and lower E-region ionosphere. Rocket measurement approaches can be divided into the differential Doppler method, probe technique, and Faraday rotation method.

1.3.7.1. Differential Doppler Method

When rockets receive radio waves transmitted from ground-based stations, the received frequency is shifted due to the Doppler effect. The Doppler shift Δf is represented as follows (Kimura et al., 1972):

$$\Delta f = -\frac{f}{c}\left(V_x \cos\beta \sin\rho_0 + V_z\sqrt{\mu^2 - \sin^2\rho_0}\right), \qquad (1\text{-}11)$$

where V_x and V_z are x- and z-direction components of rocket speed (orbital plane of the rocket: x–z plane, and z is vertically upward direction), β is an angle between the horizontally projected direction of the propagation vector and the positive x-direction, ρ_0 is the initial value of the incident angle of the radio waves from the transmitter, and μ is the refractive index described by the Appleton–Hartree formula. The value of μ is calculated from Equation (1-11). Snell's law then leads to

$$\mu \sin\rho = \sin\rho_0, \qquad (1\text{-}12)$$

where ρ is the angle between the propagation vector and the positive z-direction, and ρ is calculated from Equation (1-12) using μ obtained from Equation (1-11). The wave normal angle θ, which is the angle between the propagation vector and the external magnetic field vector, is represented as

$$\cos\theta = \sin\rho\cos\delta\sin\phi + \cos\rho\cos\phi, \qquad (1\text{-}13)$$

where δ is the angle between the horizontal component of the propagation vector and

the magnetic meridian plane, and φ is the angle between the external magnetic field vector and the z-axis. If θ is calculated from Equation (1-13), the electron plasma frequency is calculated from μ and θ based on the Appleton–Hartree formula, and the electron density can be calculated from Equation (1-3).

1.3.7.2. Probe Techniques

If we insert a probe into plasma and supply a direct voltage that varies from negative to positive, the relationship between the applied voltage and the current flowing through the probe can be described for three current regions: the ion current region, exponential region, and electron current region (Tohmatsu, 1990), as follows:

(1) ion current region

$$i = en_e S \frac{1}{\sqrt{\exp(1)}} \sqrt{\frac{kT}{m_i}} \qquad (1\text{-}14)$$

(2) exponential region

$$i = en_e S \sqrt{\frac{kT}{2\pi m_e}} \exp\left(\frac{eV_p}{kT}\right) \qquad (1\text{-}15)$$

(3) electron current region

$$i = en_e S \sqrt{\frac{kT}{2\pi m_e}}, \qquad (1\text{-}16)$$

where i is the electric current from the probe, S is the effective surface area of the probe, m_i is the ion mass, and V_p is the voltage between the probe and the plasma. If we plot experimental values of $ln(i)$ as a function of V in region (2), we have a straight line for which the gradient is $e/(kT_e)$. Thus, T_e can be estimated from the gradient, and then n_e is calculated from T_e and the measured electric current using Equation (1-15).

1.3.7.3. Faraday Rotation Method

When a linearly polarized electromagnetic wave enters into a region with a finite magnetic field, it is split into ordinary and extraordinary waves, which are elliptically polarized, and the rotating direction of the polarization vectors are opposite to each other. If the propagation direction is nearly parallel to the magnetic field line, the rotation rate of the polarization vector is given by (Tohmatsu, 1990)

$$\frac{d\psi}{ds} = \frac{\omega}{2c}\left(\mu_o - \mu_x\right) \cong \frac{\omega}{2c}\frac{XY}{1-Y^2}$$
$$X = \left(\frac{\omega_N}{\omega}\right)^2 \qquad \text{(1-17)}$$
$$Y = \frac{\omega_H}{\omega} \quad ,$$

where $\omega_N = 2\pi f_N$ (Equation 1-3), and ω_H is the electron gyro frequency. The electron density is calculated from the plasma frequency f_N based on the Appleton–Hartree formula. Smith and Gilchrist (1984) estimated the accuracy by the Faraday rotation method to be 100 cm^{-3} for variations in electron density.

The above direct measurements by sounding rockets have provided the most accurate profiles of D- and E-region electron density. However, rockets are relatively expensive and have restricted launch times and locations. For example, in the sounding rocket flights summarized by Friedrich and Torkar (1998), nighttime flights made up only about 14% of the total number. Fifteen times more flights were made when the sunspot number was lower than 50 than when it was above 150. Furthermore, twice as many flights were made at latitudes between 30º and 60º as between 0º and 30º. Thus, it is difficult to determine long-term variations in the D-region electron density from rocket measurements.

1.4. Electron Density in the D- and Lower E-region Ionosphere

This section reviews previous studies on electron density in the D- and lower E-region ionosphere considering solar-cycle variations and magnetic storms.

1.4.1. Solar-cycle Variations

Previous studies have found that the electron density in the D- and lower E-region ionosphere at solar maximum is slightly greater than that at solar minimum, as seen in Figure 1.4, in both daytime and nighttime. In daytime, the solar EUV fluxes at solar maximum are greater than those at solar minimum. These intense solar EUV fluxes lead to higher electron densities. The higher electron densities at solar maximum are considered to be a result of increased ionization production (Schunk and Nagy, 2000). This section describes previous studies of solar-cycle variations and nighttime electron density in the D- and lower E-region ionosphere. In earlier observations, a few ionosondes were designed specifically to extend to a frequency range below 1 MHz to investigate the nighttime lower E-region ionosphere (Wakai, 1971). The nighttime dependence of the ionogram parameter f_oE (critical frequency of the E region) on the sunspot number was found using the 'low-frequency sounder' with a frequency range of 50 kHz to 2 MHz (Blair et al., 1953; Wakai, 1971). The f_oE at night in the sunspot minimum period was lower by about 0.3 MHz than that in the sunspot maximum period. Lower (higher) f_oE means decreased (increased) electron density, which is consistent with the empirical expression of Equation (1-4) derived by Wakai (1971).

An empirical model of D- and lower E-region density based on rocket experiments showed that nighttime electron density at 100-km height for an average sunspot number

of R_z = 0 was about 2000 cm^{-3} (Friedrich and Torkar, 1998). Even when R_z = 180, nighttime electron density increased only by a few hundred cubic centimeters. The electron density at 90-km height was about 600 cm^{-3} when R_z = *0*, whereas it is over 1000 cm^{-3} for R_z = 180.

Using observation data by rocket measurements, ISRs, and lower frequency ionosonde and the International Reference Ionosphere 1995 (IRI-95) model, Titheridge (2003) calculated that the mid-latitude (40ºN) electron density at 105 km at midnight was about 2300 cm^{-3}. The difference in the electron density between the solar maximum and solar minimum was less than 100 cm^{-3}.

Kumar et al. (2008) examined 2428 tweeks observed at Suva Fiji in the South Pacific during a period of low solar activity and reported that the nighttime tweek reflection height range was 83–92 km. This range is higher by about 1.0–1.5 km than that found in a high solar activity period. The decrease in the tweek reflection height during periods of high solar activity corresponds to the increase in the electron density.

1.4.2. Density Variations during Magnetic Storms

Magnetic storms result from compression of the magnetosphere due to the arrival of discontinuity in the solar wind with the southward interplanetary magnetic field. During the main phase of magnetic storms, the magnetospheric electric fields, currents, and particle precipitation increase. A large amount of energy is deposited into the ionosphere–thermosphere system at high latitudes during a storm. In response to this energy input, electron densities increase in the auroral E region. At middle latitudes, the eastward electric field associated with penetration of the magnetospheric electric field moves F-region plasma to higher altitudes through **E**×**B** drift, which can result in the increase in F-region electron density. At high latitudes, auroral heating transports N_2 to

higher altitudes, causing a reduction in the O/N_2 ratio in the thermosphere. This leads to decreased electron densities in the F region through recombination. Equatorward neutral winds driven by high-latitude thermospheric heating carry this low-O/N_2 atmosphere to middle latitudes, causing the F-region density to decrease. In general, the enhancement and decrease of electron density at middle and low latitudes are referred to as positive and negative ionospheric storms, respectively.

Numerous studies of the high-latitude lower ionosphere during magnetic storms have been reported (e.g., Knuth and Lauter, 1964; Lauter and Knuth, 1967; Lauter and Nitzche, 1967; King and Fooks, 1968; Belrose and Thomas, 1968). The effects of magnetic storms on the high-latitude lower ionosphere are generally classified as the 'primary storm effect' and 'storm aftereffect.' The primary storm effect occurs during the main phase of magnetic storms and is characterized by the rapid and deep fading of artificial LF/VLF radio waves and by the phase advance that corresponds to the fall of the reflection height (Araki, 1974). The storm aftereffect indicates that the absorption of the radio waves increases several days after a storm and sometimes continues for 10 days or more. Although these effects in LF/VLF radio waves are seen only in nighttime, similar effects are observed by HF/MF absorption measurements in daytime. Thus, ionospheric changes during magnetic storms reach the level of the reflection height of HF/MF radio waves in daytime and of LF/VLF radio waves in nighttime.

In contrast to studies of high latitudes, relatively few studies of the lower ionosphere at middle and low latitudes have been reported. In early studies, Jacobs and Watanabe (1963) predicted that westward electric fields associated with the sudden commencement of a magnetic storm could cause the downward movement of charged particles in the ionosphere. Belrose and Thomas (1968) reported that the phase of artificial VLF radio waves from transmitters (short path) rapidly fluctuated during a magnetic storm and showed an anomalous diurnal variation during the several days

after the storm recovery phase. The amplitude of artificial LF radio waves from transmitters showed rapid fluctuations during a magnetic storm and severe attenuation after the recovery phase. Araki (1974) reported that the phase of trans-equatorial VLF signals from a transmitter changed anomalously during the nighttime main phase of two large magnetic storms. Kikuchi and Evans (1989) reported unusual enhancements of energetic electron fluxes over Japan at L = 1.3 during a large magnetic storm based on NOAA-6 satellite data.

Peter et al. (2006) reported an approximately 5-dB depression in VLF amplitudes from transmitters located in the USA (L = 2–3) during a magnetic storm, with a depression onset occurring later for VLF/LF paths at lower latitudes. They also reported that during two magnetic storms, amplitude fluctuations in the VLF radio waves occurred in the pre-midnight sector and continued until dawn. On the same days, increases were observed in the energetic electron flux in the loss cone by NOAA Polar Orbiting Environmental Satellites. Peter et al. (2006) suggested that both signal depressions and subsequent fluctuations were associated with variations in the precipitation flux of energetic electrons into the upper atmosphere. The fluctuations and signal depression occur when the equatorward edge of the aurora oval extends over the perturbed VLF/LF wave paths. Quantitative modeling of lower ionospheric VLF wave propagation incorporating energetic electron-flux measurements yielded results consistent with the variations in the observed VLF amplitudes. These results suggested that this variability is largely due to magnetic storm-associated increases in the energetic electron population in the slot region.

Peter and Inan (2004) reported that the occurrence rates of lightning-induced electron precipitation (LEP) events depend on geomagnetic activities. LEP events are produced by the fraction of the VLF energy radiated by lightning discharges that escapes into the magnetosphere and propagates as a whistler-mode wave. The

whistler-mode wave interacts with trapped radiation belt electrons through cyclotron-resonant pitch-angle scattering, causing some of the electrons close to the loss cone to precipitate and produce secondary ionization. The precipitating energetic electrons (~50 to 500 keV) cause secondary ionization and alter the conductivity of the D-region ionosphere. It was suggested that LEP events correlate with the energetic electron-flux levels in the radiation belts ($2 < L < 3$). However, the degree of correlation between geomagnetic activities and the loss of electrons by the LEP have not yet been quantified.

1.5. Purpose of this Thesis

The D- and lower E-region ionosphere has been studied by lower frequency ionosondes, rockets, and VLF radio waves for over 60 years, as described in sections 1.3 and 1.4. However, the nighttime lower ionosphere at low latitudes still remains a relatively blank region of study because there are few effective tools for observing these regions, where electron densities are very low (less than 10^3 cm^{-3}). In the D and lower E regions, strong coupling between plasma and the neutral atmosphere makes measurements difficult. Strong absorption causes the difficulties of the measurements. The lack of observation tools has resulted in a shortage of observation data and modeling.

This thesis presents three results obtained by analyzing tweek atmospherics: 1) the development of an automatic procedure to estimate the reflection height and propagation distance of tweek atmospherics; 2) evidence of long-term variation in the tweek reflection height; and 3) data on variation in the tweek reflection height during magnetic storms. Tweek atmospherics offer an effective tool for deriving long-term variations in the D- and lower E-region ionosphere. Passive measurements of tweeks are

much easier and cheaper than measurements by rockets or ISRs and can be used to observe the ionosphere even over sea. Chapter 2 describes observations of tweek atmospherics and the method of analysis. Long-term variations in the tweek reflection height are given in Chapter 3. Chapter 4 describes variations in the tweek reflection height during magnetic storms. Chapter 5 summarizes the results of this thesis, and an outline of the new Asia VLF Network System (AVON) is described in Chapter 6.

Chapter 2. Observations of Tweek Atmospherics and Method of Analysis

By fitting theoretical spectra to the observed tweek atmospherics, it is possible to obtain information about the D- and lower E-region ionosphere along the tweek propagation paths. The source location of the tweeks was not estimated in this thesis because of limited observations for one magnetic component. However, 78% of lightning occurs at low latitudes between 30°N and 30°S (Christian et al., 2003). Thus, we can assume that lightning was the source of the tweeks observed at Kagoshima in the lower latitudes of southern Japan. Measurement of the lower ionosphere using tweeks provides an average view of the lower ionospheric height variation for a wide horizontal area along the waveguide propagation paths of the tweeks. In the propagation model, it is assumed that the Earth and the ionosphere are spherical because the propagation distance of tweeks is over several thousand kilometers.

In Section 2.1, observation data of tweeks are described. A spherical Earth–ionosphere waveguide model is given in Section 2.2. Equivalent electron density at the tweek reflection height is presented in Section 2.3. An automatic procedure to estimate the tweek reflection height and the propagation distance is described in Section 2.4. The automatic procedure was developed to allow for statistical analysis of the D- and lower E-region ionosphere using long-term tweek measurements.

2.1. Observation Data of Tweek Atmospherics

The measurements of tweek atmospherics presented in this thesis were obtained at Kagoshima Observatory (31.48ºN, 130.72ºE) operated by Nagoya University, Japan. The observatory has been conducting tweek measurements since 1976. The receiving antennas of this system are two orthogonal loops, but only one magnetic component was used in this thesis. Output signals were analogically recorded on magnetic tapes for 2 minutes of every hour (at 50–52 minutes of the hour) from April 1976 to December 2005. The analog signals were digitized using a 16-bit A/D converter with a 20-kHz sampling frequency. Since January 2006, the signal has been digitally recorded on hard disks at a 20-kHz sampling frequency.

Because the tweek reflection height can be determined by the cut-off frequency of the tweek atmospherics rather than their intensity, degradation of the receiver sensitivity does not affect the accuracy of the measurement. In the magnetic tapes, standard oscillator signals with a frequency of 760 Hz were recorded every 1 s. We carefully calibrated the tape extension based on the oscillator signals and corrected the frequency for all tapes. The most extended tape was 1.025 times longer than a normal tape. Tape extension did not occur in tapes after 1997.

The typical waveform and dynamic spectrum of a tweek are shown in Figure 2.1. The tweek was observed at Kagoshima Observatory at 19:50:09 LT on 20 August 1978. The frequency clearly falls from 10 kHz to about 2 kHz in several tens of milliseconds. The first-order mode has characteristic frequency–time dispersion. This first-order mode cut-off frequency of tweeks corresponds to the tweek reflection heights (equivalent electron densities) in the D- and lower E-region ionosphere, where the electron density becomes 20–28 cm^{-3} (Shvets and Hayakawa, 1998).

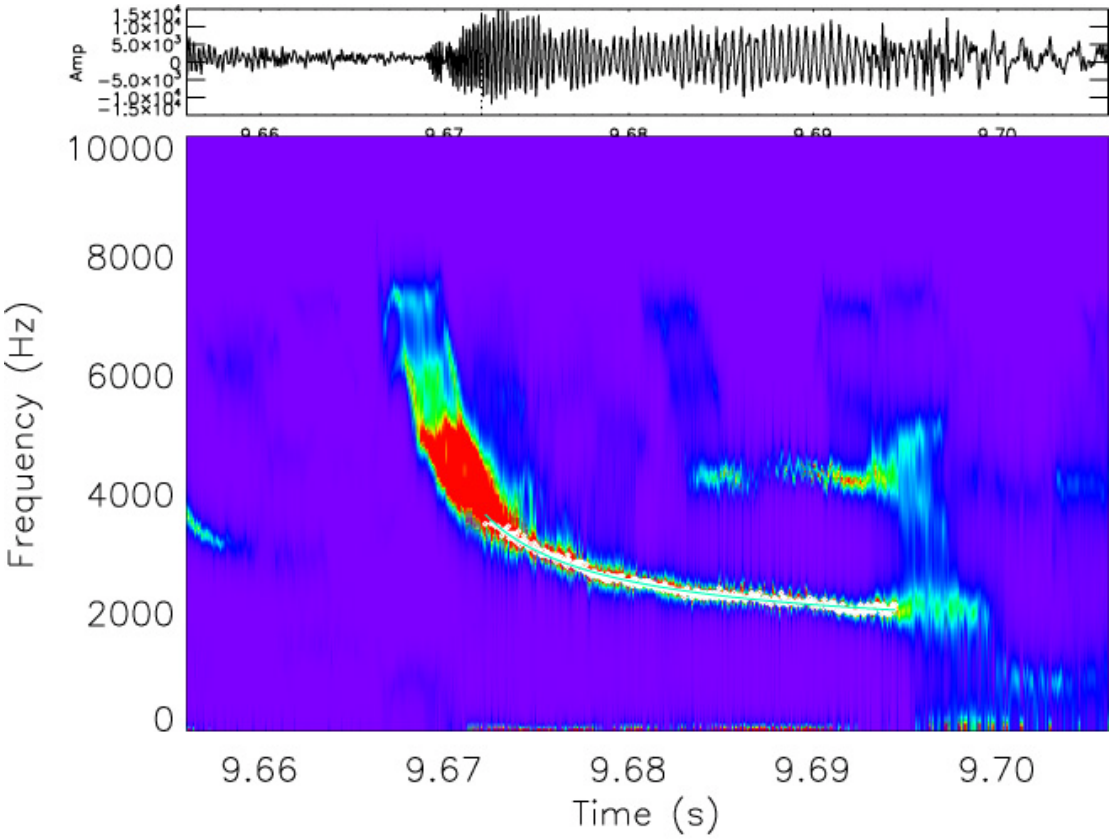

Figure 2.1. Dynamic spectrum of typical tweek atmospherics observed at Kagoshima Observatory at 19:50:09 LT on 20 August 1978.

2.2. Spherical Earth–Ionosphere Waveguide Model

In this thesis, the estimation of the tweek parameters was based on a homogeneous spherical Earth–ionosphere waveguide model (Davies, 1969). The horizontal phase velocity v_p in the homogeneous spherical Earth–ionosphere waveguide is approximated by

$$v_p \approx \frac{c\left(1-\frac{h}{a}\right)}{\sqrt{1-\left(\frac{n\lambda}{2h}\right)^2}}, \qquad (2\text{-}1)$$

where c is the speed of light, h is the height of the waveguide, a is the Earth's radius, λ

is the wavelength in free space, and n is the order of the mode. The denominator of Equation (2-1) indicates the real part of sine of the incident angle used to calculate the horizontal group velocity. The height of the waveguide h is given as

$$h = \frac{nc}{2 f_c}, \quad \text{(2-2)}$$

where f_c is the cut-off frequency. We do not need to take the number of reflections into account, although multiple reflections in the waveguide are geometrically described by image sources placed along the vertical axis at the points 0, ±2h, ±4h, …, assuming a vertical dipole for lightning discharge on the ground (Wait, 1970). Here, we estimate the cut-off frequency for the first-order mode. The cut-off frequency (or cut-off wavelength) is determined by the height of the waveguide. The horizontal group velocity v_g for the first-order mode is obtained from Equations (2-1) and (2-2) for n = 1 as follows:

$$\begin{aligned} v_g &\approx \frac{c^2}{v_p} \\ &= \frac{c\sqrt{1-\left(\frac{f_c}{f}\right)^2}}{1-\frac{c}{2af_c}}, \end{aligned} \quad \text{(2-3)}$$

where f is the frequency of the waves. The propagation time T_g for the first-order mode is obtained as

$$\begin{aligned} T_g &= \frac{d}{v_g} \\ &= \frac{d\left(1-\frac{c}{2af_c}\right)}{c\sqrt{1-\left(\frac{f_c}{f}\right)^2}}, \end{aligned} \quad \text{(2-4)}$$

where d is the horizontal propagation distance of tweeks. Consequently, the frequency–time dispersion relation of tweeks is rewritten as follows:

$$f = \frac{T_g f_c}{\left(1 - \frac{c}{2af_c}\right)\sqrt{T_g^2 - \left(\frac{d}{c}\right)^2}} \qquad \text{(2-5)}.$$

In Equation (2-5), unknown parameters are f_c, d, and T_g. Here, T_g is the time delay from the lightning to the observation point for each frequency. For easier calculation of these unknown parameters, we assumed that the unknown parameter T_g is given with the time from lightning occurrence to the first point t_0, where t_0 is the first time the tweek is identified on the dynamic spectrum. Then, we can replace T_g with t_0, $t_1 = t_0$ + time step, $t_2 = t_0$ + time step x 2, …, and $t_n = t_0$ + time step x N. Then, using the gradient-expansion algorithm, we can fit Equation (2-5) to the dataset of (t_i, f_i) for $i = 0, 1, 2, ..., N$, which was determined from the dynamic spectrum.

2.3. Tweek Reflection Height

The tweek reflection height is determined by the electron density, gradient of electron density in the ionosphere, and incident angle of the tweeks to the ionosphere. The tweeks are reflected at the bottom side of the D and lower E layer, where the vertical gradient of electron density is very steep. Thus, the tweek reflection height estimated from the cut-off frequency would not differ much from the reflection height due to the density gradient. As the tweek frequency gets closer to the cut-off frequency, the incident angle becomes zero, showing vertical incidence (Baba et al., 1991). Thus, this section presents the analytical expression of the equivalent electron density at the tweek reflection height from the tweek cut-off frequency, considering the vertical incidence.

The refractive index of wave propagation with an angular frequency ω and wave normal angle θ in magnetoactive plasma is expressed by the Appleton–Hartree formula (see for example, Budden, 1961):

$$\mu^2 = \frac{2X(1-X-jZ)}{2(1-jZ)(1-X-jZ)-Y_T^2 \pm \sqrt{4Y_L^2(1-X-jZ)^2+Y_T^4}}, \qquad (2\text{-}6)$$

where

$$X = \left(\frac{\omega_N}{\omega}\right)^2$$
$$Y = \frac{\omega_H}{\omega}$$
$$Z = \frac{\nu}{\omega} \quad , \qquad (2\text{-}7).$$
$$Y_L = Y\cos\theta$$
$$Y_T = Y\sin\theta$$

and ω_N and ν are the angular plasma frequency and collision frequency between electrons and neutrals, respectively.

The angular electron gyro-frequency ω_H is given as follows:

$$\omega_H = \frac{e\mu_0 H}{m_e}, \qquad (2\text{-}8)$$

where μ_0 (=4π × 10^{-7} H/m) is permeability in a vacuum, and H is the geomagnetic field strength. With regard to the "±" sign in the denominator of Equation (2-6), the "+" sign corresponds to ordinary-mode (O-mode) waves, and the "-" sign corresponds to extraordinary-mode (X-mode) waves.

Using quasi-longitudinal approximation, Yedemsky et al. (1992) and Hayakawa et al. (1994) demonstrated the possibility of full reflection for extraordinary waves in the lower ionosphere. O-mode waves can propagate into the ionosphere. In contrast, as the square of the refractive index (μ^2) for X-mode waves decreases with an increase in electron density (with altitude), X-mode waves undergo full reflection at the altitude at which the refraction index μ becomes zero. Thus, X-mode waves cannot propagate into the ionosphere. However, quasi-longitudinal approximation is not needed for this study because the full reflection condition can be derived directly from the Appleton–Hartree

equation (Shevts and Hayakawa, 1998).

According to equation (2-6), the X value where μ^2 becomes zero is given by the following equation, which shows wave cut-off irrespective of the propagation direction:

$$X = 1 \qquad (2\text{-}9)$$

$$X = 1 \pm Y\,. \qquad (2\text{-}10)$$

Equations (2-9) and (2-10) represent O-mode and X-mode waves, respectively. The X-mode waves correspond to $X = 1 + Y$ when $Y > 1$ ($\omega_H > \omega$) and $X = 1 - Y$ when $Y < 1$ ($\omega_H < \omega$). Therefore, only $X = 1 + Y$ is used for the ELF/VLF waves considered in this thesis.

The electron density n_e cm^{-3} at the tweek reflection height is derived from $X = 1 + Y$ as follows:

$$n_e = 1.241 \times 10^{-8} f_c \left(f_c + f_H \right), \qquad (2\text{-}11)$$

where f_c *is* the cut-off frequency of the tweeks for the first-order mode, and f_H is the electron gyrofrequency. As the tweeks examined here were mainly from lightning discharges in the low-latitude and equatorial region, we take f_H = 1.1 +/- 0.2 MHz according to the International Geomagnetic Reference Field (IGRF) model. The first-order mode cut-off frequency of tweeks usually ranges from 1.5 to 2.5 kHz. Then, $f_H \gg f_N$ is satisfied, and Equation (2-11) is rewritten as

$$n_e = 1.241 \times 10^{-8} f_c f_H\,. \qquad (2\text{-}12)$$

Thus, electron densities are estimated as n_e = 27 +/- 5 cm^{-3} if we take f_c = 2.0 kHz and f_H = 1.1 MHz. The equivalent electron densities can be estimated by the tweek method despite the long propagation paths.

2.4. Automatic Procedure to Estimate Tweek Parameters

An automatic procedure was developed to estimate reflection height, propagation distance, and propagation time of tweek atmospherics. This section presents the automatic procedure and compares it with a manual method using both artificial and observed tweek signals. Initially, after the automatic procedure was completed, we used the fast Fourier transform (FFT) to create the dynamic spectra. Later, however, we changed to the maximum entropy method (MEM) to improve estimation accuracy. The FFT results are given in sections 2.3.1 to 2.3.3. Section 2.3.4 compares the accuracies of the FFT and MEM estimations.

2.4.1. Automatic Method

The automatic procedure searches the frequency f_i of the maximum power of the spectrum at every sampling time t_i (50 μs) for time intervals from 30 ms before to 70 ms after the time triggered by shifting the window by one sampling time t_i on the dynamic spectrum. The duration of tweeks is typically ~50 ms. Considering that the longest tweeks last ~100 ms, we empirically set the time intervals of 100 ms to have sufficient fitting precision and to exclude the next (non-target) tweeks. The first time interval of 30 ms is needed to obtain the higher frequency part of the tweeks. The last time interval of 70 ms is long enough to obtain data points of the tweek tail. Then, to remove background noise emissions and other tweeks embedded on the target tweek, the procedure selects the dataset (t_i, f_i) for one tweek automatically by checking the frequency difference between two successive times, t_i and t_{i+1}. Here, the procedure picks the point of maximum intensity from the data points with intensities of more than -11

dB for each time. If two or more tweeks with comparable intensities overlap, the procedure cannot clearly distinguish them and fails to determine the parameters. Such cases can be removed because the fitting error (expressed as chi-squared below) becomes very large, and the estimated parameter *d* becomes unrealistic (either less than 1,000 km or more than 10,000 km).

For the least-square fitting, we adopted the fitting results when the mean difference between the data point f_i and the fitted curve was less than 50 Hz, which is comparable to the FFT frequency resolution (40 Hz). Fitting results with large differences should thus be ruled out.

The automated procedure first selects intense tweeks having amplitudes that exceed 80% of the maximum amplitude. By this method, the tweek level should vary among the datasets. Intensity variations of VLF data over the long term cannot be discussed here because the variations depend not only on the conditions of the D and lower E region but also on the observational system itself. On the other hand, the reflection height variations of tweeks do not depend on the observational system and are useful for investigating long-term change over tens of years.

2.4.2. Evaluation of Method Using Artificial Tweeks

To evaluate the automatic procedure, we compared the automatic procedure with a manual method using waveforms of artificial tweeks. In the manual method, the frequency and time points of a tweek on the dynamic spectrum made by the FFT are visually inspected, and the tweek parameters are estimated by spectral fitting. We calculated the frequencies *f* of the artificial tweek using Equation (2-5) and produced the waveform $y(t) = \sin(2\pi ft)$. The amplitude and initial phase were assumed to be 1 and 0, respectively.

Figure 2.2 shows a frequency–time spectrum of an artificial tweek with f_c = 1700 Hz and d = 6000 km.

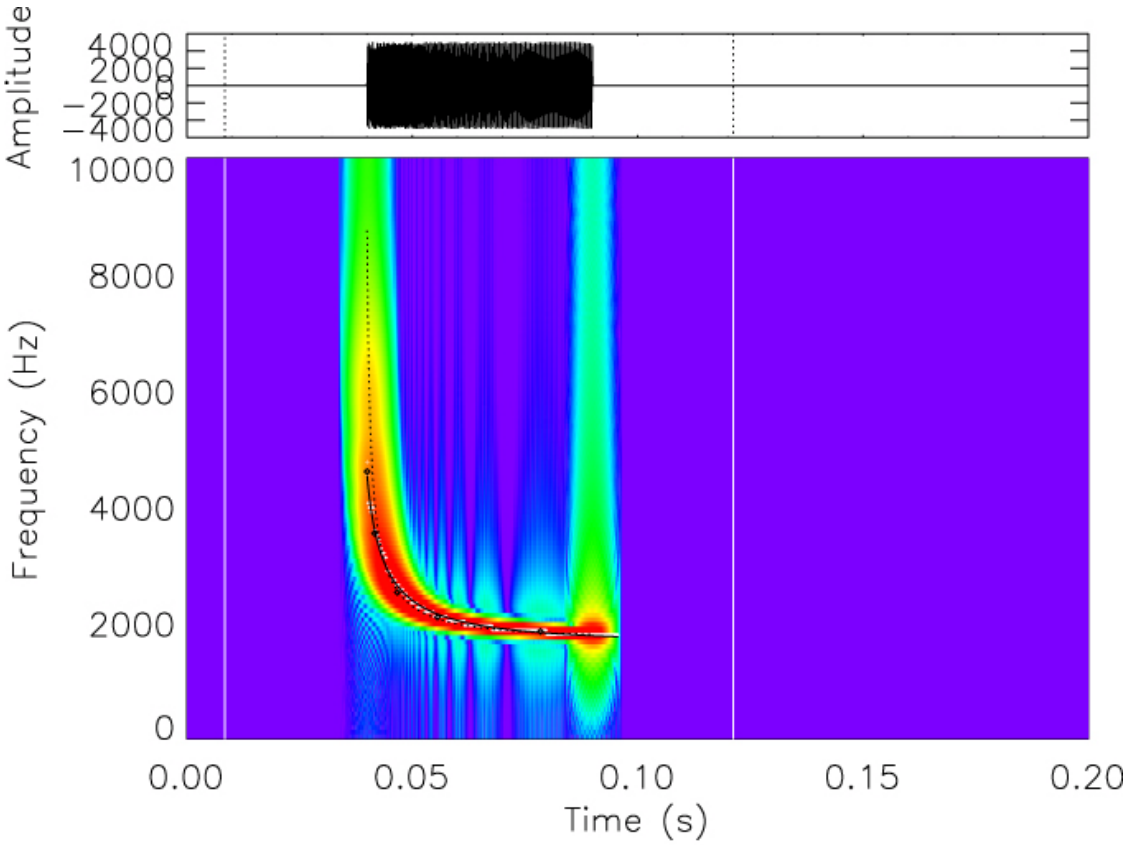

Figure 2.2. A dynamic spectrum of an artificial tweek with f_c = 1700 Hz and d = 6000 km. White points and black diamonds indicate the data points determined by the automatic procedure and by the manual method, respectively. The black solid curve and dotted curve are the fitting curves by the manual method and the input frequency–time curve, respectively.

White points and black diamonds indicate the data points determined by the automatic procedure and by the manual method, respectively. The solid and dotted curves are the fitting curves by the manual method and the input frequency–time curve, respectively. The estimation results were f_c = 1659.18 ± 0.13 Hz and d = 9408.16 ± 0.50 km for the manual method, and f_c = 1712.17 ± 0.07 Hz and d = 7125.96 ± 0.07 km for the

automated method, respectively. These results show that the automatic procedure can determine correct peaks of the tweek signals.

To investigate the fitting accuracy of the manual method, we generated nine artificial tweeks with parameter combinations of f_c = 1500, 2000, and 2500 Hz, and d=1000, 6000, and 10000 km. We estimated f_c and d for these artificial tweeks by the manual method and compared the fitting results with the original input values. The resulting average fitting error of f_c was +0.716%. The fitting error of d decreased as d became greater, i.e., the average errors were +35.494% for d = 1000 km, +18.766% for d = 6000 km, and +0.292% for d = 10000 km. This means that it is more difficult to estimate d using tweek signals with short duration of frequency–time dispersion.

Next, we checked whether the artificial tweeks could be detected by the automatic procedure according to our tweek-selection algorithm. All tweeks with non-overlapping time intervals of more than 50 ms before and after the tweek signals could be picked up by the automatic procedure (100 of 100 tweeks). Because of our tweek-selection criteria, the automatic procedure did not pick up tweeks that were overlapped by other tweeks during the interval less than 50 ms before and after the target tweek.

2.4.3. Evaluation of Method Using Observation Data

We compared tweek parameters estimated by the automated and manual methods with those estimated by the spherical model, using 77 tweeks recorded at Kagoshima at 17:50–17:52 UT (02:50–02:52 LT) on 1 November 2003. The automatic procedure picked up 266 tweeks. For 93 of those 266 tweeks, the typical dispersion relation could not be found by visual inspection by the manual method. For the remaining 173 tweeks,

96 had a large fitting error (>50 Hz). These large-error events were mainly caused by the overlapping of two or more tweeks on the dynamic spectrum, as will be discussed later. Thus, we used the other 77 tweeks for the comparison. For each tweek, we compared the automatic estimation results of h (f_c) and d with those from the manual method, in which an operator selects (t_i, f_i) based on visual inspection of the dynamic spectrum and calculates the parameters using Equation (2-5).

Figure 2.3 shows an example of a tweek with good spectral fitting by the automatic method (the mean difference between the data point f_i and the fitted theoretical curve is 9.9 Hz). The target tweek was observed at 23.58–23.59 s at frequencies of ~2 kHz. The white points and the light-blue line mark the peak frequencies of the tweek and the estimated frequency–time curve, respectively. For this case, the average and the fitting error of the automatically estimated h (f_c) were 98.53 ± 0.33 km (1521.3 ± 6.2 Hz), and those by the manual method were 93.76 ± 3.63 km (1598.7 ± 64.6 Hz). Thus, the manual method showed larger estimation error than the automatic method, possibly because of reading error in the manual method.

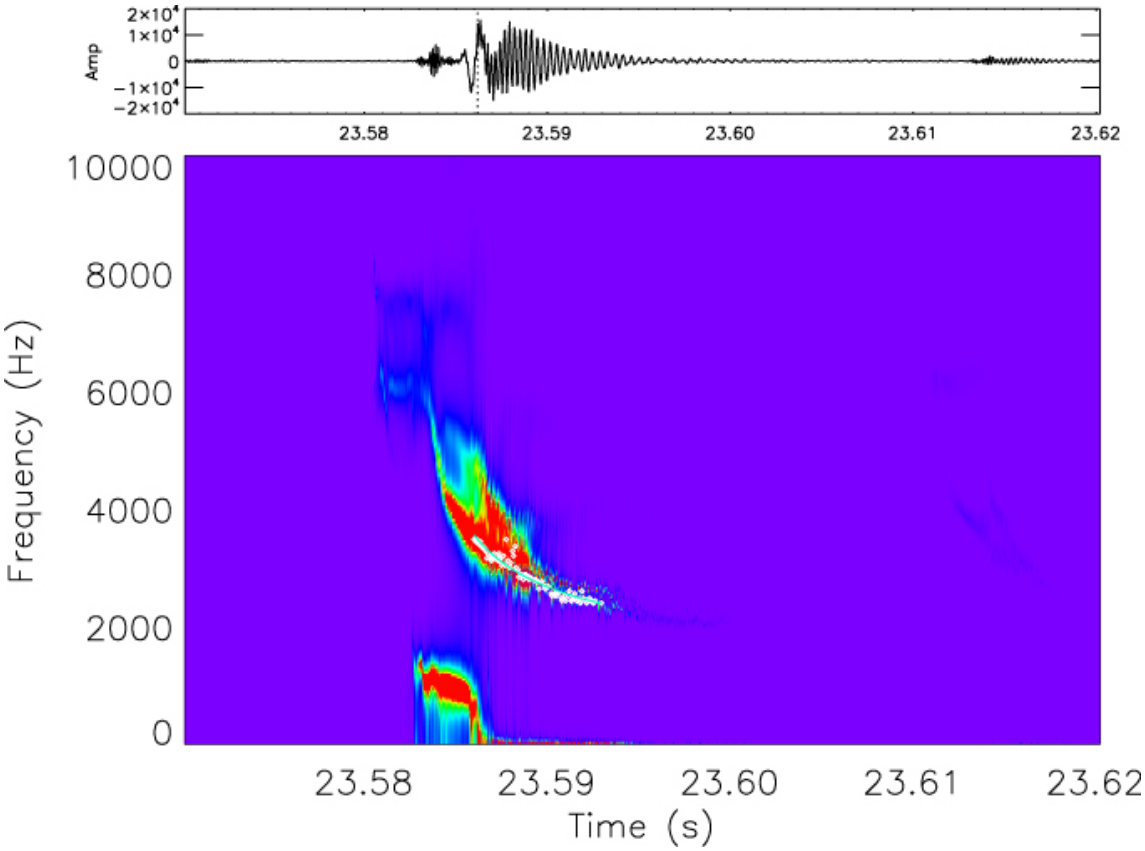

Figure 2.3. (Top) waveform and (bottom) dynamic spectrum of a clear tweek atmospheric observed at Kagoshima at 14:50:23.58–14:50:23.59 UT on 26 February 2010. White points and the light-blue curve indicate the spectral peaks and the theoretical curve determined by the automatic procedure, respectively.

Christian et al. (2003) estimated that 78% of lightning on Earth occurs at low latitudes between 30ºS and 30ºN, and Lynn and Crouchley (1967) reported that approximately four times more tweeks propagated from the east than from the west at Brisbane on the eastern coast of Australia. Interestingly, the rate of lightning occurrence was highest at the west coast of Australia (Christian et al., 2003). Such directionality has been explained by the smaller attenuation coefficient (by about 3 dB/1000 km) over sea than over land (Davies, 1969). Considering these previous findings, most tweeks observed at Kagoshima (31.48ºN) probably came from lower latitudes with propagation

over the sea.

As noted above, the main reason for erroneous fitting was the overlap of two or more tweeks on the dynamic spectrum or sequential tweeks with short separation. The automated procedure cannot separate overlapping tweeks and sequential multiple tweeks that occur within 50 ms. Figure 2.4 presents an example of a failed estimation, in which the fitting trace extends to the spectra of two tweeks.

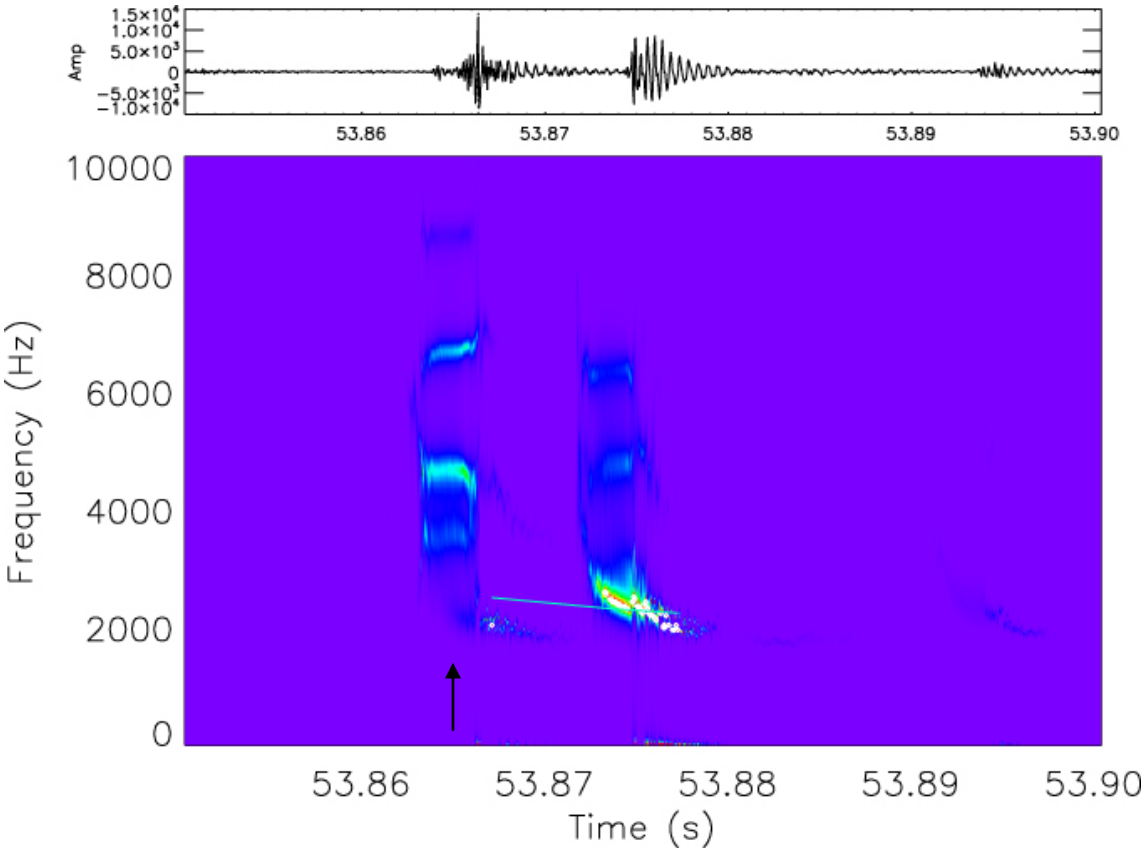

Figure 2.4. (Top) waveform and (bottom) dynamic spectrum of two sequential tweek atmospherics observed at Kagoshima at 14:50:53.86–14:50:53.88 UT on 26 February 2010. White points and the light-blue curve indicate the spectral peaks and the theoretical curve determined by the automatic procedure, respectively. The automatic procedure fails to distinguish the multiple tweeks.

In this case, the automatic procedure could not separate the target tweek (marked by

the black arrow) from the other subsequent tweeks, incorrectly recognizing them collectively as one tweek. Such errors caused by overlapping/sequential tweeks occurred in approximately 15% of the total cases. In the case of such errors, the difference between the data point f_i and the fitted theoretical curve becomes large (more than 120 Hz). Additionally, for 72% of these error cases, d was less than 1000 km, which is smaller than typical tweek d values. Thus, by checking the values of the difference between the data point f_i and the fitted theoretical curve and d, we may be able to eliminate errors caused by overlapping and multiple tweeks.

Figures 2.5 and 2.6 show a comparison of h and f_c, respectively, using the automated and manual methods.

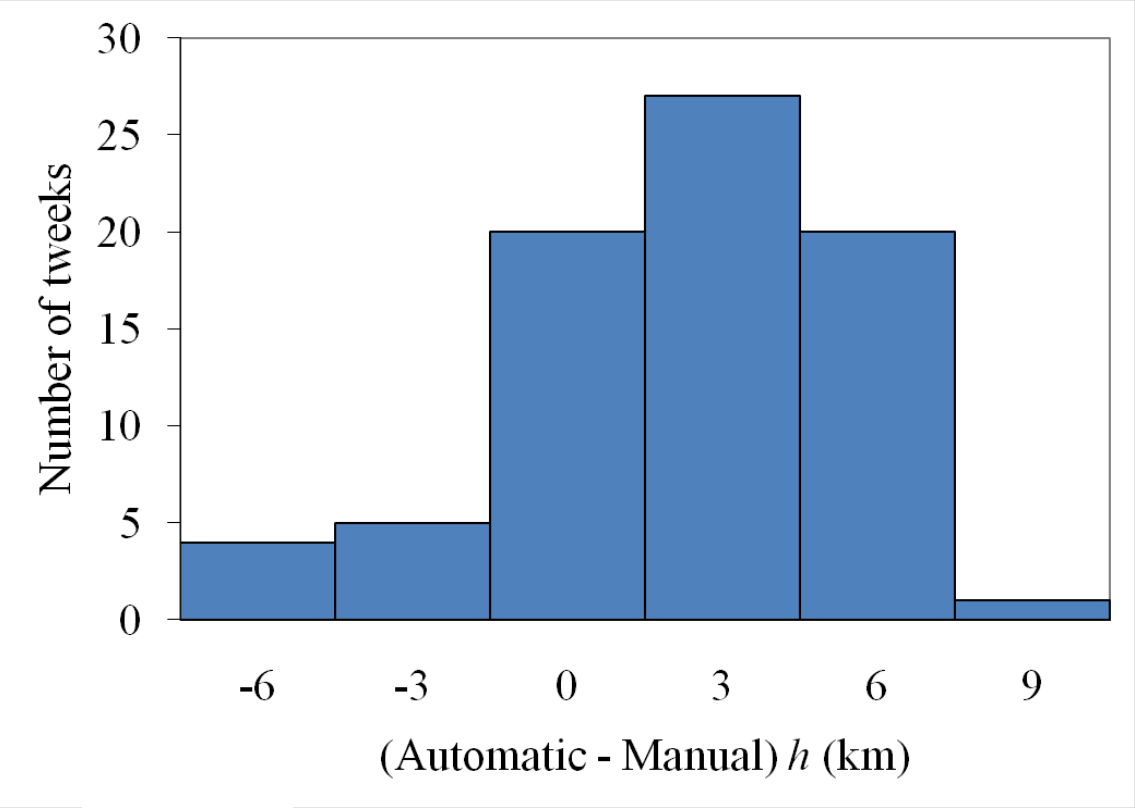

Figure 2.5. Differences δ (= automatic- manual) of the reflection height h. For the total tweeks, 61.0% fall in the range of -3 km < δ < 3 km.

We considered f_c (h) to be acceptable if the difference was less than ±50 Hz (±3.0 km at ~1600 Hz), considering the spectral resolution of the FFT (40 Hz). Acceptable values of h (-3 km < δ < 3 km, δ = automatic – manual) and f_c (-50 Hz < δ < 50 Hz) were obtained for 61.0% and 59.7% of the 77 cases, respectively.

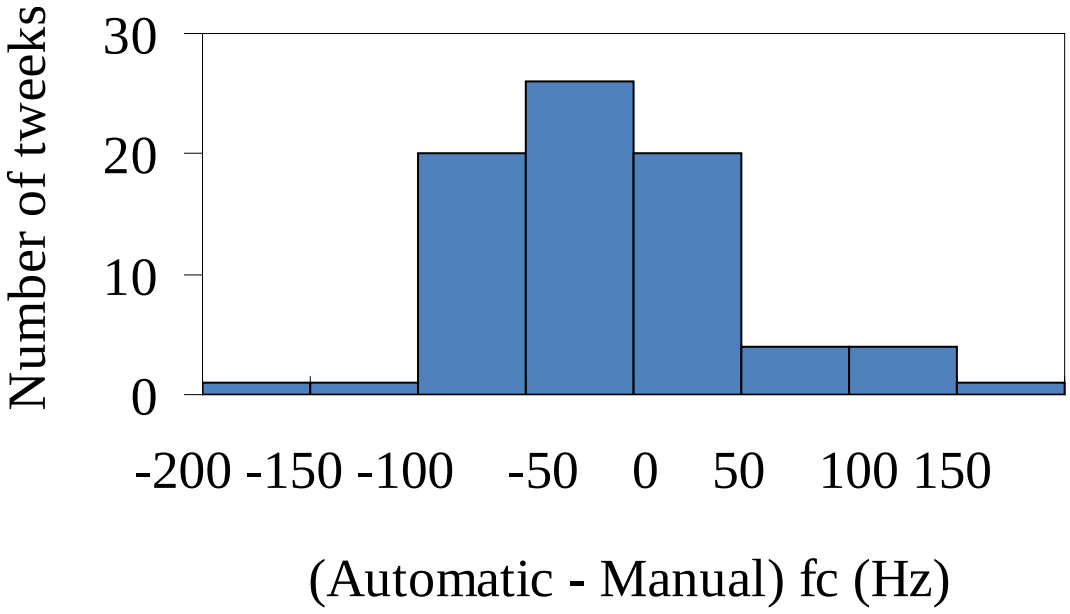

Figure 2.6. Differences δ (= automatic – manual) in the cut-off frequency for the first-order mode f_c. For the total tweeks, 59.7% are in the range of -50 Hz < δ < 50 Hz.

Comparing the results of the automated (for 194 tweeks, including 93 tweeks for which the manual method could not estimate parameters) and manual (for 77 tweeks) methods for the 2-minute averages, the averages and standard deviations of h and f_c by the automatic method (manual method) were 89.78 ± 3.60 km (89.20 ± 2.68 km) and 1672.2 ± 68.5 Hz (1682.1 ± 51.8 Hz), respectively. Thus, the differences (automatic – manual) between the mean h and f_c values are +0.58 km and -9.9 Hz, respectively. The difference for h (f_c) is less than the resolution of the FFT (40 Hz).

Figure 2.7 shows variations in tweek reflection heights obtained by the automatic procedure during an intense magnetic storm during 11–21 December 2006. The plotted data are averages and standard deviations for 2-minute intervals obtained for each hour during nighttime. The total number of tweeks during the plotted interval was 918. For such a large number of tweeks, the automatic procedure is effective in reducing the analysis time. The reflection heights abruptly rose in the initial phase (17:50–20:50 UT, 14 December) (from 91.90 to 106.72 km) and the recovery phase (9:50–12:50 UT, 15 December) (from 91.90 to 97.43 km) of the storm. These increases in reflection height occur in response to the characteristic Dst variations and may indicate temporal decrease in energetic electron fluxes in the inner radiation belt.

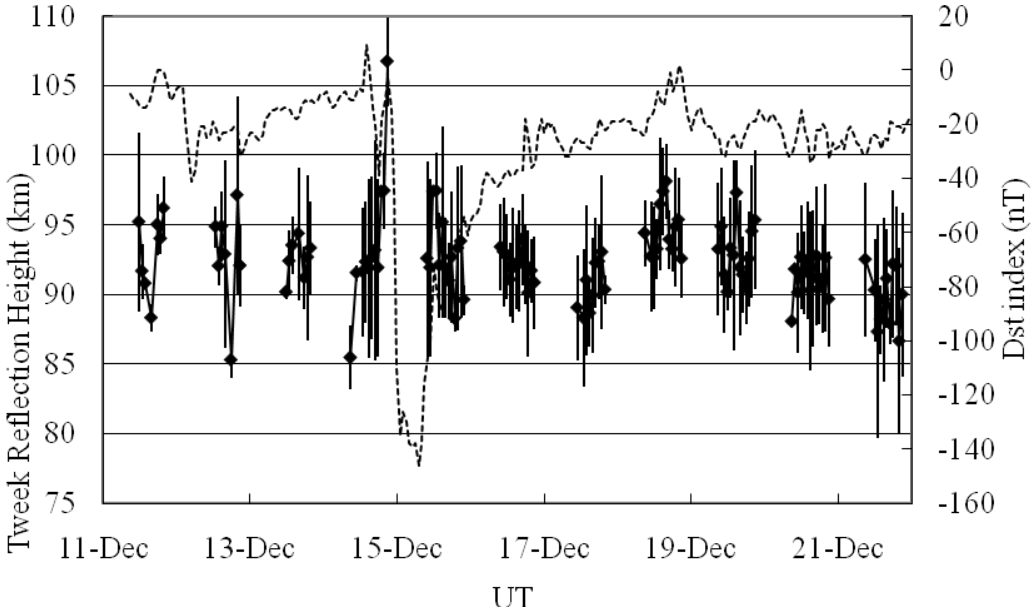

Figure 2.7. Reflection-height variations in tweeks estimated by the automatic procedure during a magnetic storm on 11–21 December 2006. The diamonds with error bars indicate 2-minute averages and standard deviations of the reflection height. The dotted line indicates the variations in the Dst index.

2.4.4. Comparison of the Fast Fourier Transform and Maximum Entropy Methods

We developed an automatic procedure to estimate the tweek parameters *h* and *d* for statistical analysis using the tweek spectra obtained by a conventional FFT. For more accurate estimation of the tweek reflection height, we compared tweek spectra obtained by the MEM and by the FFT. The MEM obtains a spectrum using an autoregression model with high resolution. Detailed explanation of the MEM is beyond the scope of this study (for details see, for example, Press et al., 1988). Figure 2.8 shows a comparison of a dynamic spectrum of an artificial tweek signal drawn by the MEM (a) and that drawn by the FFT (b).

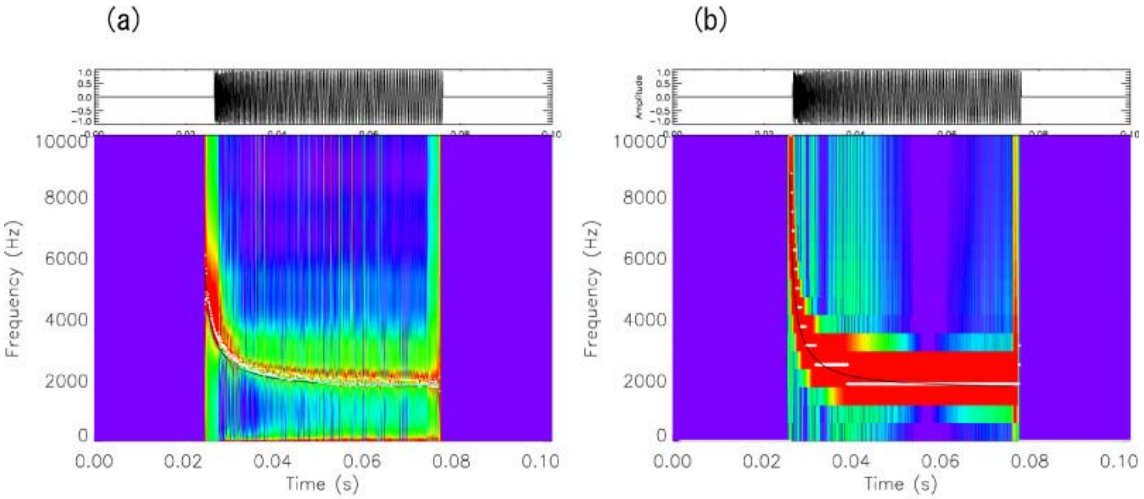

Figure 2.8. Comparison of the dynamic spectra of an artificial tweek signal with f_c = 1700 Hz and d = 6000 km calculated by the (a) MEM and (b) FFT.

To investigate the difference between the MEM and FFT, we used waveforms of an artificial tweek with f_c = 1700 Hz and d = 6000 km. We calculated the frequencies of the artificial tweek using Equation (2-5) and produced the waveform $y(t) = \sin(2\pi ft)$. The

amplitude and initial phase were assumed to be 1 and 0, respectively. White points indicate the regions of maximum intensity for each time calculated by the automatic method. The solid curves show the least-squares fit. The time step was 50 μs, and the window widths were 64 data points. The dynamic spectra were drawn by shifting the window by one time step. The results of the estimation were f_c = 1728.4 Hz (+1.7%) and d = 6320.6 km (+5.3%) for the MEM, and f_c = 1659.2 Hz (-2.4%) and d = 9408.2 km (+56.8%) for the FFT, respectively. This result indicates that the MEM could capture higher-frequency variations from about 10 kHz down to 2 kHz during several tens of milliseconds and recognize the tweek signal peak more accurately. In particular, a remarkable improvement can be seen for d, which is more sensitive to the frequency changes of the dispersion.

To compare the fitting accuracy of the MEM and FFT methods, we generated nine artificial tweeks with parameter combinations of f_c = 1500, 2000, and 2500 Hz, and d = 4000, 7000, and 10,000 km. We estimated f_c and d for these artificial tweeks by MEM and FFT and compared the fitting results with the input values. The average errors of h, f_c, and d were -2.07%, -0.51%, and -0.85% for the MEM, and -1.79%, +1.98%, and -12.35% for the FFT. The standard deviations of the h, f_c, and d errors were ±1.43%, ±4.22%, and ±9.47% for the MEM, and ±4.09%, ±4.44%, and ±43.68% for the FFT. Particularly, the fitting accuracy of d was significantly improved by the MEM. The MEM average error was slightly higher than the FFT error for h, although the FFT standard deviation was larger than that of the MEM. Based on these model calculations, we adopted the MEM instead of the FFT to estimate the tweek parameters.

Chapter 3.
Long-term Variations in Tweek Reflection Height

No systematic observations of long-term variation in the lower ionosphere below the height of 100 km have been reported. Absorption of any artificial radio frequency is large because of the high collision frequency below 100 km, making such measurements difficult. Conventional ionosondes cannot observe the region where the electron density is less than 1000 cm^{-3}. Although sounding-rocket experiments have been used to directly measure electron density profiles in the D-region and lower E-region ionosphere (e.g., Maeda, 1971), sounding rockets can only be launched at limited locations and times. Furthermore, while numerous rockets have been launched at latitudes between |35º| and |40º|, none has been launched between |15º| and |25º| (Friedrich and Torkar, 1998). Additionally, nighttime rocket flights account for only approximately 22% of all rocket launches, and only about 7% of rockets flights have taken place during a solar maximum phase (sunspot number $R_z > 150$). The electron density profile of the D region can also be estimated by MF radar (e.g., Holdsworth et al., 2002). However, nighttime MF radar measurements contain ambiguities arising from the estimation method. Moreover, MF radar requires a large facility. Standard radio-wave signals propagated from VLF/LF transmitters have also been used to measure the height variation of the D region based on phase and intensity modulations (e.g., Bickel et al., 1970; Thomas and Harrison, 1970; Thomson et al., 2007), but the possible region for electron density measurements is limited along the propagation path

between the transmitter and the receiver.

Compared with these methods, tweek atmospherics offer a rather conventional and stable source for investigating D-region height variations over many years. In this chapter, we investigate long-term variations in tweek reflection height throughout three solar cycles (1976–2010) observed at Kagoshima (31.48ºN, 130.72ºE, L = 1.17), Japan. When we analyzed the tweek data, we used only the geomagnetically quietest day for each month, as defined by the Helmholtz Centre Potsdam, GFZ German Research Centre for Geosciences, to avoid geomagnetic effects. We also carefully calibrated the tape extension based on the oscillator signals (760 Hz) and corrected the frequency for all tapes, as described in Section 2.1. We analyzed 203,649 tweek signals on the geomagnetically quietest day of each month by the automatic procedure employing MEM, as described in Section 2.4. The possible causes of the long-term variations are also discussed quantitatively in Section 3.2.

3.1. Results

Figure 3.1 shows (a) the tweek reflection height, (b) the sunspot number (red) and 10.7-cm solar radio flux (F10.7, blue), and (c) the galactic cosmic ray (GCR) counts over Tokyo (Japan, green) and Beijing (China, blue). The values in (b) are monthly averages. The dots in (a) and (c) represent the nighttime mean values for the geomagnetically quietest days of the months. The lines in (a) and (c) indicate 12-month running averages. The tweek reflection heights and GCRs used in these plots are those at 10:50–19:52 UT (LT = UT + 9 hours, 18:50–04:52 LT).

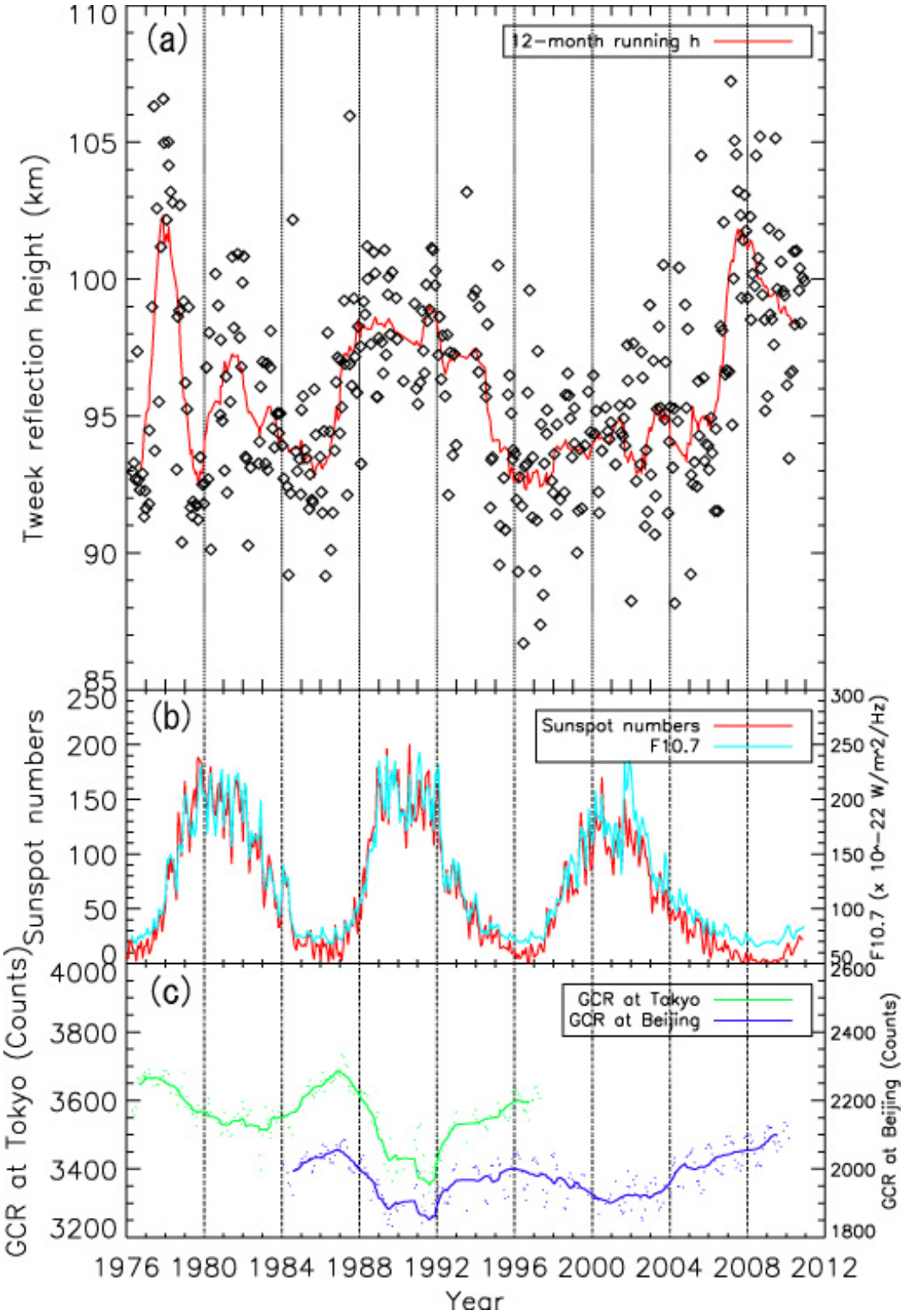

Figure 3.1. (a) Tweek reflection height, (b) sunspot number (red), and 10.7-cm solar radio flux (F10.7, blue), and (c) galactic cosmic ray (GCR) counts over Tokyo (Japan, green) and Beijing (China, blue). The lines in (a) and (c) indicate 12-month running averages.

The average and standard deviation of the reflection height for the whole plotted interval were 95.9 km and 3.1 km, respectively. The years when the tweek reflection height was lower than 93.0 km were 1976 (solar minimum), 1979 (solar maximum), 1985 (solar minimum), 1995–1997 (solar minimum), and 2002 (solar maximum). On the other hand, the years when the tweek reflection height was higher than 99.0 km were 1977–1978 (rising phase), 1987–1991 (rising phase to solar maximum), and 2006–2009 (solar minimum).

Clear correlations were not found between the tweek reflection height and the sunspot number or F10.7. Similarly, there was no clear correlation between the long-term variations in tweek reflection height and the GCR counts. The cross-correlation coefficient between the tweek reflection height and the sunspot number was 0.03. The correlations of the tweek reflection height with the GCR at Tokyo and Beijing were -0.25 and 0.17, respectively.

Looking at the long-term tweek variations in detail, the reflection height was significantly high (about 102 km) around 1978 in the rising phase of solar cycle 21. This means that the electron density in the lower ionosphere decreased in the rising phase of solar cycle 21. It decreased to 92 km in 1979 and then varied in the height range of 93–97 km. In solar cycle 22, the reflection heights were low at the solar minimum (1985) and high at the solar maximum (1987–1991). This finding is opposite to the results of a previous study that found that the electron density in the lower ionosphere in the solar maximum phase was larger than that in the solar minimum phase (e.g., Wakai, 1971). In solar cycle 23, however, the tweek reflection height was similar to previous results. In 2001–2002, the reflection height was low at the solar maximum. From 2006, it began to rise again and peaked in 2007–2008 at the solar minimum. It then continuously declined to 99 km. Converting the tweek reflection height to the electron density using the IRI-2007 model, the reductions in height from 102 to 92 km roughly

correspond to increases in the electron density from 10^1 cm^{-3} to 10^4 cm^{-3} at 102 km.

Figure 3.2 shows periodgrams of the tweek reflection height (black line), sunspot number (red line), and GCRs at Tokyo (green line) and Beijing (blue line) calculated by the MEM.

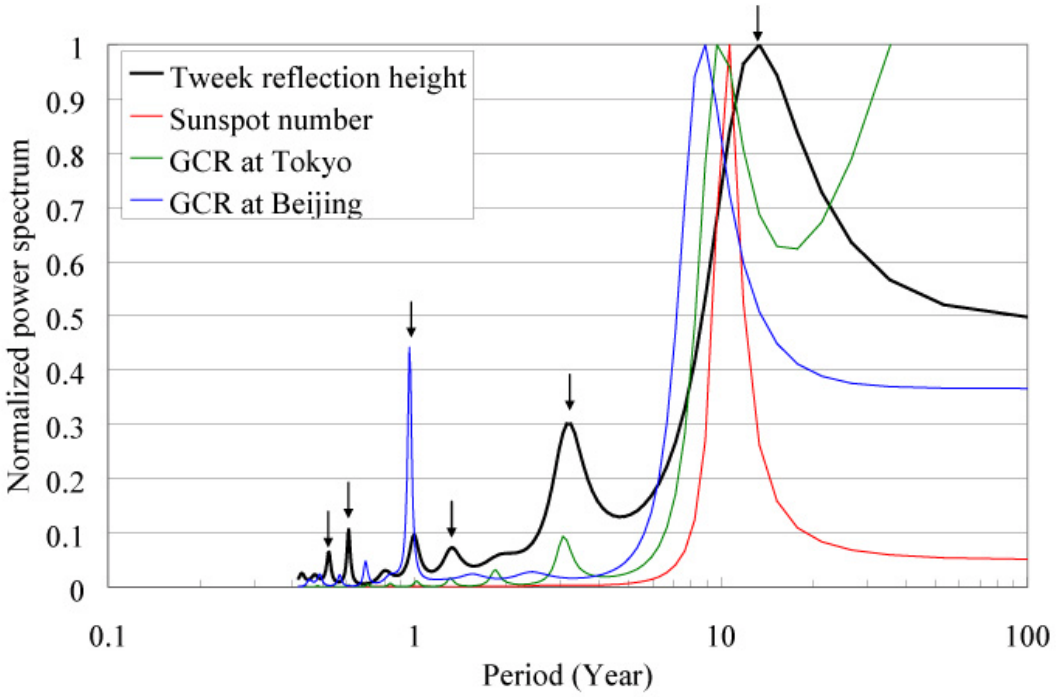

Figure 3.2. Periodgram of the tweek reflection height, sunspot number, and galactic cosmic rays (GCRs) at Tokyo and Beijing calculated by the maximum entropy method (MEM).

Arrows indicate main peaks of the tweek reflection height. Peaks of the tweek reflection height in the normalized power spectrum are shown at 13.3, 3.2, 1.3, 1.0, 0.6, and 0.5 years. The peak of the sunspot number is 10.7 years. GCR peaks at Tokyo are seen at 9.7 and 3.0 years, whereas those at Beijing are at 8.9 and 1.0 years. This result shows that the tweek reflection height had a slightly longer cycle (13.3 years) than that of the sunspot number (10.7 years) and GCRs (9.7 years at Tokyo and 8.9 years at Beijing) for

the periods near the solar cycle. For shorter periods, the tweek reflection height had similar periods (3.2, 1.3, and 1.0 years) to the GCRs (3.0 and 1.0 years).

More detailed investigation of the variations in the tweek reflection height was made using the Hilbert–Huang transform (HHT), which can separate time series into several different frequency modes (Huang et al., 1998, Huang and Wu, 1998, Kataoka et al., 2009). The HHT is a nonlinear time–frequency analysis that combines Hilbert spectral analysis and the empirical mode decomposition (Huang et al., 1998). Figure 3.3 shows two IMFs with different periods decomposed from the HHT, as well as the instant frequency for each IMF. Figure 3.3 (a) shows the IMF with the period of 0.5–l.5 years, as shown in Figure 3.3 (c), whereas Figure 3.3 (b) shows the IMF with the period of ~10 years, as shown in Figure 3.3 (d). Clear periodical variations can be seen in Figure 3.3 (a), suggesting the existence of 0.5–1.5-year modulations. However, the cross-correlation coefficient between the variation in Figure 3.3 (a) and sunspot number through the whole data period was -0.03.

On the other hand, the ~10-year variation is shown in Figure 3.3 (b). Compared with the sunspot number, a positive correlation would be expected between the tweek reflection height and the solar activity. The cross-correlation coefficient between them was 0.64 in 1976–2006. Similarly, the cross-correlation coefficient with GCR at Tokyo in 1976–1997 was -0.48 and that at Beijing in 1984–2006 was -0.57. After 2006, the variations in the tweek reflection height seem to differ from those of the previous cycles, but the data period is too short to analyze the correlation.

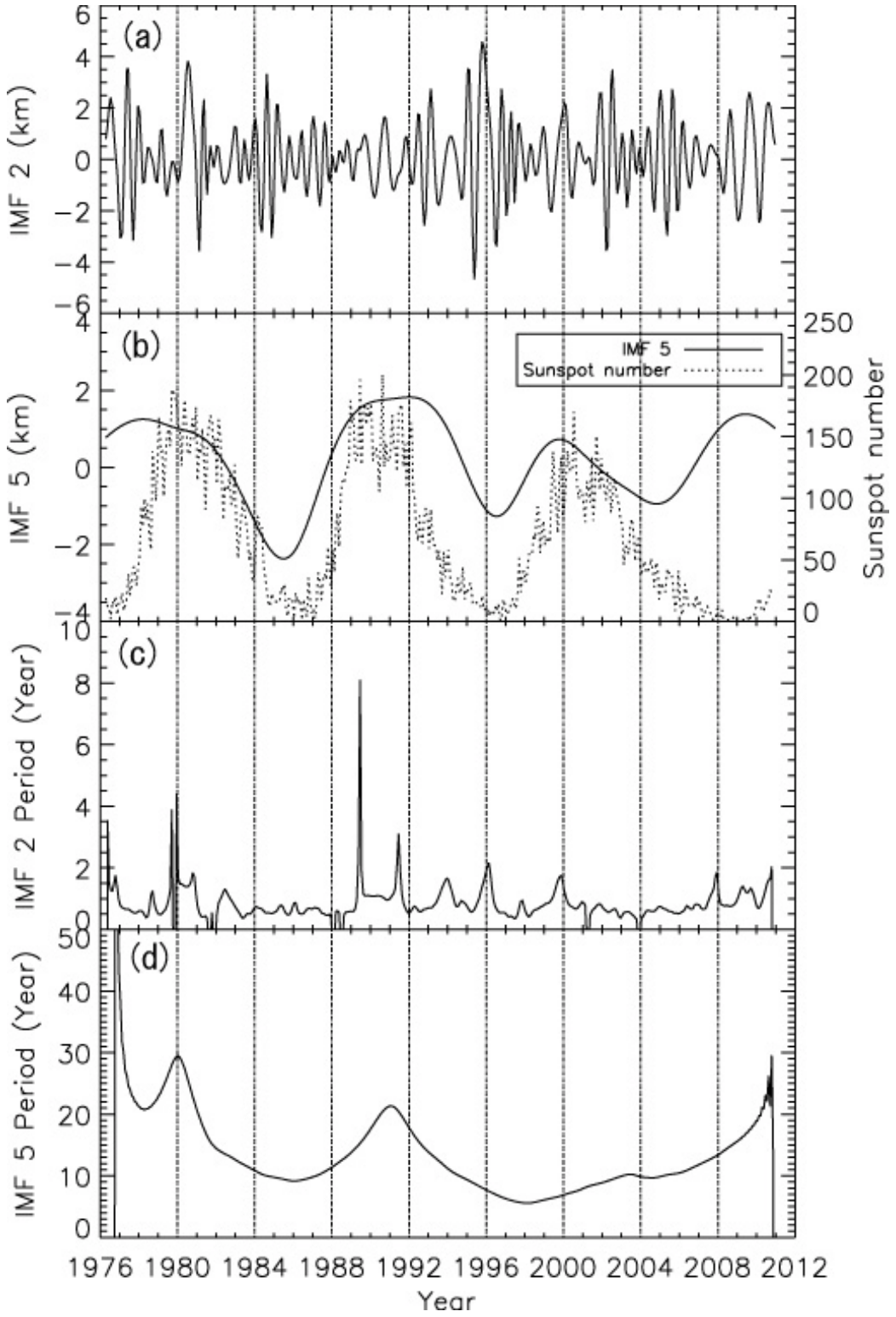

Figure 3.3. Intrisic mode functions (IMFs) of the tweek reflection height derived from the HHT. (a) IMF for the period of 0.5–1.5 years. (b) Same as (a) but IMF for the long-term variations. Corresponding instantaneous frequencies for (a) and (b) are shown in (c) and (d), respectively.

Figure 3.4 shows (a) nocturnal and (b) seasonal variations in the tweek reflection height for the geomagnetically quietest day of each month over the three solar cycles.

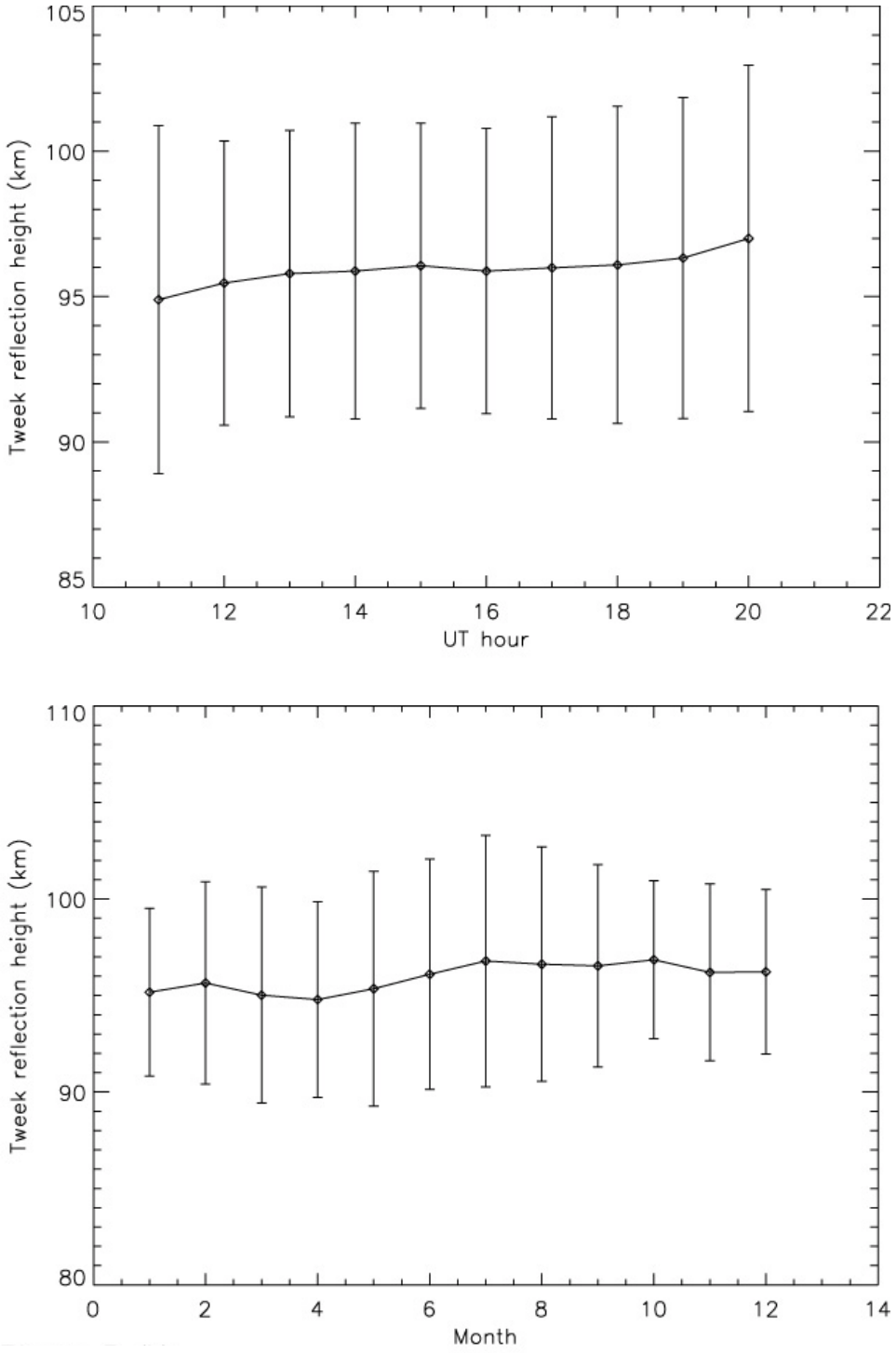

Figure 3.4. (a) Nocturnal and (b) seasonal variations in the tweek reflection height for geomagnetically quiet days over three solar cycles.

The tweek reflection heights gradually increased from evening to morning. Values were relatively high in July–October and low in March–April. However, these variations were only a few kilometers and much smaller than the error bars showing the variations over the three solar cycles.

3.2. Discussion

The complicated long-term variation in the tweek reflection height revealed in this study differs substantially from previous findings obtained by various methods. Previous studies suggested that the electron density in the nighttime lower ionosphere increased at solar maximum and decreased at solar minimum (Wakai, 1971; Kürschner and Jacobi, 2002; Laštovička, 2005; Kumar et al., 2008).

Wakai (1971) determined an empirical expression for the midnight peak electron concentration versus the smoothed relative sunspot number for middle latitudes, as described in Section 1.4.1 of this paper. This expression was based on f_oE measurements by an ionosonde specifically designed with a frequency range below 1 MHz. Kürschner and Jacobi (2002) and Laštovička (2005) reported that the reflection heights of LF radio waves at 177 kHz frequency that propagated a short distance (150 km) over Germany between a transmitter and a receiver decreased (increased) at the solar maximum (minimum) during 1983–2001. Kumar et al. (2008) found that tweek reflection height in low solar activity periods was higher by about 1.0–1.5 km than that in high solar activity periods from September 2003 to July 2004. However, these observations were for only limited intervals or for different techniques/frequencies compared with the present study.

The ionization sources in the nighttime lower ionosphere have not been clearly identified. Possible sources include (1) geocorona emission, (2) GCRs, (3) energetic

particle precipitation from the inner radiation belt, and (4) metal ions (Tohmatsu, 1990). Here we discuss these sources separately.

3.2.1. Geocorona

First, we estimate the amount of ionization in the nighttime lower ionosphere due to geocorona emissions. The hydrogen Lyman-α and Lyman-β emissions from the geocorona photoionize NO and O_2, respectively. The ions NO^+ and O_2^+ play important roles in the nighttime D- and lower E-region ionization. The electron density from this photoionization is given as (Brekke, 1997; Thomson et al., 2007)

$$n_e = \sqrt{\frac{q}{(1+\lambda)\alpha_{eff}}}, \qquad (3\text{–}1)$$

where q is the ionization production rate (in $cm^{-3}s^{-1}$), $\lambda(=n^-/n_e)$ is the ratio of negative ions, and α_{eff} is the effective recombination rate (in cm^3s^{-1}). The value of λ_n can be assumed to be ~3.0×10^{-1} at 95 km at night (Brekke, 1997).

Nagata and Tohmatsu (1973) noted that the nighttime ionization rate q for NO^+ is ~2.0×10^{-1} $cm^{-3}s^{-1}$ at 95 km, with a peak of ~1 $cm^{-3}s^{-1}$ at 105 km. For O_2^+, q is ~10^{-1} $cm^{-3}s^{-1}$ at 95 km, with a peak of ~10 $cm^{-3}s^{-1}$ at 105 km. The recombination rates α_{eff} for $NO^+ + e^-$ and $O_2^+ + e^-$ at 176 K (the nighttime neutral temperature at 95 km by the MSIS90 model) are ~5.1×10^{-7} cm^3s^{-1} and ~2.8×10^{-7} cm^3s^{-1}, respectively (Sheehan and St.-Maurice, 2004). If we calculate the nighttime electron densities at 95 km for NO^+ and O_2^+ based on (3-1), they become 5.5×10^2 cm^{-3} and 5.2×10^2 cm^{-3}, respectively. Using the IRI-2007 model, the nighttime electron density at 95 km is 1.6×10^3 cm^{-3}. Accordingly, about 67% of total electron density at 95 km is produced at night by both the hydrogen Lyman-α and -β of the geocorona.

The Lyman-α intensity increases by 1.7–2.7 times at solar maximum compared with

that at solar minimum (Lean, 1987; Danilov, 1998). If the ionization production rate of the NO^+ (Lyman-α) increased threefold, the electron density would increase by about 4.0×10^2 cm^{-3}, which corresponds to almost a doubling in the electron density at an altitude of 95 km.

The α_{eff} values for NO^+ and O_2^+ vary depending on the neutral temperature (Sheehan and St.-Maurice, 2004). In the MSIS90 model, solar-cycle variations in the nighttime neutral temperature at 95 km are not seen. However, we may have to consider the solar-cycle variations in the recombination rates caused by the variation in the neutral temperature. According to long-term sodium lidar measurements by She et al. (2009), the difference in nighttime neutral temperature at 85–95 km between solar maximum and solar minimum is ~9.5 K. We assumed that the nighttime neutral temperatures at 95 km at solar maximum and minimum are 194.0 K and 184.5 K, respectively. The q values for NO^+ and O_2^+ at both solar maximum and minimum are 2.0×10^{-1} $cm^{-3}s^{-1}$ and 10^{-1} $cm^{-3}s^{-1}$, respectively. When the neutral temperature is 194.0 K, the α_{eff} values for NO^+ and O_2^+ are 4.7×10^{-7} cm^3s^{-1} and 2.6×10^{-7} cm^3s^{-1}, respectively. For 184.5 K, the α_{eff} values for NO^+ and O_2^+ are 4.9×10^{-7} cm^3s^{-1} and 2.7×10^{-7} cm^3s^{-1}, respectively. The electron densities for NO^+ and O_2^+ at 194.0 K are 5.7×10^2 cm^{-3} and 5.4×10^2 cm^{-3}, respectively, while they are 5.6×10^2 cm^{-3} and 5.3×10^2 cm^{-3}, respectively, at 184.5 K. The nighttime electron density changes only by a factor of 10^1 cm^{-3} due to variations in the neutral temperature caused by the recombination effect. Thus, we conclude that the neutral temperature effects on the electron density are one order smaller than the effect of solar-cycle variations in the geocoronal intensity.

Danilov (2001) examined rocket mass-spectrometer measurements and suggested that an increase in the E-layer peak density, f_oE, is associated with a decrease in the NO^+/O_2^+ ratio in the low–mid-latitude E region in both daytime and nighttime. For E-region heights, a negative trend in NO^+/O_2^+ which causes a decreasing effective

recombination coefficient (as the dissociative recombination coefficient of the NO^+ ions is about twice that of the O_2^+ ions) and therefore an increase of the electron density at the E-region peak height (Bremer, 1998). In the IRI-2007 model, the NO^+/O_2^+ ratio is constant at low latitudes at midnight, showing no variation with solar activity. The solar-cycle variation in the intensity of geocoronal Balmer-α (6562.7Å), which is excited by the solar Lyman-β flux, has been investigated using Fabry-Perot interferometer observations (Nossal et al., 2006). The intensity observed in Wisconsin, USA, was about 50% higher at solar maximum than at solar minimum for a shadow altitude of 3000 km during solar cycles 22 and 23. However, opposite results were found for an observation at Arecibo, Puerto Rico, in 1983; the Balmer-α intensity was about 50% higher during the solar minimum than during the solar maximum for shadow altitude less than about 2000 km (Kerr et al., 2001).

3.2.2. Galactic Cosmic Rays

The second ionization source in the nighttime lower ionosphere is GCRs, for which the ionization rate is ~10^{-3} $cm^{-3}s^{-1}$ at 95 km (Nagata and Tohmatsu, 1973). Thomson et al. (2007) reported a GCR nighttime ionization rate of ~3×10^{-4} $cm^{-3}s^{-1}$ at 85 km, and Nagata and Tohmatsu (1973) reported that the GCR ionization rate was larger by about 3×10^{-3} $cm^{-3}s^{-1}$ at 95 km at solar minimum than at solar maximum. At solar maximum, GCRs are prevented from penetrating the heliosphere by the stronger interplanetary magnetic field. Thus under solar maximum conditions, the GCR ionization is less intense.

The HHT analysis identified the existence of an ~10-year variation in the tweek reflection height as an IMF, as shown in Figure 3.3 (b). The obvious correlations between the ~10-year variation in the tweek reflection height and the sunspot number

and GCRs were obtained until 2006. Thus, until around 2006, high (low) solar activities may have caused the decrease (increase) in the GCRs. This decrease (increase) in the GCRs may have led to a decrease (increase) in the electron density in the D-region and lower E-region ionosphere, which corresponded to the rise (decline) in the tweek reflection height. This suggests that GCRs could be major ionization sources for the ~10-year variation in the lower ionosphere. From 2006 to 2010, the reflection height seems to be more complicated.

GCRs have been found to have not only an 11-year period but also a 22-year period (e.g., McCracken and McDonald, 2004). At present, however, the period of the VLF observation data is too short to investigate longer variations. Further continuous observations of tweek atmospherics are necessary for detailed discussion.

3.2.3. Particle Precipitation from the Inner Radiation Belt

Another possible ionization source of the lower ionosphere is particle precipitation from the inner radiation belt. The energetic electrons trapped along magnetic field lines can precipitate into the lower ionosphere through pitch-angle scattering in the magnetosphere. Electrons with energies of 30–300 keV can penetrate into the D-region altitude (e.g., Helliwell et al., 1973; Inan et al., 1985). At lower latitudes over Japan (L = 1.3), electron precipitation during a large geomagnetic storm was reported (Kikuchi and Evans, 1989). The electron flux of the radiation belts increased depending on the L shell (Miyoshi et al., 2004; Miyoshi and Kataoka, 2011). Additionally, electrons with energies below a few hundred keV were reported to decrease in the region below L ~1.3 during the solar active period (Abel et al., 1994), probably due to neutral density enhancement in the upper atmosphere at solar maximum, as occurs with radiation belt protons

(Miyoshi et al., 2000).

3.2.4. Metal Ions

Metal ions (Fe^+ and Mg^+) are also likely to contribute to nighttime ionization. The electron density due to metal ions is ~10^3 cm^{-3} near 90 km (Aikin and Goldberg, 1973; Swider, 1984; Kopp, 1997). Metal ions and related sporadic E layers appear temporarily, although the long-term variations in metal ion content in the lower ionosphere have not yet been resolved. The midnight occurrence of f (flat)-type sporadic E (Es) layers at 100–105 km has been reported to increase at solar maximum (Abdu et al., 1996). The f-type is a classification for nighttime Es at lower heights below 140 km. The height stays the same with increased ionosonde frequency, producing an ionogram with a flat-line. If the occurrence of the f-type sporadic Es increases at solar maximum, it could have an influence on tweek reflection height.

3.2.5. Comparison with Empirical Models

Next, we compare our tweek observations with empirical models of the atmosphere and ionosphere. Figure 3.5 shows the variations in (a) annual electron density at 96-km altitude at midnight calculated from the IRI-2007 model, (b) midnight neutral mass density at 96 km (the mean tweek reflection height) calculated by the extended version of the MSIS90 model (MSIS-E-90), and (c) the midnight neutral temperature at 96 km calculated by the MSIS-E-90 model. The parameters were those at Kagoshima Observatory. The dotted lines in (a), (b), and (c) represent 12-month running averages of the tweek reflection height taken from Figure 3.1(a). The black dots in (b) and (c) represent the midnight mean values for the geomagnetically quietest day in each month.

The black lines in (b) and (c) mark 12-month running averages.

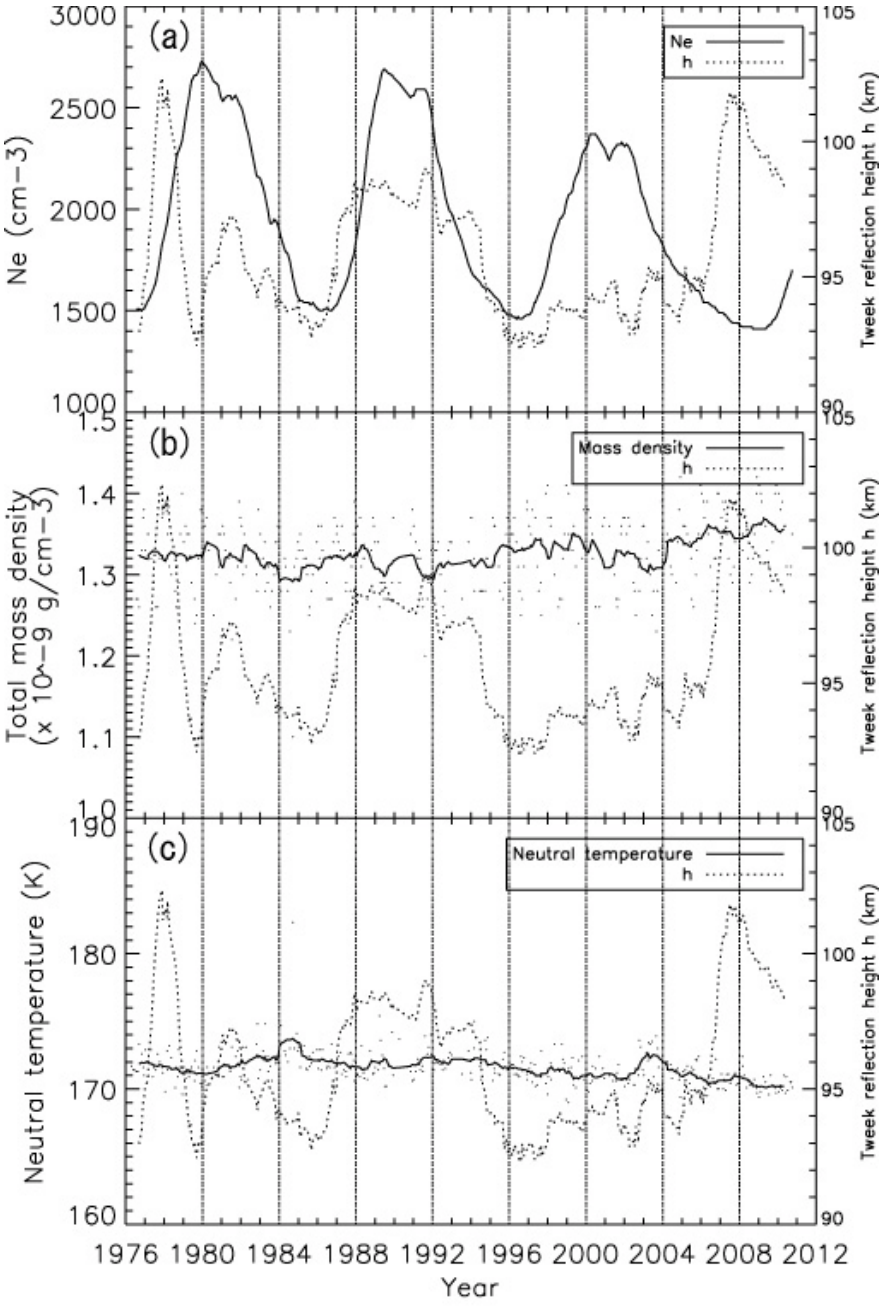

Figure 3.5. Variations in (a) the annual electron density at 96-km altitude at midnight calculated by the International Reference of Ionosphere 2007 model, (b) the midnight neutral mass density at 96 km calculated by the extended version of the Mass Spectrometer Incoherent Scatter 90 model (MSIS-E-90), and (c) the midnight neutral temperature at 96 km calculated by the MSIS-E-90 model.

The midnight electron density calculated by the IRI-2007 model shows clear solar-cycle variation in (a), whereas the tweek reflection height *h* indicates more complicated variations, as described above. The overall comparison does not show clear correlation between the electron density and the tweek reflection height. There were no long-term variations in the total mass density (b) and the neutral temperature (c) at midnight calculated by the MSIS-E-90 model.

The electron density in the lower ionosphere varies due to temperature changes caused by atmospheric waves (Sugiyama, 1988). Three main types of atmospheric waves can be considered: gravity waves (cycles: tens of minutes to hours), tides (6, 8, 12, 24 hours, and their harmonics), and planetary waves (2–30 days) (Laštovička, 2009). The cycles of these variations in the electron density are in agreement with each wave cycle. However, clear long-term variations in the atmospheric wave activity have not been found (e.g., Gavrilov et al., 2002; Jacobi et al., 2006; Laštovička, 2008). Thus, it is unlikely that atmospheric waves cause the long-term variations in the tweek reflection height.

3.2.6. Cooling Effects of the Upper Atmosphere

Greenhouse gases cause cooling in the upper atmosphere because CO_2 and other greenhouse gases emit infrared emissions toward space, reducing the temperature in the atmosphere. The cooling of the upper atmosphere causes an increase in electron concentration in the lower ionosphere below 100 km (Laštovička, 2009), which corresponds to the descent of the lower ionospheric height. The cooling is expected to result in thermal contraction of the upper atmosphere, and a decline in thermospheric density at fixed heights as well as a downward displacement of ionospheric layers. Bremer (2008) reported a rate of descent of -0.029+/-0.020 km/year based on the *h'E*

parameter of ionosonde observations. No significant trend was seen in the tweek reflection height (Figure 3.1). If the tweek reflection height descends at the rate of -0.029 km/year, the height would descend by 1.015 km in 35 years. However, this value is very small compared with the variations in the tweek reflection height shown in Figure 3.1. Thus, the long-term variations in the tweek reflection height do not seem to be caused by cooling effects in the upper atmosphere.

3.2.7. Geomagnetic Effects

In this study, we estimated the tweek reflection height on the geomagnetically quietest days of each month to alleviate geomagnetic effects. However, if geomagnetic storms had occurred several days before, their effects might still be seen even on the geomagnetically quietest day. Considering this issue, we investigated the minimum Dst index for the 10-day interval before the corresponding geomagnetically quiet day. Figure 3.6 shows the correlation between the tweek reflection height and the minimum Dst index.

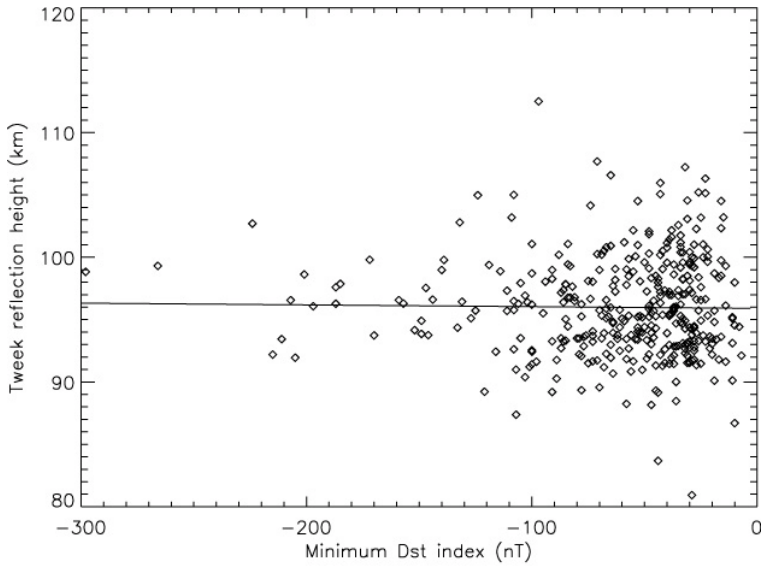

Figure 3.6. Correlation between the tweek reflection height and the minimum Dst index.

The reflection heights are the average values through the night for the geomagnetically quietest day of each month. The correlation coefficients were -0.01. We thus concluded that geomagnetic storm effects are not included in the estimated tweek reflection heights.

3.2.8. Nocturnal and Seasonal Variations

In Figure 3.4 (a), tweek reflection heights seem to increase slightly from evening to morning. Note that the error bars in this figure are not the errors due to measurements and data reduction but are the standard deviation of the height data due to nocturnal, seasonal, and long-term variations. Thus, it is possible to discuss the variations in the lower ionosphere even if the derived variations in the averages are smaller than the standard deviations.

Nocturnal variation in the tweek-reflection height was first reported by Burton and Boardman (1933a) for the second half of August 1932 at a mid-latitude site (44.0ºN, 71.1ºW). The reflection height was 61 km at sunset, rising to 88.5 km around 21:00 LT. At 30 minutes before sunrise, the height was 87 km, and at 15 minutes after sunrise, it decreased to 61 km. Kumar et al. (2008) reported that the tweek reflection heights for the first-order mode observed at Suva, Fiji (18.2ºS), during September 2003–July 2004 rose from ~82 km to ~86 km at 18:00–23:00 LT and then fell to about 83 km at ~01:00 LT. The height then gradually rose to ~93 km toward 05:00 LT. On the basis of low-frequency ionograms obtained at Boulder, CO (40º02’N), on the magnetically quiet night of 20–21 August 1960, Wakai (1967) showed that the nighttime electron density at 95 km decreased from 3×10^4 cm^{-3} at 18:00 LT to 2×10^3 cm^{-3} at 00:00 LT and then increased to 5×10^3 cm^{-3} at 01:30 LT, after which it again decreased to 1×10^3 cm^{-3} toward 03:00 LT. In terms of the general trend, the increase in the tweek reflection

height shown in Figure 3.4 (a) agrees with the results of Wakai (1967) and Kumar et al. (2008).

Regarding the seasonal variations in Figure 3.4 (b), Burton and Boardman (1933) showed that the intensity of tweeks observed in New Hampshire, USA, increased in spring. The intensity was higher from May to September and smaller from October to the beginning of March. Strobel et al. (1980) calculated the seasonal variation in the midnight O_2^+ ionization rate due to starlight at 120 km at 18ºN. The O_2^+ ionization rate was smaller in March and September and larger in January, May–June, and December. However, the seasonal variations in the tweek reflection height in Figure 3.4(b) do not correspond with those of starlight.

Regarding seasonal variation in the D region, a winter anomaly has been observed in radio wave absorption resulting from the remarkable enhancement of electron density in winter (e.g., Kawahira, 1985). The winter anomaly is likely associated with stratospheric sudden warming (SSW), and stratosphere–ionosphere coupling due to gravity waves and/or planetary waves has been discussed. However, the direct mechanism of the coupling has still not been clarified (e.g., Goncharenko and Zhang, 2008). If the anomaly in winter always occurred in the analyzed period, the tweek reflection height would become low in winter. However, lower reflection height in winter is not seen in Figure 3.4 (b).

3.2.9. Periodicity in the Tweek Reflection-height Variation

As illustrated in Figure 3.2, the tweek reflection height had a slightly different period (13.3 years) from the periods of the sunspot number (10.7 years) and GCRs (9.7 years at Tokyo and 8.9 years at Beijing) for the periods near the solar cycle. For shorter

periods, the tweek reflection height had similar periods (3.2 and 1.0 years) to GCRs (3.0 and 1.0 at Tokyo and Beijing, respectively). However, the GCR peaks at Tokyo had different periods from those at Beijing. The intervals of GCR data differed between Tokyo (1976–1996) and Beijing (1984–2009). GCRs may be a possible cause of the variations in the tweek reflection height, although the GCRs showed slightly different periods from those of the tweek reflection height. Many factors cause the solar-cycle variations in the nighttime D-region height, including the geocorona, GCRs, particle precipitations, and neutral atmosphere. Thus, we can expect that the time variations in the tweek reflection height will have slightly different periods from each factor such as GCRs.

3.3. Summary

This study newly investigated long-term (1976–2010) variations in tweek reflection heights. The long-term variations in the nighttime lower ionosphere at low to mid-latitudes were revealed by VLF observations at Kagoshima, Japan. The tweek reflection heights on the geomagnetically quietest day of each month were analyzed over three solar cycles with an automated procedure of spectral fitting to obtain the tweek cut-off frequency. The results are summarized as follows.

1. The average and standard deviation of the reflection height were 95.9 km and 3.1 km, respectively.

2. The typical periods embedded in the variations were identified as 13.3, 3.2, 1.3, 1.0, 0.6, and 0.5 years.

3. The variations in the tweek reflection heights did not show simple anti-correlation with solar activity. The correlation coefficient between the tweek reflection height and the sunspot numbers was 0.03 throughout the three solar cycles.

4. The HHT analysis indicated the existence of long-time variations with periods of ~10 years as an IMF. Positive correlation between the IMF and the sunspot cycle and GCRs was found during 1976–2006, whereas more recent variations in the tweek reflection height after 2007 seem to differ from those in the previous period.

5. The tweek reflection height slightly increased by a few kilometers from evening to morning. The tweek reflection height tended to be high in July–October and low in March–April, varying by a few kilometers. The nocturnal and seasonal variations were smaller than the long-term variations.

Based on these results and comparison with some models and previous results, we propose that these variations in the tweek reflection heights could be caused by the mixture of several D- and lower E-region ionization effects by the geocorona, GCRs, and particle precipitation and by variations in the neutral density of the lower thermosphere. Among these possible sources, GCRs may have played a role in the long-term variations until 2006. The geocorona and particle precipitation could cause negative correlation, whereas GCRs and the neutral density could cause positive correlation with solar activity.

Chapter 4.
Variations in the Tweek Reflection Height during a Magnetic Storm

This chapter describes variations in the tweek reflection height during a magnetic storm in October 2000 based on tweek observations at Moshiri (44.37°N, 142.27°E) and Kagoshima, Japan. We compared these tweek observations with measurements by LF transmitter signals (40 kHz), an MF radar, ionosondes, and GPS receivers.

4.1. Results

Reflection-height measurements were obtained from analysis of nighttime tweek atmospherics observed at Moshiri and Kagoshima during the great magnetic storm in October 2000. Figure 4.1(a) shows hourly/daily variations in the mean reflection heights for Moshiri (asterisks) and Kagoshima (open diamonds) for 2–12 October 2000. Mean reflection heights were obtained by averaging all propagation paths of tweek atmospherics in a wide area of low to middle latitudes. Vertical segments represent variances in the mean values. Hatched horizontal bars show the nighttime hours when the tweek observations were available. Variation in the hourly D_{st} index indicating global geomagnetic activity is also shown. The D_{st} index shows a small bay variation with a minimum value (~–80 nT) on 2–3 October. Thereafter, D_{st} exhibits major

decreases, with large magnetic fluctuations on 4–5 October, and attains the minimum value of −182 nT on 5 October, followed by a gradual recovery until 12 October. This D_{st} variation is classified as a great geomagnetic storm. During this magnetic storm, most of the tweek atmospheric sources (lightning discharges) were located in the equatorial region including Indonesia and Southwest Asia.

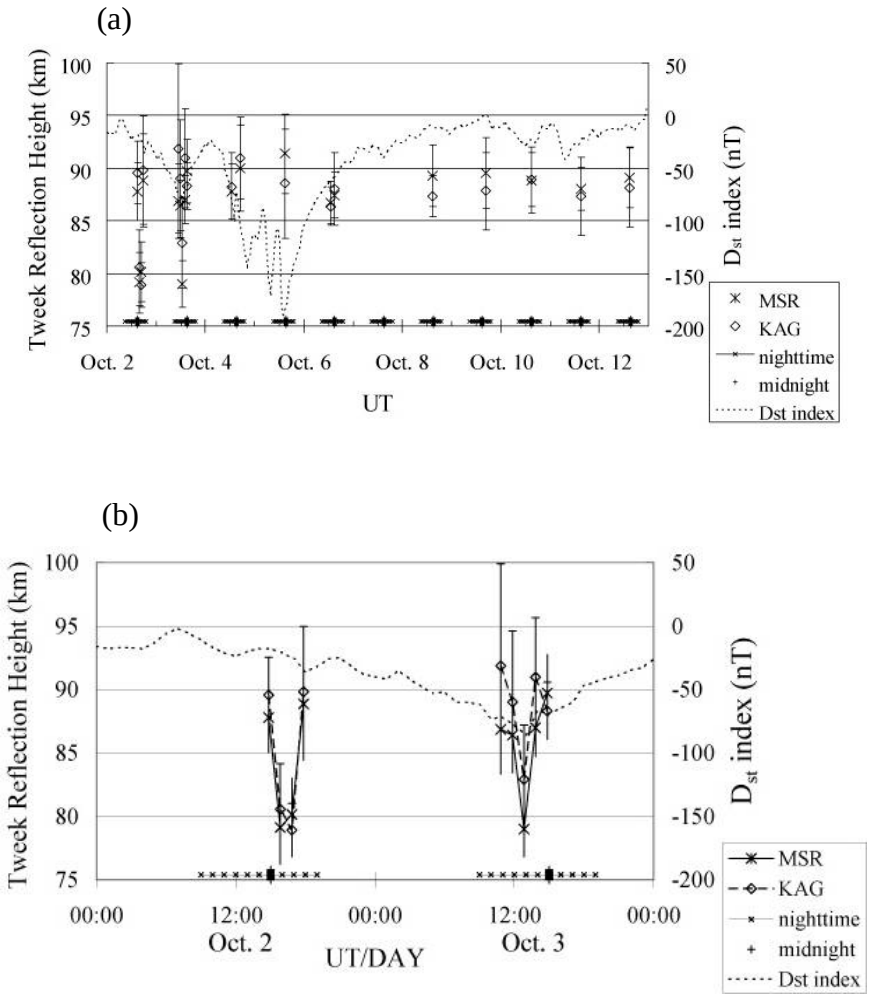

Figure 4.1. (a) Hourly/daily variations in mean reflection heights at Moshiri (MSR, asterisks) and Kagoshima (KAG, diamonds) during 2–12 October 2000. Vertical segments represent variances in the mean values. Horizontal hatched lines at the bottom of the figure show the nighttime hours of tweek observation. The dotted line indicates the variation in the Dst index. (b) Enlargement of (a) for 2–3 October.

Figure 4.1 (b) shows an enlargement of the mean reflection height variations for 2–3 October. The mean reflection heights in the magnetically quiet period prior to the small bay variation were 88.8 km and 88.3 km at Moshiri and Kagoshima, respectively. Local time (LT) at these observatories is 9 hours ahead of Universal Time (UT): LT = UT + 9 h. We observed a change in the mean reflection height from 87.8 to 79.1 km at Moshiri and from 89.6 to 80.6 km at Kagoshima between 14:50 UT (23:50 LT) and 15:50 UT (00:50 LT) on 2 October, with the decrease remaining for more than 1 hour; the mean reflection heights then returned to 88.8 km at Moshiri and 89.6 km at Kagoshima at 17:50 UT.

On 3 October, the mean reflection heights were high for both Moshiri and Kagoshima at 10:50 UT and 11:50 UT. Then, the reflection heights decreased to 79.0 km at Moshiri and 82.9 km at Kagoshima at 12:50 UT and returned to the quiet-time height at 13:50 UT within 1 hour. At 10:50–13:50 UT on 3 October, reflection heights at Moshiri were lower than those at Kagoshima.

Figure 4.1 (a) also shows that the mean reflection height ranged from 87 to 91 km for both Moshiri and Kagoshima during the major decreasing-D_{st} variation on 4–5 October. At the maximum depression of D_{st} on 5 October, the mean reflection height showed a small increase to 91.4 km at Moshiri, while remaining at 88 km at Kagoshima. Thereafter, the reflection height was fairly settled in the height range of 86–89 km for both Moshiri and Kagoshima in the D_{st} recovery phase after 6 October 6.

Summarizing the above variations, the mean reflection height showed a transient lowering/rising response twice during the small bay D_{st} variation on 2–3 October. However, on 3 October, the lowering feature at Moshiri differed from that at Kagoshima. The reflection height showed a small rising response at Moshiri near the major D_{st} depression on 5 October.

4.2. Discussion

In this section, we compare the tweek observations described in the previous chapter with the LF transmitter signals (40 kHz), MF radar data, ionograms, and total electron content (TEC) data.

4.2.1. Comparison with Low-frequency Transmitter Signals

Here, we compare the tweek reflection height with the amplitude of LF transmitter signals (40 kHz) propagating from Fukushima to Kagoshima, Japan. Predominantly, 40-kHz radio waves propagate as ground waves for distances less than 600 km. These waves are commonly used as standard radio-wave signals in Japan. However, for distances greater than 600 km, ground waves are mixed with reflection waves (one-hop sky waves) in the D-region ionosphere. During nighttime in particular, one-hop sky waves are dominant for long distances, e.g., greater than 800 km (Watt, 1967). The propagation distance from the transmitter at Fukushima to the receiver at Kagoshima is about 1200 km; thus, the 40-kHz radio-wave signals received at Kagoshima are useful for detecting D-region disturbances near the middle point in the propagation path. Figure 4.2 shows the locations of the observation stations for tweeks, LF transmitter signals, MF radars, and an ionosonde.

Figure 4.3 (a) shows amplitude variations of the 40-kHz radio-wave signals received at Kagoshima.

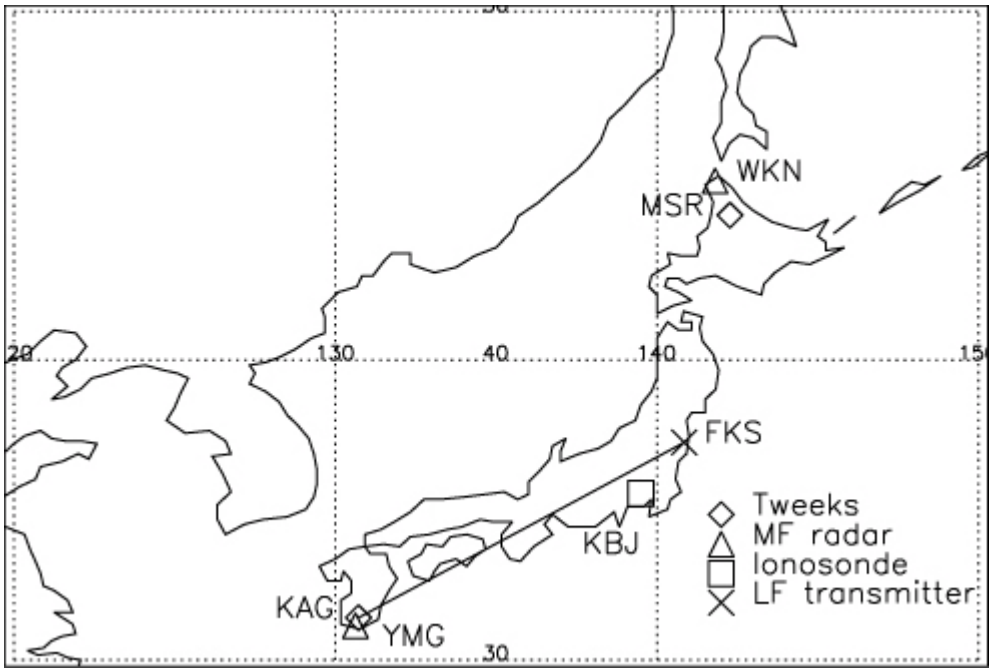

Figure 4.2. Tweek observation stations at Moshiri (MSR) and Kagoshima (KAG), the propagation path of the 40-kHz radio waves between the transmitter at Fukushima (FKS) and the receiver at KAG, and two MF radar stations at Wakkanai (WKN) and Yamagawa (YMG).

A solid black line represents the amplitude variation on 2 October, and a black dotted line shows the monthly mean amplitude averaged for geomagnetically quiet days in October. Red lines indicate times of significant descent in tweek reflection heights, as shown in Section 4.1. The amplitude variation on 2 October shows a broad decrease/increase, with a minimum near 11:00 UT (20:00 LT) due to the sunset effect and a sharp decrease/increase just before 20:00 UT (5:00 LT) due to the sunrise effect. Note that the amplitude around 17:00 UT corresponding to the time of lowering of tweek reflection heights at 16:50 UT [see Figure 4.1(b)] is 4.1 dB smaller than the monthly mean value. This indicates that the one-hop sky waves were disturbed in the D region in the propagation path. However, at 15:50 UT, variations in the amplitude were not seen. The amplitude also decreased around 15:00 UT, although the tweek reflection

heights did not decrease (88~89 km) at 14:50 UT. The inconsistency may be due to the latitudinal difference between the 40-kHz wave path and the tweeks paths: the 40-kHz wave path is located over the Japanese mainland, whereas the tweek paths are mainly located at latitudes lower than Japan. Figure 4.4 shows the distributions of tweek reflection heights at 14:50 UT with geographical latitude. The distribution of the tweek reflection heights at Moshiri (solid line) tends to be a lower than that at Kagoshima (broken line). A vertical solid line represents the latitude (~34˚) of the middle point in the 40-kHz wave path. Thus, we consider that the D-region disturbances occurred at the higher latitudes in Japan near 15:00 UT but did not occur in the lower latitudes at this time.

Figure 4.3 (b) shows amplitude variations of the 40-kHz radio wave signals received at Kagoshima on 3 October 2000, with the lines representing the same meanings as those in Figure 4.3 (a). The amplitude at 12:50 UT corresponding to lowering of the reflection height was almost the same as the average on geomagnetically quiet days. The variations for both 3 October and the average on geomagnetically quiet days show broad minimums around 11:00 UT due to the sunset effect.

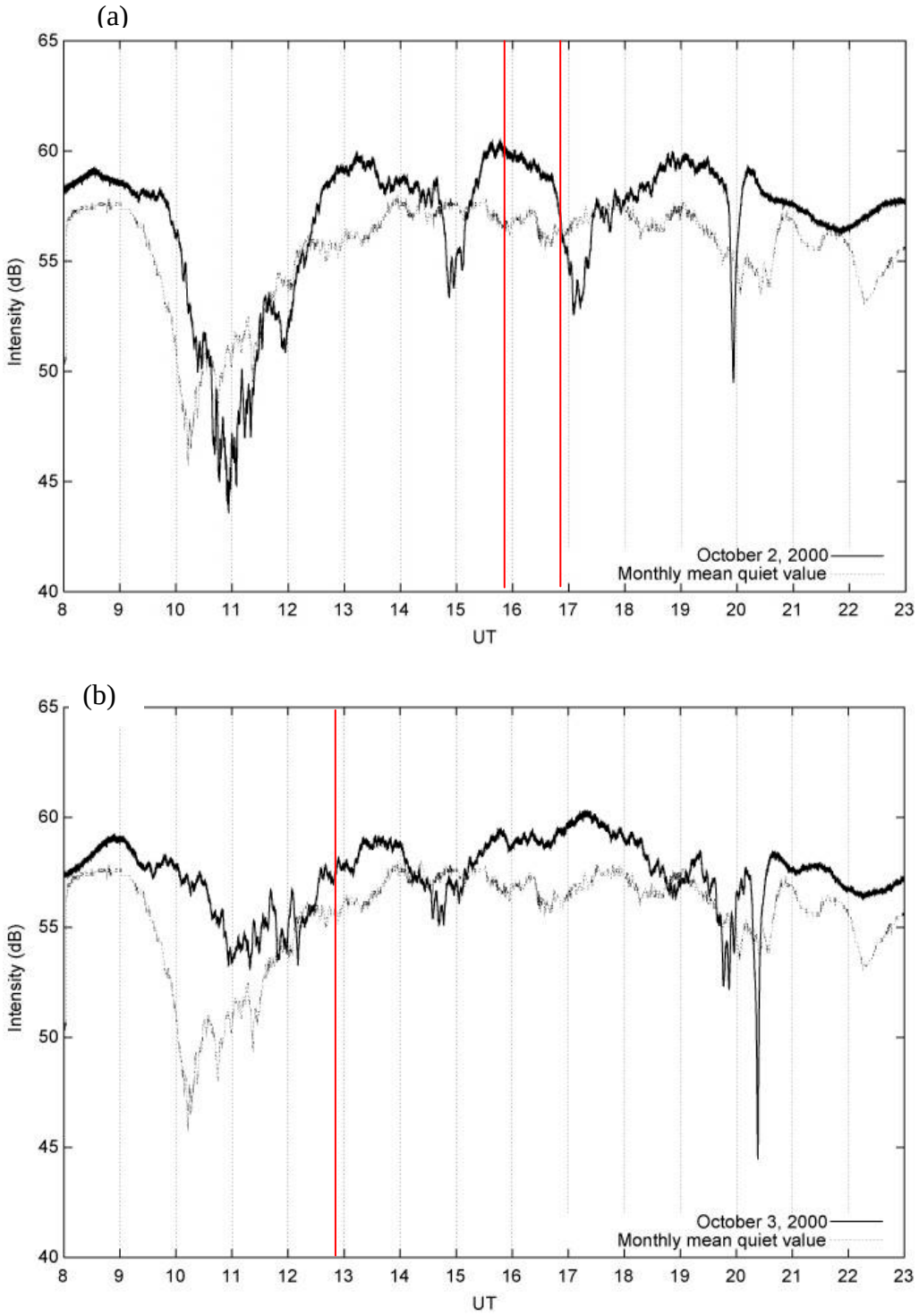

Figure 4.3. Amplitude variation (solid line) of the 40-kHz radio-wave signals received at KAG (a) on 2 October and (b) on 3 October. The dotted line shows the monthly mean amplitude averaged during quiet days in October. Red lines indicate times when the tweek reflection heights significantly descended.

Summarizing the result in Figure 4.3, the 40-kHz radio-wave signals showed an abnormal change related to the lowering of the reflection heights, but the amplitude changes did not always show one-to-one correspondence for the lowering/rising of the reflection heights. The amplitude is probably affected by other mechanisms such as focusing, scattering loss, and spatial loss in the D-region propagation (Davis, 1965). Thus, data on both the amplitude and phase of the 40-kHz radio-wave signals are needed. Phase data have been recorded since July 2001 at Kagoshima, and thus we do not have phase data for the October 2000 event in this case study.

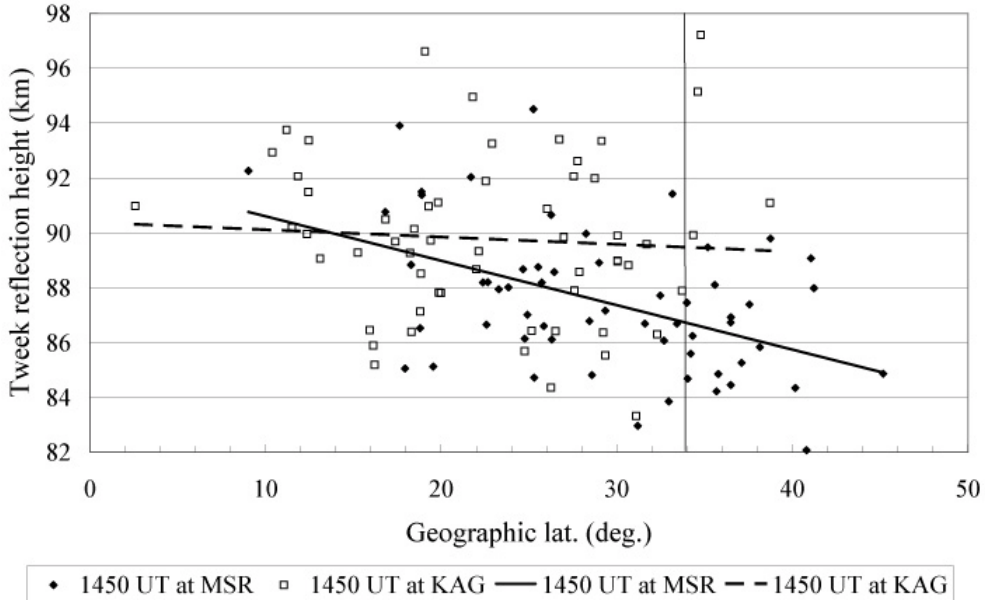

Figure 4.4. Distributions of tweek reflection heights at 14:50 UT on 2 October 2000 with latitude at Moshiri (MSR) and Kagoshima (KAG). The solid and broken lines are linear least-square fittings. The vertical solid line represents the latitude (~34˚) at the midpoint of the 40-kHz wave path.

4.2.2. Comparison with Medium-frequency Radar

In this section, we compare tweek reflection heights with electron density profiles estimated from two MF radars. Figure 4.5 shows variations in the mean reflection

heights at Moshiri (red asterisks) and Kagoshima (blue open diamonds) in each of the 2-minute observation periods on 2–3 October. The mean reflection heights on the vertical axis are converted to equivalent electron densities on the horizontal axis using Equations (2-2) and (2-12) to allow for comparison with the electron density profiles obtained from the MF radars at Wakkanai and Yamagawa.

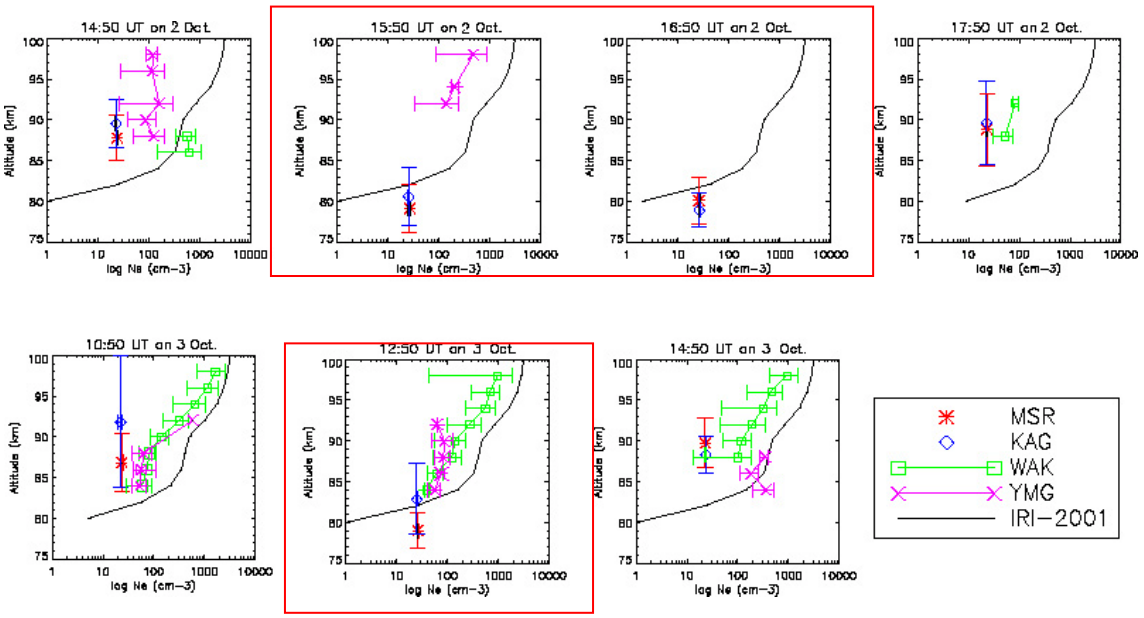

Figure 4.5. Variations in the mean tweek reflection heights at Moshiri (MSR, red asterisks) and Kagoshima (KAG, blue diamonds) in the 2-minute nighttime observations on 2–3 October. Height profiles of electron density from the IRI model (solid line) and electron densities with variances measured by the MF radars at Wakkanai (WAK, green squares) and Yamagawa (YMG, pink 'x' marks) are also shown. Red rectangulars indicate times when the tweek reflection heights significantly descended.

The electron density profiles (solid curve) from the IRI model in these panels are almost identical because the profiles were modeled for quiet-time conditions. The mean equivalent electron densities were smaller than those in the IRI model, except for those at 15:50 UT and 16:50 UT on 2 October and 12:50 UT on 3 October, which showed lowering of the D-region reflection heights [see Figure 4.1 (b)]. The average of the

equivalent electron densities at Kagoshima is 23 cm^{-3}, whereas the average electron density from the model is 402 cm^{-3} at 88-km height. This difference may have resulted from our assumption that tweeks have a propagation velocity equaling the speed of light *c* in Equation (2-3). Because the propagation velocity (the group velocity) is actually smaller than the light velocity, true reflection heights should be lower. If we take the propagation velocity to be 7.3% smaller than the speed of light, the equivalent electron density is ~21 cm^{-3} (~82-km reflection height), which approximately agrees with the electron density from the IRI model (~30 cm^{-3}) at a height of 82 km.

A comparison between the equivalent electron densities and electron densities measured by the MF radars at Wakkanai (green squares) and Yamagawa (pink 'x' marks) indicates that the average equivalent electron densities (~23 cm^{-3}) are smaller than the electron densities (35–1195 cm^{-3}) at >84-km height measured by the Wakkanai and Yamagawa radars on 2–3 October. This difference may arise because the tweek method measures average values over various long propagation paths, whereas the MF radars only measure electron densities directly above Wakkanai and Yamagawa, in addition to the assumption of the group velocity of tweeks. Unfortunately, MF radar data at Wakkanai were not recorded at 15:50 and 16:50 UT on 2 October. However, the increase in electron density above 94 km was seen in Yamagawa data at 15:50 UT when compared with values at 14:50 UT. If the electron density in the entire D region increased at 15:50 UT, it could be associated with the decrease in the tweek reflection height.

On 3 October, reflection height dropped at both Moshiri and Kagoshima at 12:50 UT. The electron densities obtained from the Yamagawa MF radar decreased at higher altitudes (>90 km) at 12:50 UT, whereas those obtained from the Yamagawa MF radar at 10:50 UT were similar with those obtained from the Wakkanai radar. This may indicate that the horizontal distribution of electron densities was not uniform over Japan

at 12:50 UT.

4.2.3. Comparison with Ionograms

In this section, we compare the tweek reflection heights with the ionospheric parameter *h'F* (minimum virtual height of the F layer) measured by the ionosonde at Kokubunji, Japan (see Fig. 4.2). Figure 4.6 shows temporal variations in *h'F* (a solid line with diamonds) and their monthly mean quiet values (solid line with open squares) for 2–3 October 2000. Shaded arrows represent the times of lowered tweek reflection heights. At 16:00 and 17:00 UT on 2 October, *h'F* decreased by about 42–52 km from the quiet value, indicating downward motion of the F layer, which is consistent with the drop in the tweek reflection heights at 15:50 and 16:50 UT on 2 October. At 18:00 UT, *h'F* increased by about 100 km relative to the quiet values, indicating upward motion of the F layer, which is consistent with the rising of the tweek reflection heights at 17:50 UT on 2 October. This result suggests a coupling between the D- and F-region ionosphere.

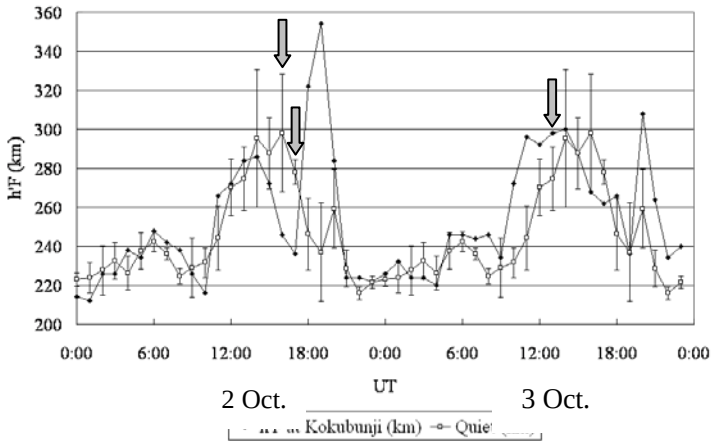

Figure 4.6. Temporal variations in the ionospheric *h'F* (a solid line with diamonds) parameter and their monthly mean quiet values (solid line with open squares) during 2–3 October 2000. Shaded arrows represent times when the tweek reflection heights became lower.

At 13:00 UT on 3 October, *h'F* increased to 23 km above the monthly mean quiet value, indicating upward motion of the F layer, which is inconsistent with the drop in the tweek reflection heights at 12:50 UT. At 15:00 UT, *h'F* decreased, indicating downward motion of the F region, in contrast to the rise in tweek reflection height at 14:50 UT. This inconsistency suggests a lack of coupling between the D- and F-region ionosphere, in contrast to the events on 2 October.

4.2.4. Comparison with Total Electron Content

In this section, we compare the tweek reflection height with TEC data obtained by GPS receivers. The TEC data were obtained from the Global Positioning System Earth Observation Network (GEONET), which includes more than 1,000 GPS receivers over Japan. The TEC data represent the electron density integrated over the entire ionosphere, although electrons in the F region dominate. TEC perturbations are measured by subtracting the TEC values from their 60-minute running average (Saito et al., 1998).

First, we discuss the 2 October events. Figure 4.7 shows hourly TEC values over the point of (35ºN, 135ºE) from 16 September to 15 October 2000. The black arrow indicates 2 October 2000 (day of year 276). The maximum and minimum values of the *z*-axis are 70 TEC units in red and 20 TEC units in black, respectively. One TEC unit is 1×10^{16} electrons/m^2. When the tweek reflection height significantly decreased at 15:50–16:52 UT, the hourly TEC value seemed to be larger than that at the same time on other days. However, TEC values were generally larger throughout this day. No significant variation can be seen in these TEC values at 12:50 UT on 3 October 2000, when the second D-layer descent was observed in the tweek reflection height.

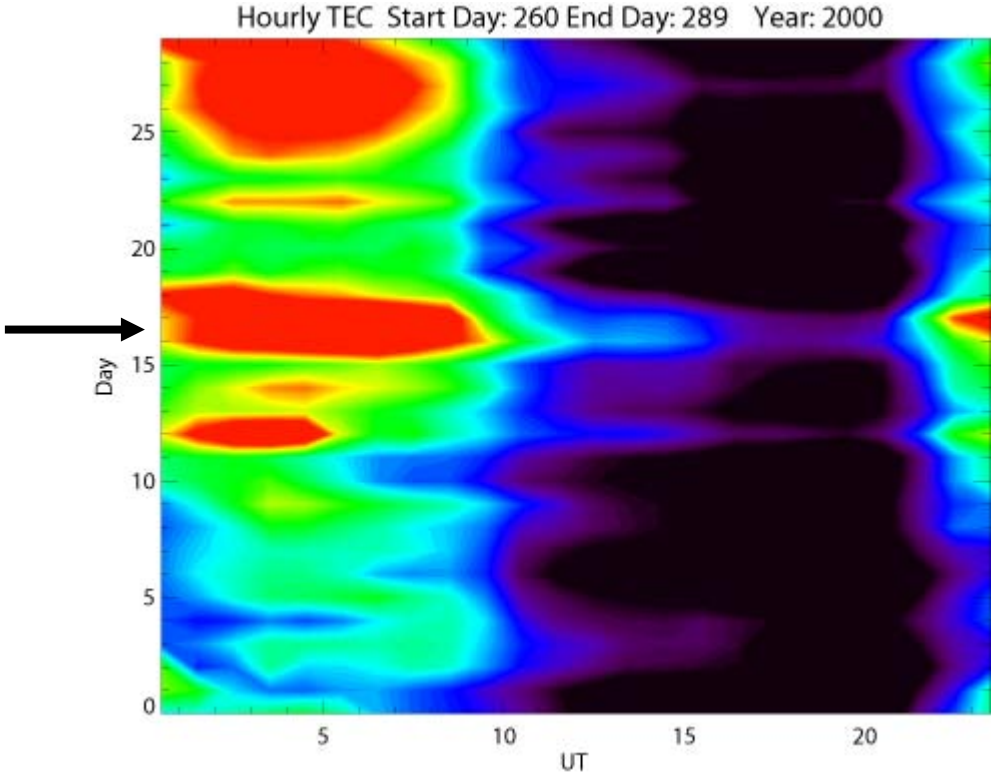

Figure 4.7. Hourly TEC value over the point of (35ºN, 135ºE) on 16 September to 15 October 2000. The black arrow indicates 2 October 2000. The maximum and minimum values on the *z*-axis are 70 TEC units in red and 20 TEC units in black, respectively. One TEC unit is 1×10^{16} electrons/m^2.

Jacobs and Watanabe (1963) suggested that westward electric fields associated with sudden commencement of geomagnetic variations could cause a downward motion of charged particles in the ionosphere, resulting in charged particle accumulations in the lower ionosphere. They calculated electron density profiles between altitudes of 80 km and 160 km assuming westward electric fields of 0.6 mV/m lasting 5 minutes. The results showed that the electron density increased from 1.0×10^5 cm^{-3} to 2.0×10^5 cm^{-3} at a height of 95 km with an average velocity of 20 m/s for the downward motion. Furthermore, if the downward velocity decreased at lower altitudes because of lower electron mobility, the electron density recovered in 8 minutes due to chemical recombination processes in the D-region ionosphere, assuming a recombination

coefficient of about 10^{-8} cm^3s^{-1}. Because hydrated ions are extremely rich in the D region below 100-km altitude, the electrons would immediately recombine with ions. If the positive-ion density were equal to the electron density, the electron density would recover in a very short time of about 95 ms under quiet-time conditions. However, the increase in equivalent electron densities measured by the tweek method appears to last for more than 1 hour in the D region. Therefore, we may expect the existence of ionospheric westward electric fields during this time period. Unfortunately, no data were available on the ionospheric electric fields; thus, we referred to electric field data from the low to middle latitudes measured during previous magnetic storms.

It is known that westward electric fields occur on the night side of the Earth during the main phase of magnetic storms (e.g., Kikuchi et al., 2008). Spiro et al. (1988) showed westward electric fields measured by the Jicamarca (Peru) incoherent-scatter (IS) radar (77°W, 12°S) in the phase of sharp decrease of the D_{st} variation (minimum, about 60 nT) at 19:00–01:00 LT on 6 October 1984. They also showed evidence for lowering of *h'F* (~200 km) at Cachoeira Paulista, Brazil (45°W, 23°S), synchronized with the westward electric fields associated with substorm activities at high latitudes. Xiaoqing et al. (2000) presented observations of westward electric fields for several hours in the post-midnight period measured by the Arecibo (Puerto Rico) IS radar (L = 1.43). These fields were associated with substorm activities during a moderate geomagnetic storm (D_{st} ~–50 nT).

The subsequent rising of the tweek reflection height at 16:50–17:50 UT appears to be coupled with the F-region upward motion at 18:00 UT shown in Figure 4.6. Thus, we can expect eastward electric fields in the ionosphere. Spiro et al. (1988) and Xiaoqing et al. (2000) presented evidence of eastward electric fields succeeded by westward electric fields in measurements by low-middle latitude IS radars. Consequently, a possible mechanism for the transient response of the D-region ionosphere is the existence of

electric fields in the low- to middle-latitude ionosphere associated with high-latitude substorm activities.

Next, we compare the lowering of tweek reflection height on 3 October with the TEC data. Figure 4.8 shows two-dimensional maps of TEC perturbations over Japan every 10 minutes at 12:20–12:50 UT on 3 October. According to these images, enhanced TEC perturbations first appeared over northeastern Japan at 12:20 UT, propagated southwestward with time, and reached central Japan at 12:50 UT. The large-scale and southwestward motion of the perturbations identifies them as a large-scale traveling ionospheric disturbance (LSTID) (Tsugawa et al., 2004). Thus, the higher equivalent electron densities at Moshiri during 11:50–12:50 UT were likely caused by passing LSTIDs. However, the measurement of this effect is not exact because the tweek measurements consist of 2-minute observations every hour. The LSTIDs are generated by acoustic gravity waves (AGWs) that are produced by energy input from the magnetosphere to the auroral ionosphere. Consequently, the transient response of the D-region ionosphere on 3 October could have been induced by LSTID propagation in the F region.

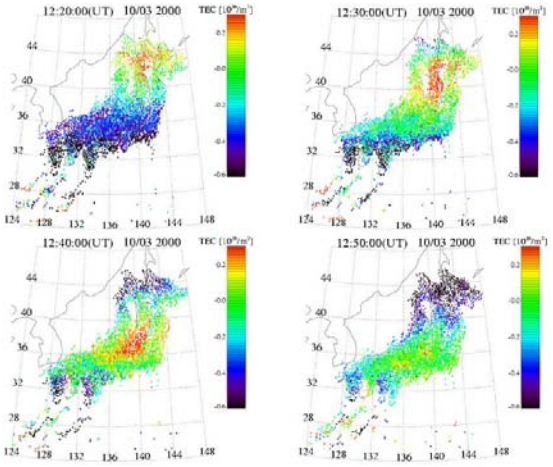

Figure 4.8. A time sequence of two-dimensional maps of TEC perturbations between 12:20 and 12:50 UT on 3 October 2000.

4.2.5. Comparison with 210 Magnetic Meridian Magnetic Field Data

Next, we examined the case of D-region ionospheric lowering by considering the presence of substorm occurrences at 14:50–15:50 UT at high-latitude stations according to the 210 (degree) Magnetic Meridian magnetic field data (Yumoto et al., 1992; Yumoto et al., 1996). Figure 4.9 shows H-component magnetic field variations of the 210 Magnetic Meridian magnetic field data on 2 and 3 October. Three red vertical lines indicate the time when the tweek reflection height significantly fell. All lowerings of the tweek reflection height occurred simultaneously with positive geomagnetic bays at low latitudes and negative bays at high latitudes at CHD (Chokurdakh, Russia), ZYK (Zyryanka, Russia), and MCQ (Macquarie Island, Australia) on both 2 and 3 October, indicating that magnetic substorms took place at these times. However, similar magnetic field variations associated with substorms were also observed on 4 and 5 October, when the tweek reflection height did not decrease.

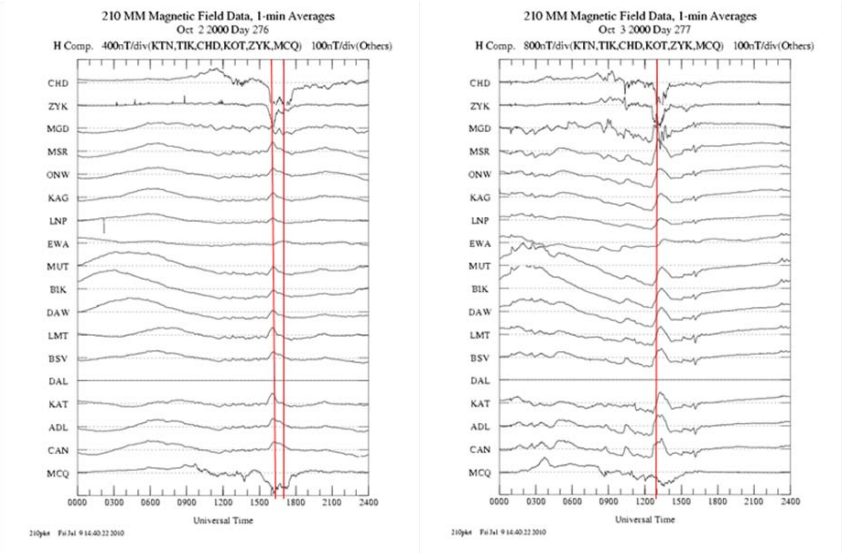

Figure 4.9. H-component magnetic field variations in 210 Magnetic Meridian magnetic field data on 2 and 3 October 2000. The three red vertical lines indicate times of lowering tweek reflection height.

4.2.6. Comparison with Galactic Cosmic Rays

In this section, we compare the tweek variations with variations in GCRs. Figure 4.10 shows the GCR variations at Beijing on 2 and 3 October 2000. The red and blue lines indicate the GCR counts on that day and monthly mean value on magnetically quiet days in October 2000, respectively. Three black arrows indicate the time of the lowering reflection heights. The GCR data were almost the same as the monthly mean value during all the episodes of decreased reflection height. Thus, GCRs are unlikely to have been the cause of the lowering of the tweek reflection height on 2 and 3 October 2000.

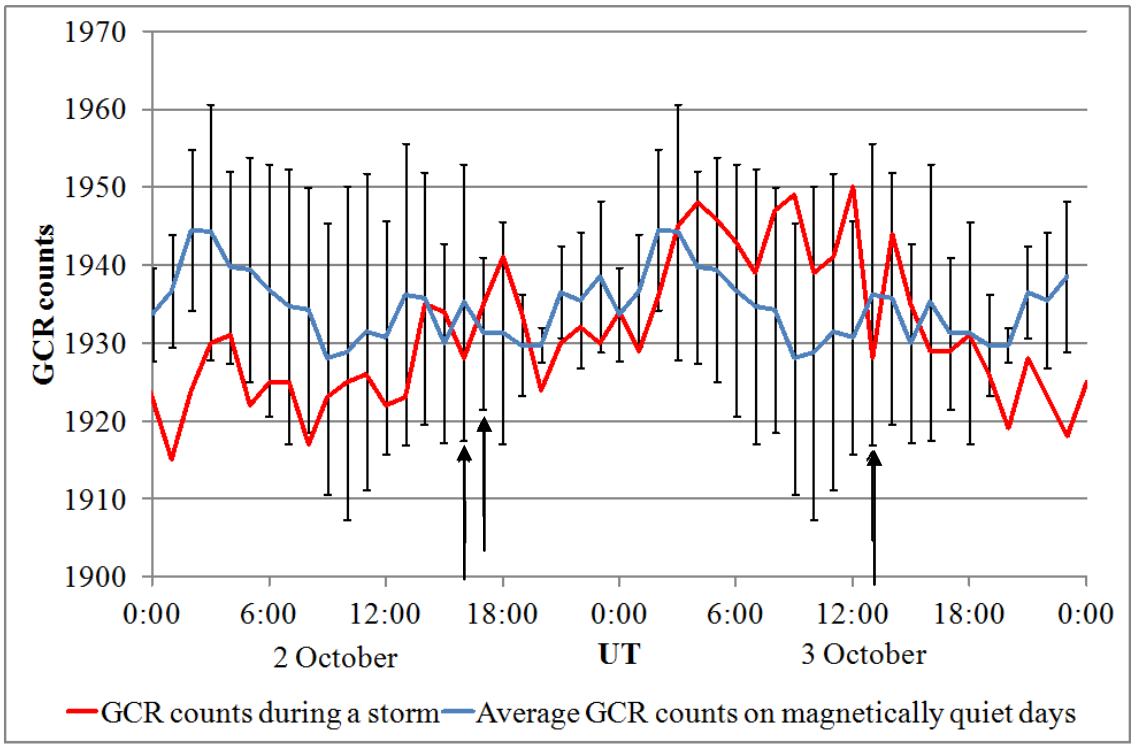

Figure 4.10. Galactic cosmic rays (GCRs) at Beijing, China, on 2 and 3 October 2000. The red and blue lines indicate the GCRs on that day and monthly mean value on magnetically quiet days in October 2000, respectively.

4.3. Summary

We examined the response of the nighttime D-region ionosphere to the great magnetic storm of 2–12 October 2000 by analyzing tweek atmospherics. The tweek reflection height fell significantly at 15:50–16:50 UT on 2 October and 12:50 UT on 3 October. This study is the first report of variations in the tweek reflection height during a magnetic storm. We compared the variations in the tweek reflection heights with amplitude variations in 40-kHz radio-wave signals, electron-density profiles obtained by two MF radars, the *h'F* parameter measured by an ionosonde, 210 Magnetic Meridian magnetic field data, and GCRs. Then, we considered possible mechanisms for the fall of the tweek reflection heights. Below we summarize our conclusions for these two events.

1. The 2 October event

The tweek reflection heights were significantly lowered at 15:50–16:50 UT. The amplitude of 40-kHz transmitter signals showed a decrease relative to the quiet-time level at 16:50 UT, synchronized with the lowering of the reflection heights, although the amplitudes of the 40-kHz signals were almost the same as the quiet-time level at 15:50 UT. The increase in the electron density above 94 km measured by the MF radars at Yamagawa at 15:50 UT was confirmed. The *h'F* parameter indicated downward motion of the F region at 15:50–16:50 UT. The hourly TEC value was larger through the night on 2 October than on the other days. However, significant TEC variations were not observed during the time of lowered tweek heights. At 15:50–16:50 UT, a substorm occurred simultaneously with the lowering of the reflection heights. We therefore suggest that the lowering of the D-region ionosphere could be coupled with the F-region downward motion caused by the ionospheric westward electric fields associated with substorm activities during the great magnetic storm.

2. The 3 October event

The tweek reflection heights decreased at 12:50 UT, although the lowering (increase in equivalent electron density) recorded at Moshiri was larger than that at Kagoshima. The variations in the amplitude of the 40-kHz signals were not seen at 12:50 UT. The *h'F* parameter indicated upward motion of the F region. The TEC perturbations indicated LSTIDs propagating from the northern to central regions of Japan. On the basis of these findings, we suggest that the lowering of the D-region ionosphere could have been associated with the LSTIDs propagating from auroral latitudes to low latitudes.

Chapter 5. Conclusions

This thesis has presented a method for monitoring the nighttime D- and lower E-region ionosphere using tweek atmospherics and variations in the reflection height associated with solar activities and a magnetic storm. Tweek atmospherics (1.5–10.0 kHz) originate from lightning discharge and propagate in the Earth–ionosphere waveguide, reflecting between the bottom edge of the ionosphere and the Earth over several thousand kilometers. This thesis has three important aspects. It (1) shows that the tweeks are useful tool for statistically investigating the D- and lower E-region ionosphere (Chapter 2), (2) presents long-term variations in the tweek reflection height (Chapter 3), and (3) documents variations in the tweek reflection height during a magnetic storm (Chapter 4).

Regarding aspect (1) above, although relatively few tweek studies have examined lower ionospheric variations to date, tweeks are useful for investigating long-term variations in the D- and lower-E region ionosphere. Because the reflection height can be determined by the cut-off frequency of the tweek atmospherics rather than their intensity, degradation of the receiver sensitivity does not affect the measurement accuracy. We developed an automatic procedure to estimate the reflection height and propagation distance of tweeks to investigate long-term variations in the tweek reflection height. Use of the maximum entropy method (MEM) instead of the conventional fast Fourier transform (FFT) greatly improved the accuracy of the estimations of the reflection height, particularly the propagation distance. The results indicate that the automatic procedure can clearly detect the rapid frequency changes of tweeks.

The most important results obtained in this thesis are those for aspect (2) above, i.e., the long-term variations in the tweek reflection height that show complicated variations rather than a simple anti-correlation with solar activity. In this study, the average and standard deviation of the reflection height were 95.9 km and 3.1 km, respectively. Typical temporal variations in the reflection height were identified as 13.3, 3.2, 1.3, 1.0, 0.6, and 0.5 years. The correlation coefficient between the tweek reflection height and the sunspot number was 0.03 throughout the three examined solar cycles. More detailed analysis by the Hilbert–Huang transform showed 0.5–1.5-year and ~10-year variations as intrinsic mode functions (IMFs). The decomposed IMF with the ~10-year variation was positively correlated with sunspot numbers and negatively correlated with galactic cosmic rays (GCRs). Based on these results and comparison with some models and previous results, we consider that these variations in the tweek reflection heights could have been caused by the mixture of D- and lower E-region ionization effects by the geocorona, GCRs, and particle precipitation and by variations in the neutral density of the lower thermosphere. Among these possible sources, GCRs may have played a role in the long-term variations until 2006.

Regarding aspect (3) above, we first showed that the tweek reflection heights significantly dropped for about 1 hour during a magnetic storm. We compared these variations in the tweek reflection heights with amplitude variations of 40-kHz radio-wave signals, electron-density profiles obtained by two MF radars, the *h'F* parameter measured by an ionosonde, as well as total electron content (TEC) data, ground magnetic field data, and GCRs to discuss possible mechanisms for the fall in the tweek reflection heights during the magnetic storm. The comparisons suggest two possibilities: the lowering of the tweek reflection heights could have been caused by the ionospheric westward electric fields associated with substorm activities during the great magnetic storm and/or by a large-scale traveling ionosphere disturbance (LSTID)

propagating from auroral latitudes to low latitudes.

The results for tweek reflection heights associated with solar activity and a magnetic storm are just a part of all nighttime D-region phenomena whose mechanisms have not yet been fully revealed. Regarding the effects of magnetic storms, statistical analysis of tweeks from many more storms is necessary.

Chapter 6.
Future Research

This thesis has presented average variations in the tweek reflection height over a wide area of low and mid-latitudes because only one magnetic component at each station was available. If the timing and propagation direction of tweeks can be determined for more than three stations, the distribution of the tweek reflection height could be estimated. As future work, we will introduce findings from the Asia VLF Observation Network (AVON), which consists of three stations: Tainan in Taiwan (at National Cheng Kung University, 23.1ºN, 120.1ºE), Saraburi in Thailand (at Chulalongkorn University, 14.5ºN, 101.0ºE), and Pontianak in Indonesia (at Lembaga Penerbangan Dan Antariksa Nasional, LAPAN; 0.0ºN, 109.4ºE). The purpose of AVON is to monitor the lower ionosphere and lightning activities.

Figure 6.1 shows the locations of the AVON sites. Using an orthogonal loop antenna, a monopole antenna, and a dipole antenna, electromagnetic waves originated from lightning and transmitters in the frequency range of 0.1–60 kHz are measured at each site. The obtained data will be analyzed to monitor the lower ionosphere and lightning activities in Southeast Asia.

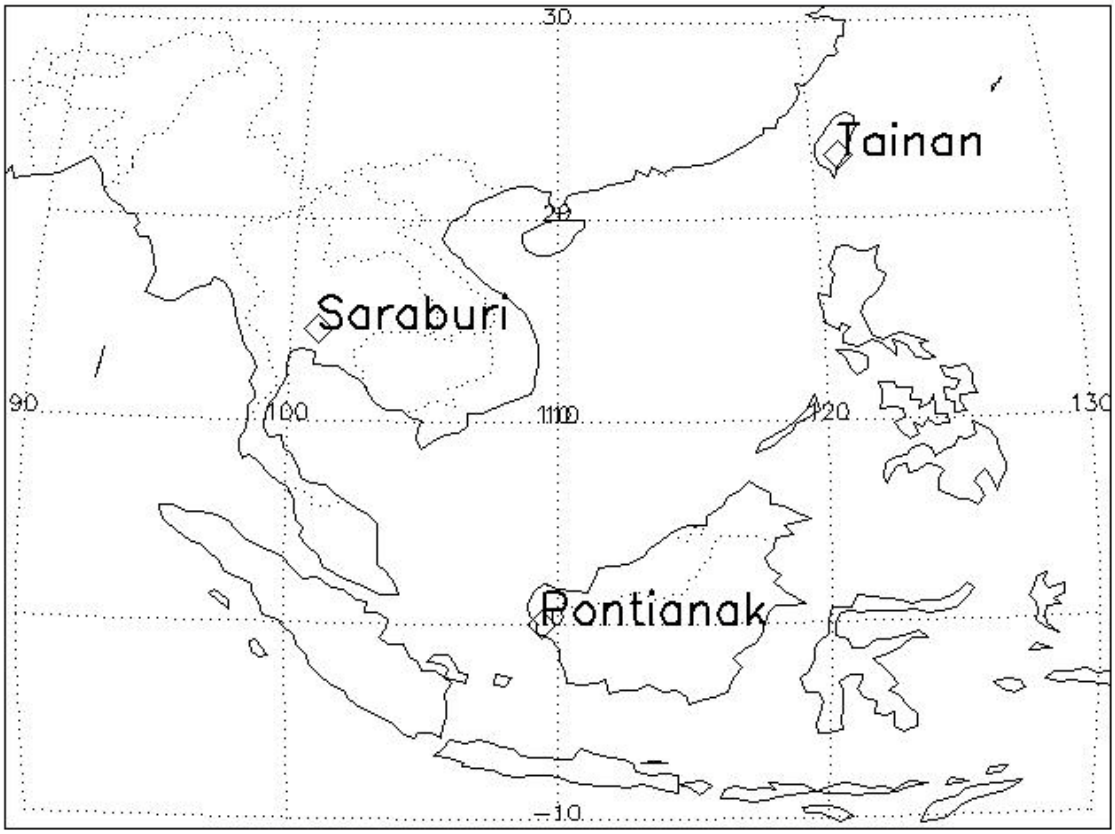

Figure 6.1. AVON observation sites.

Tweek observations over Southeast Asia are important for revealing variations in the tweek reflection height associated with energetic particle precipitation at low latitudes. During a large magnetic storm, energetic particle precipitation was confirmed over Japan (L = 1.3) based on NOAA-6 satellite data (Kikuchi and Evans, 1989). However, it is not known whether such particle precipitation occurs at lower latitudes. In this project, we will reveal variations in tweek reflection height at low latitudes by analyzing both AVON data and data collected at Moshiri and Kagoshima by the Solar–Terrestrial Environment Laboratory, Nagoya University.

Another topic of research in the low ionosphere is Trimpi effects. Trimpi effects are transient changes in the amplitude and phase of VLF/LF radio waves due to the

precipitation of energetic electrons (~keV) by whistlers (Helliwell et al., 1973; Nunn, 1997). Typically, Trimpi effects last for some tens of seconds, although significantly longer Trimpi events (10–20 minutes) have been observed by AVON (Tsuchiya et al., 2010). The time from the onset to the peak of typical Trimpi events is the same as that for the longer Trimpi events, but the recovery times are greatly different. The cause of the longer Trimpi events has not yet been revealed.

Table 6.1 shows system specifications for AVON. At each site, a set of orthogonal loop antennas is used to observe the horizontal magnetic field components of

Table 6.1. Specifications of AVON.

	Dipole antenna	Orthogonal loop antennas		Monopole antenna
Observation target	E field of lightning atmospherics	B field of lightning atmospherics		E field of radio waves
Size of antenna element	Length = 2 m	1 × 1-m square or 2-m triangle, 30 turns		Length = 2 m
Observation frequency	1–40 kHz	100 Hz – 40 kHz	100 Hz – 10 kHz	For example, 40, 60 kHz
Recording system	PC1 (Desktop)		PC2 (Desktop)	PC3 (Desktop)
Sampling	100 kHz, 16-bit resolution		20 kHz, 16-bit resolution	200 kHz, 16-bit resolution (10 Hz record)
Data amount	~24 TB/year		215 GB/year	15 GB/year

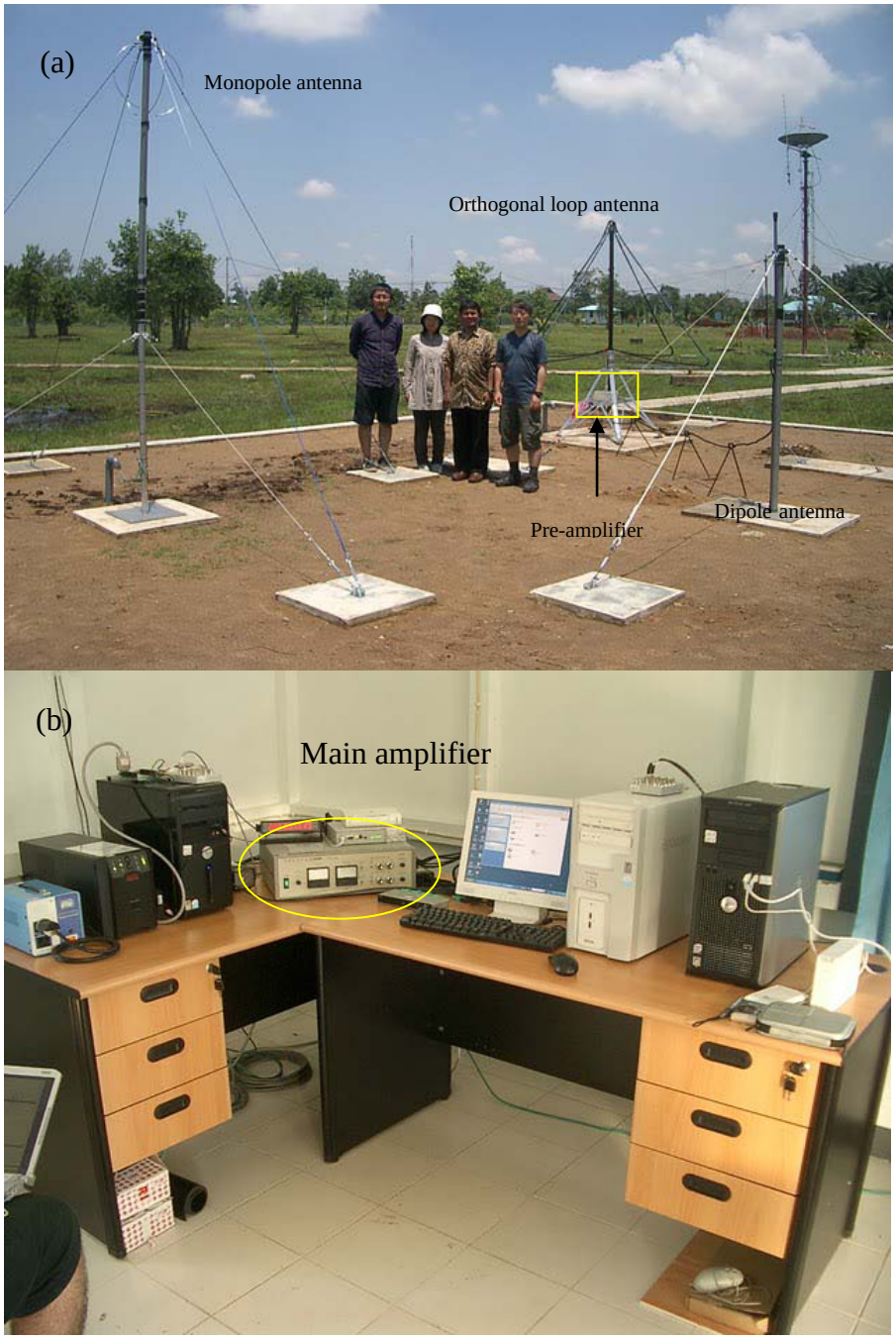

Figure 6.2. Photos of the AVON system. (a) Monopole, dipole, and orthogonal loop antennas in the field, and (b) a main amplifier and data recording system installed inside a room.

north–south (N-S) and east–west (E-W) directions induced by lightning discharges. A set of dipole and monopole antennas is also used to observe the vertical electric field

component of electromagnetic waves radiated by lightning and artificial transmitters, respectively. Figures 6.2 and 6.3 show a photograph and a block diagram of the observation system installed at each site, respectively. Signals are amplified by a pre-amplifier and a main amplifier and then recorded by three personal computers (PCs) together with the GPS time code signals.

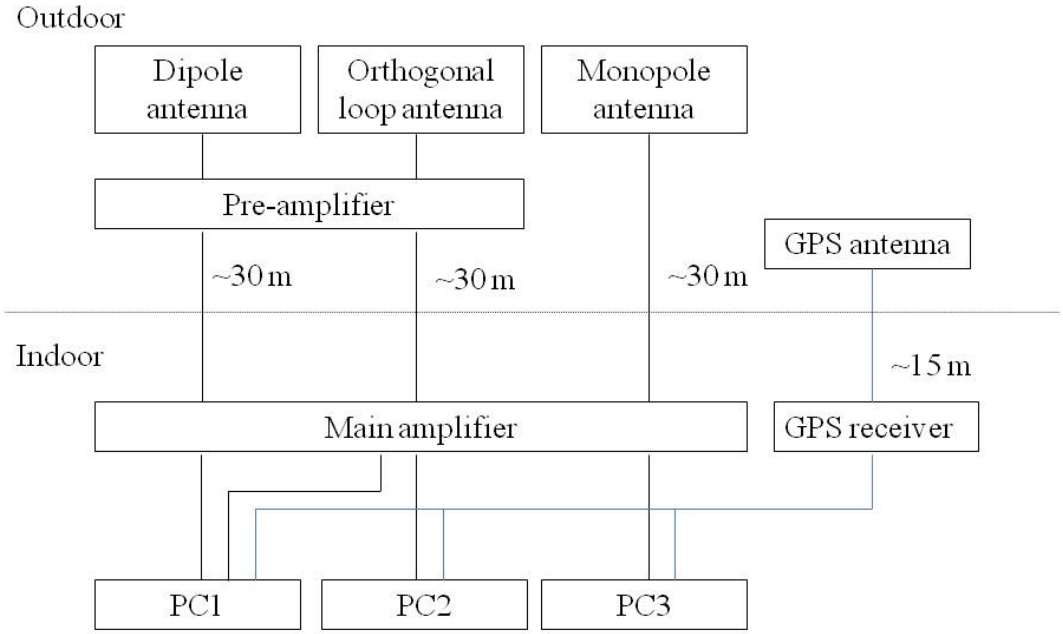

Figure 6.3. Block diagram of the AVON system.

The first PC (PC1) is used for monitoring lightening, and the second (PC2) and third (PC3) PCs are used for monitoring the lower ionosphere. PC1 regularly records the waveforms of lightning atmospherics in both the electric and magnetic field components. The sampling frequency is 100 kHz. The obtained data allow us to detect the occurrence location and the timing of source lightning with accuracies of 10 km and 10 μs, respectively. Furthermore, because the system detects atmospherics in a wide frequency range of 1–60 kHz, it is possible to derive the current moment change of lightning, which is an important parameter in the production of transient luminous events (TLEs)

such as sprites, elves, and blue/gigantic jets (Adachi et al., 2008). PC2 records the waveforms of two-component (N-S and E-W) magnetic-field data of tweeks for 2 minutes every 10 minutes. The measured frequency range is from 100 Hz to 10 kHz, with a sampling frequency of 20 kHz. PC3 records the vertical electric-field component of radio waves emitted from artificial transmitters. Such radio waves are used for the purpose of navigations and time synchronizations in many countries. PC3 samples the radio waves with a sampling frequency of 200 kHz and by analyzing the real-time data, records the power and phase of the pre-set transmitter signals at a rate of 10 Hz. The obtained data are used for monitoring the D- and lower E-region ionosphere.

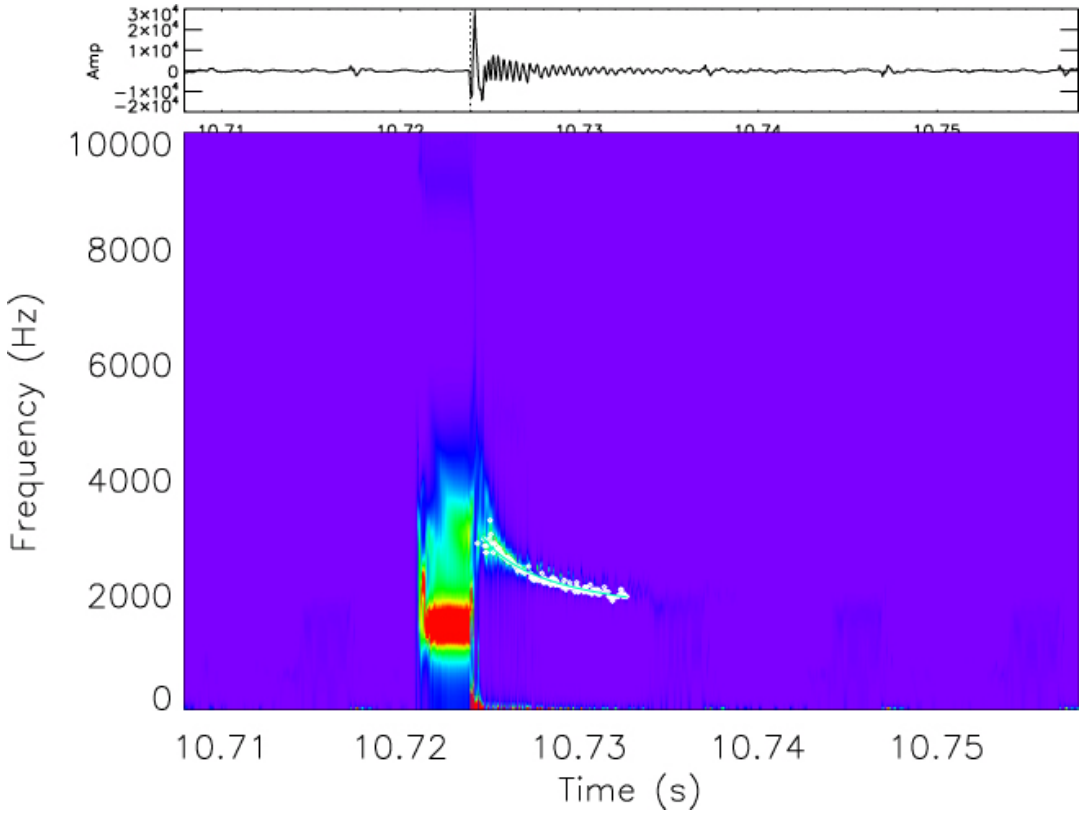

Figure 6.4. Waveform and dynamic spectrum of a tweek observed at Pontianak, Indonesia, at 17:10:43 UT on 28 August 2010.

Figure 6.4 shows an example of a tweek observed by the AVON system. The

reflection height and propagation distance of the tweek were estimated to be 101.4 km and 5847 km, respectively.

In the future, we will estimate the locations of tweek sources (lightning) and the distributions of tweek reflection heights over tweek paths. Currently, the estimation of propagation distance is not sufficiently accurate. We need to improve the method of estimating propagation distance, such as by using the time-of-arrival (TOA) method (e.g., Cummins et al., 1998).

References

Abdu, M. A., I. S. Batista, P. Muralikrishna, and J. H. A. Sobral, Long term trends in sporadic E layers and electric fields over Fortaleza, Brazil, *Geophysical Research Letters, 23(7)*, 757–760, 1996.

Abel, B., R. M. Thore, and A. L. Vampola, Solar cyclic behavior of trapped energetic electrons in Earth's inner radiation belt, *Journal of Geophysical Research, 99*, 19427–19431, 1994.

Adachi, T., Y. Hiraki, Y. Yamamoto, Y. Takahashi, H. Fukunishi, R. R. Hsu, H. T. Su, B. Chen, S. B. Mende, H. U. Frey, L. C. Lee, Electric fields and electron energies in sprites and temporal evolutions of lightning charge moment, *Journal of Physics D, 41*, 234010, 2008.

Aikin, A. C., and R. A. Goldberg, Metallic ions in the equatorial ionosphere, *Journal of Geophysical Research, 78(4)*, 734–745, 1973.

Al'pert, Ya. L., *Radio wave propagation and the ionosphere*, Consultants Bureau, New York, 394pp, 1960.

Appleton, E. V., and M. A. F. Barnett, Local reflection of wireless waves from the upper atmosphere, *Nature, 115*, 333, 1925.

Araki, T., Anomalous phase changes of transequatorial VLF radio waves during geomagnetic storms, *Journal of Geophysical Research, 79(31)*, 4811–4816, 1974.

Baba, K., K. Ohta, T. Tomomatsu, and M. Hayakawa, Frequency dependence of wave characteristics of tweek atmospherics, トウィーク空電の波動特性の周波数依存性, The Institute of Electronics, *Information and Communication Engineers(IEICE) Transactions on Communications, J74-B-II(11)*, 587–593, 1991 (in Japanese).

Baba, K., K. Ohta, O. Takahashi, and S. Ishiguro, Location of causative sferic of

whistler at one observatory, 1 観測点によるホイスラ先行空電の発生位置測定, *Research Letter on Atmospheric Electricity, 12*, 173–183, 1992 (in Japanese).

Backus, G., and F. Gilbert, Uniqueness in the inversion of inaccurate gross earth data, *Philosophical Transactions of the Royal Society A, 266*, 123–192, 1970.

Bain, W. C., and M. D. Harrison, Model ionosphere for D region at summer noon during sunspot maximum, *Proceedings of the Institute of Electrical and Electronics Engineers, 119*, 790–796, 1972.

Bain, W. C., and B. R. May, D-region electron density distributions from propagation data, *Proceedings of the Institute of Electrical and Electronics Engineers, 114*, 1593–1597, 1967.

Belrose, J. S., and M. J. Burke, Study of the Lower Ionosphere Using Partial Reflection, 1. Experimental Technique and Method of Analysis, *Journal of Geophysical Research, 69(13)*, 2799–2818, 1964.

Belrose, J. S., and L. Thomas, Ionization changes in the middle latitude D-region associated with geomagnetic storms, *Journal of Atmospheric and Terrestrial Physics, 30*, 1397–1413, 1968.

Bickel, J. E., J. A. Ferguson, and G. V. Stanley, Experimental observation of magnetic field effects on VLF propagation at night, *Radio Science, 5*, 19-25, 1970.

Blair, J. C., J. N. Brown, and J. M. Watts, An ionosphere recorder for low frequencies, *Journal of Geophysical Research, 58(1)*, 99–107, 1953.

Breit, G., and M. A. Tuve, A radio method of estimating the height of the conducting layer, *Nature, 116*, 357, 1925.

Brekke, A., *Physics of the Upper Polar Atmosphere*, Praxis Publishing Ltd, 1997.

Bremer, J., Trends in the ionospheric E and F regions over Europe, *Annales Geophysicae, 16*, 986–996, 1998.

Bremer, J., Long-term trends in the ionospheric E and F1 regions, *Annales Geophysicae*,

26, 1189–1197, 2008.

Budden, K. G., *Radio Waves in the Ionosphere*, Cambridge University Press, 1961.

Burton, E. T., and E. M. Boardman, Audio-frequency atmospherics, *Proceedings of the Institute of Radio Engineers, 21(10)*, 1476–1494, 1933a.

Burton, E. T., and E. M. Boardman, Effects of solar eclipse on audio frequency atmospherics, *Nature, 131*, 81–82, 1933b.

Christian, H. J., R. J. Blakeslee, D. J. Bocchippio, W. L. Boeck, D. E. Buechler, K. T. Driscoll, S. J. Goodman, J. M. Hall, W. J. Koshak, D. M. Mach, and M. F. Stewart, Global frequency and distribution of lightnings as observed from space by the Optical Transient Detector, *Journal of Geophysical Research, 108*, ACL4–1–ACL4–15, 2003.

Cummins, K. L., M. J. Murphy, E. A. Bardo, W. L. Hiscox, R. B. Pyle, and A. E. Pifer, A Combined TOA/MDF Technology Upgrade of the U.S. National Lightning Detection Network, *Journal of Geophysical Research, 103(D8)*, 9035-9044, doi:10.1029/98JD00153, 1998.

Danilov, A. D., Solar activity effects in the ionospheric D region, *Annales Geophysicae, 16*, 1527–1533, 1998.

Danilov, A. D., Do ionospheric trends indicate to the greenhouse effect?, *Advances in Space Research, 28(7)*, 987–996, 2001.

Davies, K., *Ionospheric Radio Waves*, Waltham, MA:Blaisdell, 1969.

Deeks, D. G., D-region electron distributions in middle latitudes deduced from the reflection of long radio waves, *Proceedings of the Royal Society A, 291*, 413–437, 1966.

Friedrich, M., and K. M. Torkar, Comparison between an empirical and a theoretical model of the D-region, *Advances in Space Research, 21(6)*, 895–904, 1998.

Gardner, F. F., and J. L. Pawsey, Study of the ionospheric D-region using partial

reflections, *Journal of Atmospheric and Terrestrial Physics, 3*, 321–344, 1953.

Gavrilov, N. M., S. Fukao, T. Nakamura, C. Jacobi, D. Kürschner, A. H. Manson, and C. E. Meek, Comparative study of interannual changes of the mean winds and gravity wave activity in the middle atmosphere over Japan, Central Europe and Canada, *Journal of Atmospheric and Solar-Terrestrial Physics, 64*, 1003–1010, 2002.

Goncharenko, L., and S.-R. Zhang, Ionospheric signatures of sudden stratospheric warming: Ion temperature at middle latitude, *Geophysical Research Letters, 35*, L21103, doi:10.1029/2008GL035684, 2008.

Hargreaves, J. K., *The solar–terrestrial environment*, Cambridge University Press, 1992.

Hayakawa, M., K. Ohta, and S. Shimakura, High accuracy method of locating distant lightning by means of tweek atmospherics, *11th Symposium and Exhibition on Electromagnetic Compatibility*, 566, Wroclaw, Poland, 1992.

Hayakawa, M., K. Ohta, and K. Baba, Wave characteristics of tweek atmospherics deduced from the direction –finding measurement and theoretical interpretation, *Journal of Geophysical Research, 99*, 10733–10743, 1994.

Heaps, M. G., Parametrization of the cosmic ray ion-pair production rate above 18 km, *Planetary and Space Science, 26*, 513–517, 1978.

Helliwell, R. A., J. P. Katsufrakis, and M. L. Trimpi, Whistler-induced amplitude perturbation in VLF propagation, *Journal of Geophysical Research, 78*, 4679–4688, 1973.

Holdsworth, D. A., R. Vuthaluru, I. M. Reid, and R. A. Vincent, Differential absorption measurements of mesospheric and lower thermospheric electron densities using the Buckland Park MF radar, *Journal of Atmospheric and Solar-Terrestrial Physics, 64*, 2029–2042, 2002.

Huang, N. E., The empirical mode decomposition and the Hilbert spectrum for

nonlinear and non-stationary time series analysis, *Proceedings of the Royal Society of London, A, 454*, 903–993, doi:10.1098/rspa.1998.0193, 1998.

Huang, N. E., and Z. Wu, A review on Hilbert-Huang Transform: Method and its applications to geophysical studies, *Reviews of Geophysics, 46*, RG2006, doi:10.1029/2007RG000228, 2008.

Inan, U. S., D. L. Carpenter, R. A. Helliwell, and J. P. Katsufrakis, Subionospheric VLF/LF phase perturbations produced by lightning-whistler induced particle precipitation, *Journal of Geophysical Research, 90*, 7457–7469, 1985.

Jacobi, C., N. M. Gavrilov, D. Kürschner, and K. Fröhlich, Gravity wave climatology and trends in the mesosphere/lower thermosphere region deduced from low-frequency drift measurements 1984-2003 (52.1ºN, 13.2ºE), *Journal of Atmospheric and Solar–Terresyrial Physics, 68*, 1913–1923, 2006.

Jacobs, J. A., and T. Watanabe, The equatorial enhancement of sudden commencements of geomagnetic storms, *Journal of Atmospheric and Terrestrial Physics, 25*, 267–279, 1963.

Jones, T. B., and I. C. Wand, An investigation of the reflection properties of various ionospheric models for radio waves in the frequency range 16-3000 kHz, *Journal of Atmospheric and Terrestrial Physics, 32*, 1705–1719, 1970.

Kashiwagi, M., J. Ohtsu, and A. Iwai, Observation of tweeks, *Proceedings of the Research Institute of Atmospherics*, Nagoya University, 125–128, 1970.

Kataoka, R., Y. Miyoshi, and A. Morioka, Hilbert-Huang Transform of geomagnetic pulsations at auroral expansion onset, *Journal of Geophysical Research, 114*, A09202, doi:10.1029/2009JA014214, 2009.

Kawahira, K., The D region winter anomaly at high and middle latitudes induced by planetary waves, *Radio Science, 20(4)*, 795-802, 1985.

Kawamura, S., H. Mori, and Y. Murayama, A comparative study of the electron density

estimated with MF radar DAE method and cosmic noise absorption at Poker Flat, Alaska, *Journal of the National Institute of Information and Communications Technology (NICT), 54*, 57–65, 2007.

Kerr, R. B., R. Garcia, X. He, J. Noto, R. S. Lancaster, C. A. Tepley, S. A. Gonzalez, J. Friedman, R. A. Doe, M. Lappen, and B. McCormack, Periodic variations of geocoronal Balmer-alpha brightness due to solar-driven exospheric abundance variations, *Journal of Geophysical Research, 106(A12)*, 28797–28817, 2001.

Kikuchi, T., and D. S. Evans, Energetic electrons observed by NOAA–6 over Japan (L=1.3) at the time of geomagnetic storm on February 8–9, 1986, *Proceedings of the Research Institute of Atmospherics, Nagoya University, Japan, 36(2)*, 137–150, 1989.

Kikuchi, T., K. K. Hashimoto, and K. Nozaki, Penetration of magnetospheric electric fields to the equator during a geomagnetic storm, *Journal of Geophysical Research, 113*, A06214, doi:10.1029/2007JA012628, 2008.

Kimura, I., K. Hiraishi, and T. Tomimoto, Measurement of wave normal direction of VLF waves propagated through the ionosphere by means of the VLF Doppler technique, Doppler 法による電離層中の VLF 電波の伝搬ベクトル方向の測定, *Bulletin of the Institute of Space and Aeronautical Science*, University of Tokyo, 8(1_B), 97–107, 1972 (in Japanese).

King, J. W., and J. L. Fooks, Long-lasting storm effects in the ionospheric D-region, *Journal of Atmospheric and Terrestrial Physics, 30*, 639–643, 1968.

Kishore, A., S. Kumar, and V. Ramachandran, Observations of ELF-VLF sferics in the South Pacific region, *XXVIIIth International Union of Radio Science (URSI) General Assembly and Scientific Symposium*, URSI, New Delhi, India, 2005.

Knuth, R., and E. A. Lauter, Effects of trapped particles in lower ionosphere at medium latitude, *Space Research, 4*, 673–680, 1964.

Kopp, E., On the abundance of metal ions in the lower thermosphere, *Journal of Geophysical Research, 102(A5)*, 9667–9674, 1997.

Krasnushkin, P. E., and T. A. Knyazeva, Diurnal, seasonal, and 11-year variations in electron density profiles in the lower ionosphere, *International Journal of Geomagnetism and Aeronomy, 10*, 789–796, 1970.

Kumar, S., A. Kishore, and V. Ramachandran, Higher harmonic tweek sferics observed at low latitude: estimation of VLF reflection heights and tweek propagation distance, *Annales Geophysicae*, *26*, 1451–1459, 2008.

Kürschner, D., and Ch. Jacobi, Trends and periodicities in nighttime LF radio wave reflection heights, *Symposium ST11, 27th EGS General Assembly*, Nice, Italy (http://www.uni-leipzig.de/~jacobi/docs/EGS2002_3.pdf), 2002.

Laštovička, J., On the role of solar and geomagnetic activity in long-term trends in the atmosphere-ionosphere system, *Journal of Atmospheric and Solar-Terrestrial Physics, 67*, 83–92, 2005.

Laštovička, J., Global pattern of trends in the upper atmosphere and ionosphere: Recent progress, *Journal of Atmospheric and Solar-Terrestrial Physics, 71*, 1514–1528, 2009.

Laštovička, J., R. A. Akmaev, G. Beig, J. Bremer, J. T. Emmert, C. Jacobi, M. J. Jarvis, G. Nedoluha, Y. I. Portnyagin, and T. Ulich, Emerging pattern of global change in the upper atmosphere and ionosphere, *Annales Geophysicae, 26*, 1255–1268, doi:10.5194/angeo-26-1255-2008, 2008.

Lauter, E. A., and R. Knuth, Precipitation of high energy particles into the upper atmosphere at medium latitude after geomagnetic storms, *Journal of Atmospheric and Terrestrial Physics, 29*, 411–417, 1967.

Lauter, E. A. and P. Nitzche, Seasonal variations of ionospheric absorption deduced from A3-measurements in the frequency range 100-2000 kc/s, *Journal of*

Atmospheric and Terrestrial Physics, 29, 533–544, 1967.

Lean, J., Solar ultraviolet irradiance variations: A review, *Journal of Geophysical Research, 92*, 839–868, 1987.

Lynn, K. J. W., and J. Crouchley, Night-time sferic propagation at frequencies below 10 kHz, *Australian Journal of Physics, 20*, 101–108, 1967.

Maeda, K.-I., Study on electron density profile in the lower ionosphere, *Journal of Geomagnetism and Geoelectricity, 23*, 133–159, 1971.

McCracken, K. G., and F. B. McDonald, A phenomenological study of the long-term cosmic ray modulation, 850-1958 AD, *Journal of Geophysical Research, 109*, A12103, doi:10.1029/2004JA010685, 2004.

Miyoshi, Y., V. K. Jordanova, A. Morioka, and D. S. Evans, Solar cycle variations of the electron radiation belts: Observation and radial diffusion simulation, *Space Weather, 2*, S10S02, doi:10.1029/2004SW000070, 2004.

Miyoshi, Y., and R. Kataoka, Solar cycle variations of outer radiation belt and its relationship to solar wind structure dependences, *Journal of Atmospheric and Terrestrial Physics, 73*, 77–87, 2011.

Miyoshi, Y., A. Morioka, and H. Misawa, Long term modulation of low altitude proton radiation belt by the Earth's atmosphere, *Geophysical Research Letters, 27(14)*, 2169–2172, 2000.

Murayama, Y., K. Igarashi, D. D. Rice, B. J. Watkins, R. L. Collins, K. Mizutani, Y. Saito, and S. Kainuma, Medium Frequency Radars in Japan and Alaska for Upper Atmosphere Observations, *Information and Communication Engineers(IEICE) Transactions on Communications, E83–B(9)*, 1996–2003, 2000.

Nagano, I., S. Yagitani, M. Ozaki, Y. Nakamura, and K. Miyamura, Estimation of lightning location from single station observations of sferics, *Electronics and Communications in Japan, Part 1, 90(1)*, 25–34, 2007.

Nagata, T., and T. Tohmatsu, *Modern Aeronomy*, 超高層大気の物理学, Shokabo, Tokyo, 1973 (in Japanese).

Nossal, S. M., E. J. Mierkiewicz, F. L. Roesler, R. J. Reynolds, and L. M. Haffner, Geocoronal hydrogen studies using Fabry-Perot interferometers, part 2: Long-term observations, *Journal of Atmospheric and Solar-Terrestrial Physics, 68*, 1553–1575, 2006.

Nunn, D., On the numerical modelling of the VLF Trimpi effect, *Journal of Atmospheric and Solar Terrestrial Physics*, 59 (5), 537–560, 1997.

Obayashi, T., *Space Science–Solar Terrestrial Physics–*, 宇宙空間物理学, Syokabo, Tokyo, 1970 (in Japanese).

Ohta, K., M. Hayakawa, S. Shimakura, and T. Tomomatsu, Correlation of whistlers at a low latitude with causative lightnings at conjugate regions, *The Institute of Electronics, Information and Communication Engineers(IEICE) Transactions on Communications, B–II*, 276, 1991.

Ohya, H., M. Nishino, Y. Murayama, and K. Igarashi, Equivalent electron densities at reflection heights of tweek atmospherics in the low-middle latitude D-region ionosphere, *Earth, Planets and Space, 55*, 627–635, 2003.

Ohya, H., M. Nishino, Y. Murayama, K. Igarashi, and A. Saito, Using tweek atmospherics to measure the response of the low-middle latitude D-region ionosphere to a magnetic storm, *Journal of Atmospheric and Solar-Terrestrial Physics, 68*, 697–709, 2006.

Ohya, H., K. Shiokawa, and Y. Miyoshi, Development of an automatic procedure to estimate the reflection height of tweek atmospherics, *Earth, Planets and Space, 60*, 837–843, 2008.

Outsu, J., Numerical study of tweeks based on waveguide mode theory, *Proceedings of the Research Institute of Atmospherics, Nagoya University, 7*, 58–71, 1960.

Peter, W. B., M. W. Chevalier, and U. S. Inan, Perturbations of midlatitude subionospheric VLF signals associated with lower ionospheric disturbances during major geomagnetic storms, *Journal of Geophysical Research, 111*, doi:10.1029/2005JA011346, A03301(1–14), 2006.

Peter, W. B., and U. S. Inan, On the occurrence and spatial extent of electron precipitation induced by oblique nonducted whistler waves, *Journal of Geophysical Research, 109*, doi:10.1029/2004JA010412, A12215, 2004.

Prasad, R., Effects of land and sea parameters on the dispersion of tweek atmospherics, *Journal of Atmospheric and Terrestrial Physics, 43(12)*, 1271–1277, 1981.

Press, W. H., B. P. Flannery, S. A. Teukolsky, and W. T. Vetterling, *Numerical recipes in C*, Cambridge University Press, UK., 1988.

Rafalsky, V. A., A. V. Shvets, and M. Hayakawa, One-site distance-finding technique for locating lightning discharges, *Journal of Atmospheric and Terrestrial Physics, 57(11)*, 1255–1261, 1995.

Ratcliffe, J. A., The ionosphere and the engineer, *Proceedings of the Institute of Electrical and Electronics Engineers (London), 114*, 1 , 1967.

Ryabov, B. S., Tweek propagation peculiarities in the Earth-ionosphere waveguide and low ionosphere parameters, *Advances in Space Research, 12(6)*, (6)255–(6)258, 1992.

Saito, A., S. Fukao, and S. Miyazaki, High resolution mapping of TEC perturbations with the GSI GPS network over Japan, *Geophysical Research Letters, 25*, 3079–3082, 1998.

Schunk, R. W., and A. F. Nagy, *Ionospheres–Physics, Plasma Physics, and Chemistry*, Cambridge University Press, 2000.

Sechrist, C. F. Jr., Comparisons of techniques for measurement of D-region electron densities, *Radio Science, 9(2)*, 137–149, 1974.

Sen, H. K., and A. A. Wyller, On the Generalization of the Appleton-Hartree Magnetoionic Formulas, *Journal of Geophysical Research, 65(12),* 3931–3950, 1960.

She, C.-Y., D. A. Krueger, R. Akmaev, H. Schmidt, E. Talaat, and S. Yee, Long-term variability in mesopause region temperatures over Fort Collins, Colorado (41°N, 105°W) based on lidar observations from 1990 through 2007, *Journal of Atmospheric and Solar-Terrestrial Physics, 71,* 1558–1564, 2009.

Sheehan, C. H., and J. P. St.-Maurice, Dissociative recombination of N_2^+, O_2^+, and NO^+: Rate coefficients for ground state and vibrationally excited ions, *Journal of Geophysical Research, 109,* A03302, doi:10.1029/2003JA010132, 2004.

Shellman, C. H., Electron density distributions in the lower ionosphere with associated error limits derived from VLF and LF sounder data, *Radio Science, 5,* 1127–1135, 1970.

Shvets, A. V., and M. Hayakawa, Polarization effects for tweek propagation, *Journal of Atmospheric and Solar-Terrestrial Physics, 60,* 461–469, 1998.

Silberstein, R., The origin of the current nomenclature for the ionospheric layers, *Journal of Atmospheric and Terrestrial Physics, 13,* 382, 1959.

Singh, A. K., and R. P. Singh, Propagational features of higher harmonic tweeks at low latitudes, *Earth, Moon and Planets, 73,* 277–290, 1996.

Spiro, R. W., R. A. Wolf, and B. G. Fejer, Penetration of high-latitude electric field effects to low latitudes during SUNDIAL 1984, *Annales Geophysicae, 6,* 39–50, 1988.

Strobel, D. F., C. B. Opal, and R. P. Meier, Photoionization rates in the night-time E- and F-region ionosphere, *Planeary and Space Science, 28,* 1027–1033, 1980.

Sugiyama, T., Response of electrons to a gravity wave in the upper mesosphere, *Journal of Geophysical Research, 93(D9),* 11083-11091, 1988.

Swider, W., Ion and neutral concentrations of Mg and Fe near 92 km, *Planetary and Space Science, 32*, 307–312, 1984.

Thomas, L., and M. D. Harrison, The electron density distributions in the D-region during the night and pre-sunrise period, *Journal of Atmospheric and Terrestrial Physics, 32*, 1–14, 1970.

Thomson, N. R., M. A. Clilverd, and W. M. McRae, Nighttime ionospheric D region parameters from VLF phase and amplitude, *Journal of Geophysical Research, 112*, A07304, doi:10.1029/2007JA012271, 2007.

Titheridge, J. E., Ionization below the night F2 layer-a global model, *Journal of Atmospheric and Solar-Terrestrial Physics, 65*, 1035–1052, 2003.

Tohmatsu, T., *Compendium of Aeronomy*, Terra Scientific Publishing Company, Tokyo, Kluwer Academic Publishers, 1990.

Tsuchiya, F., Y. Takahashi, K. Yamashita, T. Adachi, H. Ohya, H. Misawa, A. Morioka, Y. Miyoshi, K. Shiokawa, and T. Kikuchi, Statistical analysis on occurrences of the lightning induced VLF/LF events observed in the East Asia, *2010 Asia-Pacific Radio Science Conference (AP-RASC)*, GEH2a-4, Toyama, Japan, 2010.

Tsugawa, T., A. Saito, and Y. Otsuka, A statistical study of large-scale traveling ionospheric disturbances using the GPS network in Japan, *Journal of Geophysical Research, 109*, A06302, 2004.

Villard, O. G., The ionospheric sounder and its place in the history of radio science, *Radio Science, 11*, 847, 1976.

Wait, J. R., *Electromagnetic Waves in Stratified Media*, Pergamon Press, 147, 1970.

Wakai, N., Quiet and disturbed structure and variations of the night-time E-region, *Journal of Geophysical Research, 72*, 4507–4517, 1967.

Wakai, N., Study on the nighttime E region and its effects on the radio wave propagation, *Journal of the Radio Research Laboratories, 18*, 245–348, 1971.

Watson-Watt, R. A., Weather and wireless, *Quarterly Journal of the Royal Meteorological Society, 55*, 273, 1929.

Watt, A. D., *VLF Radio Engineering*, International Series of Monographs in Electromagnetic Waves, Pergamon Press, Oxford, 1967.

Xiaoqing, P., M. Mendillo, W. J. Haughes, M. J. Buonsanto, D. P. Sipler, L. Kelly, O. Zhou, G. Lu, and T. Hughes, Dynamical effects of geomagnetic storms and substorms in the middle latitude ionosphere: an observational campaign, *Journal of Geophysical Research, 105(A4)*, 7403–7417, 2000.

Yamashita, M., Propagation of tweek atmospherics, *Journal of Atmospheric and Terrestrial Physics*, *40*, 151–153, 1978.

Yedemsky, D., B. S. Ryabov, A. Shchokotov, and V. S. Yarotsky, Experimental investigation of the tweek field structure, *Advances in Space Research, 12*, 251–254, 1992.

Yumoto, K., Y. Tanaka, T. Oguti, K. Shiokawa, Y. Yoshimura, A. Isono, B. J. Fraser, F. W. Menk, J. W. Lynn, M. Seto, and 210 (deg) MM magnetic meridian observation group, Globally coordinated magnetic observations along 210 (deg) magnetic meridian during STEP period: 1. Preliminary results of low-latitude Pc 3's, *Journal of Geomagnetism and Geoelectricity, 44*, 261-276, 1992.

Yumoto, K., and the 210 (deg) MM Magnetic Observation Group, The STEP 210 (deg) magnetic meridian network project, *Journal of Geomagnetism and Geoelectricity, 48*, 1297-1309, 1996.